STEREO-DIRECTING EFFECTS OF MOLECULARLY IMPRINTED POLYMERS ON CINNAMIC ACIDS

By

Nontlantla Regina Maseko
(17023723)

A dissertation submitted in fulfillment of the requirements for the degree of

Master of Science

in the

Department of Chemistry

Faculty of Science, Engineering and Agriculture

University of Venda

Thohoyandou, Limpopo

South Africa

Supervisor

PROFESSOR S.S MNYAKENI-MOLEELE

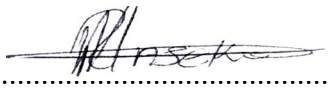
Co-supervisor

DOCTOR N.T TAVENGWA

© University of Venda

Declaration

I, Nontlantla Regina Maseko (student number: 17023723), declare that the research is my original work and has not been submitted for any degree at any other university or tertiary institution. The research does not contain any other person's writing unless specifically acknowledged and referenced accordingly.

Signed (Student):  Date: 19 March 2025

© University of Venda

Abstract

The pursuit of enantiomerically and diastereomerically pure compounds is a paramount concern in pharmaceutical synthesis and various other industries, as different isomers often exhibit drastically different even opposite and toxic biological activities. Traditional separation methods are often inefficient, costly, and environmentally unsustainable, necessitating an exploration of good separation and purification techniques. The study addresses this challenge by exploring, for the first time, the stereo-directing potential of molecularly imprinted polymers (MIPs) in reactions involving cinnamic acid derivatives, specifically focusing on (2E)-3-(4-methoxyphenyl) prop-2-enoic acid (trans-4-methoxy cinnamic acid (t-4MCA)). To the best of our knowledge, no prior studies have reported the synthesis of MIPs using t-4MCA as a template, nor the application of MIPs as catalysts in the Wittig reaction or for the selective separation of *cis* and *trans* isomers resulting from photoisomerization. The work represents a novel approach to stereoselective synthesis and purification.

MIPs were synthesized via precipitation polymerization using t-4MCA as the template, methacrylic acid (MAA) as the functional monomer, and ethylene glycol dimethacrylate (EEDGMA) as the cross-linker in a 1:4:20 molar ratio. A "dummy" template paracetamol (PCM) was also used to create a comparative MIP. Non-imprinted polymers (NIPs) were synthesized as controls. Complete template removal was verified after 8 washing cycles using UV-VIS spectroscopy. Brunauer-Emmert-Teller (BET), Fourier transform Infra-red (FTIR), thermogravimetric analysis (TGA), and ultraviolet (UV) spectroscopy were employed to characterize the unwashed MIPs, washed MIPS and NIPs. The characterization confirmed the formation of amorphous, mesoporous material with high surface areas, particularly after template removal. The disappearance of the vinyl C=C stretch (1635 cm^{-1}) in the FTIR spectra confirmed complete polymerization while the peaks for the polymer backbone were confirmed by C-H vibrations at ~2980 cm^{-1} and ~1451 cm^{-1}. The t-4MCA MIP exhibited a BET surface area of 175.2 $m^2 g^{-1}$ and a pore volume of 0.190 $cm^3 g^{-1}$, markedly higher than the NIP (7.9 $m^2 g^{-1}$ and 0.009 $cm^3 g^{-1}$). TGA showed maximum decomposition temperatures of 375°C, 379°C and 389°C for the washed t-4MCA MIP, unwashed t-4MCA MIP, and NIP, respectively, highlighting the good thermal stability of the polymer network. Swelling studies showed differential swelling behavior dependent on solvent, with acetonitrile showing a high degree of swelling for MIPs and ethanol for the NIPs.

© University of Venda

Adsorption studies, optimized using a 5:5 v/v methanol/water washing solution 10 mg of polymer mass, pH 7, and a 60-min contact time, revealed a maximum adsorption capacity (q_m) of 3.00 mg g^{-1}, for t-4MCA on the MIP, significantly exceeding that of the NIP (2.60 mg g^{-1}) and PCM MIPs (2.4 mg g^{-1}), with an imprinting factor of 1.14. Selectivity studies using structurally analogues ferulic acid, (E)-3-(4-hydroxyphenyl)prop-2-enoic acid (trans-4-hydroxy cinnamic acid (t-4HCA)), and ethyl (E)-3-(4-methoxyphenyl) acrylate (Et-MOPA) demonstrated a significant cross-reactivity with ferulic acid (k` = 0.356), moderate cross-reactivity with t-4HCA (k` = 2.340) and minimal cross-reactivity with Et-MOPA (k` = 1.635).

Optimum photoisomerization of t-4MCA at 3 h resulted in the MIP increasing the reaction rate by a 21.63% increase in the *cis* isomer proportion. At 12 h, after total equilibration, there was evidence of an increased yield of the *cis* isomer of almost 10%.

The Wittig reaction of 4-methoxybenzaldehyde yielded a percentage *cis/trans* ratio of 3/97. Crucially, conducting the reaction in the presence of the t-4MCA MIP improved the ratio to 6/94, an increase in the *cis* isomer ratio.

This research demonstrated, for the first time, an attempt at the application of t-4MCA-imprinted MIPs as both selective adsorbents and stereo-directing agents. The MIPs significantly enhanced the proportion of the *cis* isomer in the photoisomerization reaction and, uniquely, in the Wittig reaction, highlighting their potential for efficient and sustainable production of diastereomerically pure pharmaceuticals and fine chemicals.

© University of Venda

Dedication

The research is dedicated to my late father, **Thomas Maseko**, who was a constant source of inspiration and encouragement throughout my academic journey. Your unwavering belief in my abilities and your wise guidance will forever remain etched in my heart. To my beloved mother, **Matshediso Maseko**, thank you for your endless love, sacrifice, and unwavering support. Your belief in me and in miracles has been my driving force, it has propelled me through the challenging moments. To my cherished son, **Letlhogonolo Maseko**, I dedicate this research while acknowledging the sacrifices it demanded from our time together.

© University of Venda

Acknowledgments

"'Gratitude' comes from the same word as freedom (gratis = free). Gratitude is the freeing expression of a free heart toward one who freely gave." Ravi Zacharias

I express my utmost gratitude to the **Lord God Almighty** for granting me the strength and perseverance required to successfully accomplish this significant undertaking. The divine guidance and resilience provided by my faith have been essential throughout this journey.

Furthermore, I would like to extend my sincerest appreciation to my esteemed supervisor, **Professor SS Myakeni-Moleele**, a distinguished senior lecturer at the University of Venda. His continuous academic input, guidance, and constructive criti*cis*m have been invaluable, shaping the course of my research. I am especially grateful for their unwavering determination and steadfastness, which has undoubtedly become an inspiration to me. I also extend my heartfelt thanks to **Dr. NT. Tavengwa**, an adjunct senior research fellow at the University of Venda, for his invaluable guidance, unwavering support, and diligent supervision throughout this project. His remarkable patience and unwavering belief in the eventual success of my endeavors have been a source of encouragement and motivation.

Sincerest gratitude goes to the Drug Synthesis and Isolation Research Group (DSI), the Analytical Chemistry Research Group, Council for Scientific and Industrial Research (CSIR) for their generous assistance with data acquisition, Mr Patrick Pandelani for NMR data acquisition, and the Environmental Science Lab for the SEM data acquisition. Sincerest gratitude also goes to Professor Edwin Ntakadzeni Madala for his thoughtful assistance with data acquisition using the LC-MS.

To my son **Letlhogonolo Maseko**, the countless hours spent immersed in this pursuit sometimes separated us, but please know that every moment away from you was not without a pang of longing. Your infectious laughter and innocent smile have been my greatest motivation, propelling me forward, and reminding me of the importance of my work. To my family and parents, I could never express fully how thankful I am for all your support.

© University of Venda

University of Venda
Creating Future Leaders

Table of contents

Declaration i

Abstract ii

Dedication iv

Acknowledgments v

Table of contents vi

List of abbreviations xi

List of figures xv

List of tables xviii

List of schemes xix

Chapter 1 1

1. Introduction 2

1.1 Background 2

1.2. Problem statement 4

1.3. Aim of the study 5

1.3.1. Broad objective of the study 5

1.3.2 Specific objectives of the study 5

1.3.3 Research questions 6

Chapter 2 8

2. Literature review 9

Part A 9

2.1 Importance of cinnamic acid and its derivatives 9

2.1.1 Sources and abundance 10

2.1.2 Pharmacological activities 11

© University of Venda

University of Venda
Creating Future Leaders

2.1.3 Biosynthesis and structural diversity of cinnamic acid and its derivatives.....11
2.1.4 Anthropogenic sources..... 12
2.2 Challenges in cinnamic acid and derivatives production and separation..... 13
2.3 Techniques for stereoisomer separation..... 14
2.3.1 Chiral high-performance liquid chromatography..... 14
2.3.2 Gas chromatography with chiral columns..... 15
2.3.3 Super critical chromatography..... 17
2.3.4 Solid phase extraction..... 19
Part B..... 19
2.4 Stereoisomerism in drug development..... 19
2.4.1 Effects of *cis/trans* isomerism in drug development..... 20
2.4.2 The importance of early isomer separation in drug development..... 23
2.5 Molecular imprinting technology..... 25
2.5.1 Pre-polymerization reagents..... 26
Chapter 3..... 31
Materials and Methods..... 31
3.1 Chemicals and reagents..... 33
3.2 Equipment and instruments..... 33
3.3 LC-MS analysis..... 35
3.4 HPLC analysis..... 36
Part A..... 37
3.5 Synthesis of molecularly imprinted polymers MIPs and respective NIPs..... 37
3.6 Synthesis of analogs of trans-4-methoxy cinnamic acid..... 39
3.6.1 Paracetamol (7)..... 39
3.6.2 Ferulic acid (3)..... 40

© University of Venda

University of Venda
Creating Future Leaders

3.6.3 4-hydroxy cinnamic acid (2) 41

3.7 Synthesis of control MIPs using a dummy template 41

3.8 Template removal protocol of MIPs 41

3.9 Swelling behavior of polymers 42

3.10 Optimisation of adsorption parameters affecting the adsorption of the template to the MIPs. 42

3.10.1 The effect of adsorption solvent 43

3.10.2 Effect of polymer mass 43

3.10.3 Point of zero charge pH_{pzc} 44

3.10.4 Effect of sample pH 45

3.10.5 Effect of contact time 45

3.10.6 Effect of initial concentration 45

3.10.6.1 Adsorption isotherms 46

3.11 Selectivity studies 48

Part B 48

3.12 Procedure for photoisomerization to generate *cis/trans* mixtures 48

3.12.1 Selective extraction of t-4MCA from a *cis/trans* mixture using MIPs - Batch binding method 49

3.12.2 Photoirradiation experiment in the presence of t-4MCA MIPs - Batch binding method 49

3.13 Synthesis of ethyl (E)-3-(4-methoxyphenyl) acrylate (Et-MOPA) (8) Wittig reaction 50

3.13.1 Synthesis of ethyl 2-(triphenylphosphoranylidene) (ylide) acetate, a substrate in the Wittig reactions 50

3.13.2 Synthesis of (Et-MOPA) (8) using the Wittig reaction 51

3.13.3 Synthesis of t-4MCA using Wittig reaction 51

© University of Venda

University of Venda
Creating Future Leaders

3.14 Wittig reactions in the presence of synthesized MIPs 52
Chapter 4 53
Results and discussion 53
4. Results and discussion 54
Part A characterization 54
4.1 Chemical computational analysis 54
4.2 Mechanism of synthesis of MIPs 56
4.3 Synthesis and characterization of MIPs 58
4.4 Removal profile of t-4MCA and PCM templates from MIPs synthesized with MAA and chloroform 59
4.5 Batch binding studies for all MIPs and NIPs synthesized 62
4.6 Characterization of synthesized MIPs 64
4.6.1 Functional group analysis 64
4.6.2 Thermogravimetric analysis of polymers 66
4.6.3 Nitrogen gas adsorption analysis 68
4.6.4 Morphology analysis of polymers 71
4.7 Swelling studies 75
4.8 Enhancing the parameters that influence adsorption capacity 76
4.8.1 Solvent effects on adsorption capacity of t-4MCA imprinted polymers 76
4.8.2 Effect of polymer mass on adsorption capacity of *t*-4MCA imprinted polymers 77
4.8.3 Investigating the impact of pH on polymer adsorption capacity and determining the point of zero charge pH_{PZC} 79
4.8.4 Effect of contact time on the adsorption capacity of the polymers 81
4.8.5 Effect of initial concentration on t-4MCA adsorption 83
4.9 Selective adsorption and competitive evaluation of t-4MCA 87

© University of Venda

University of Venda
Creating Future Leaders

4.9.1 Selectivity studies, binding of t-4MCA and structural analogs 89

4.9.2 Competitive binding of t-4MCA and structural analogs 90

Part B 93

4.10 Photoisomerization of t-4MCA to generate c-4MCA and t-4MCA mixture 93

4.11 Selective extraction of *trans*-4-MCA from *cis/trans* mixtures using MIPs 95

4.12 Photoisomerization of t-4MCA in the presence of t-4MCA MIP, NIP with a control sample 97

4.12.1 Kinetic analysis of photoisomerization 99

4.12.2 Equilibrium shift and isomer selectivity 100

4.13 Synthesis of ethyl (E)-3-(4-methoxyphenyl) acrylate using the Wittig reaction (8) 102

4.14 Synthesis of ethyl (E)-3-(4-methoxyphenyl) acrylate using the Wittig reaction (8) in the presence of MIPs and NIPs 107

4.14.1 Synthesis in the in the presence of the NIPs 107

4.14.2 Synthesis in the in the presence of the MIPs 109

5.1 Conclusion 113

References 116

Figure A4: ^{1}H-NMR/^{13}C-NMR spectra of paracetamol 147

Figure A6: The reported Rf value of Hydroxycinnamic acid was 0.3 with 50/50 % ethyl acetate and petroleum ether (a) without UV-light (b) Under UV-light 148

Figure A8: FTIR spectra and TLC visualization of ferulic acid 150

Figure A9: The reported Rf value of ferulic acid was 0.56 with 50/50 % ethyl acetate and petroleum ether (a) without UV-light (b) Under UV-light 150

Figure A11: FTIR spectra and TLC visualization of hydroxycinnamic acid 152

Figure A12: The reported Rf value of hydroxycinnamic acid was 0.69 with 50/50 % ethyl acetate and petroleum ether (a) without UV-light (b) Under UV-light 153

Figure A13: ^{1}H-NMR/13C-NMR spectra of 4-methoxy cinnamic a 154

© University of Venda

Figure A14: ^{13}C-NMR/dept-90 spectra of Ethyl 2-(triphenylphosphoranylidene) acetate 155

Table A1: Computational study results for the optimization of synthesis solvent..... 156

Table A5: Swelling % of MIPs in different solvents..... 157

© University of Venda

List of abbreviations

^{13}C NMR	Carbon nuclear magnetic resonance
^{1}H NMR	Proton nuclear magnetic resonance
4-VP	4-Vinylpyridine
AA	Acrylic acid
ACHN	1,1'-Azobis (cyclohexanecarbonitrile)
ACN	Acetonitrile
AURO	Aurothioglucose
BET	Brunauer-Emmett-Teller
BIS	N,N'-Methylenebisacrylamide
BPA	Bisphenol A
c-4MCA	*Cis*-4-methoxy cinnamic acid
CA	Cinnamic acid
$CDCl_3$	Chloroform
CE	Capillary electrophoresis
COD	Chemical oxygen demand
COSY	Correlation spectroscopy
CSIR	Council for Scientific and Industrial Research
DCM	Dichloromethane
DEPT	Distortionless enhancement by polarization transfer
dHCA	Dihydroxy cinnamic Acid
DI	Deionized water
DMF	Dimethyl formamide
DMSO	Dimethyl sulfoxide

© University of Venda

DSI	Drug Synthesis and Isolation Research Group
EDX	Energy-dispersive x-ray spectroscopy
EGDMA	Ethylene glycol dimethacrylate
Et-MOPA	Ethyl(E)-3-(4-methoxyphenyl) acrylate
EtOH	Ethanol
FTIR	Fourier-transform infrared spectroscopy
GC	Gas chromatography
H_2SO_4	Sulfuric acid
HCA	Hydroxycinnamic acid
HCl	Hydrochloric acid
HDAC	Histone deacetylase
HEMA	2-Hydroxyethyl methacrylate
HPLC	High performance liquid chromatography
ITC	Isothermal titration calorimetry
IUPAC	International Union of Pure and Applied Chemistry
LC	Liquid chromatography
LD	Minimum lethal dose
MAA	Methacrylic acid
MeOH	Methanol
MIP	Molecularly imprinted polymer
MISPE	Molecularly imprinted solid-phase extraction
MRM	Multiple reaction monitoring
MS	Mass spectrometry
N_2	Nitrogen gas

© University of Venda

NaOH	Sodium hydroxide
NIP	Non-imprinted polymer
NIPs	Non-imprinted polymers
NMR	Nuclear magnetic resonance
NSAID	Non-steroidal anti-inflammatory drug
O	Oxygen
OMWW	Olive will wastewater
p-4HCA	Para 4-hydroxycinnamic acid
PAL	Phenylalanine ammonia-lyase
PCM	Paracetamol
PMMA	Polymethyl methacrylate
QCM	Quartz crystal microbalance
Rf	Retention factor
SAHPRA	South African Health Products Regulatory Authority
SD	Standard deviation
SEM	Scanning electron microscopy
SPE	Solid-phase extraction
SPME	Solid phase micro-extraction
SPR	Surface plasmon resonance
t-4HCA	*Trans*-4-hydroxycinnamic acid
TD	Time-dependent
TFMAA	Trifluoromethyl acrylic acid
TGA	Thermogravimetric analysis

© University of Venda

THF	Tetrahydrofuran
TLC	Thin layer chromatography
TMS	Tetramethylsilane
TSA	Transition state analogue
UV	Ultraviolet light
UVA	Ultraviolet A
UVB	Ultraviolet B
WHO	World Health Organization
XRD	X-ray diffraction

© University of Venda

University of Venda
Creating Future Leaders

List of figures

Figure 1: General structure of cinnamic acid, R_1, R_2, R_3 and R_4 are OCH_3/OH/H 9
Figure 2: Structures of cinnamic acid and its derivatives. 10
Figure 3: Cholesterol esters derivatives I and II. 12
Figure 4: The three-step molecular imprinting process. 25
Figure 5: Commonly used functional monomers in the non-covalent approach of MIP synthesis 27
Figure 6: Commonly used cross-linkers 30
Figure 7: Optimized structures of t-4MCA, PMC, 4-VP and MAA 55
Figure 8: Proposed reaction mechanism for the synthesis of the polymerization 57
Figure 9: Synthesis of t-4MCA polymers and respective NIPs 58
Figure 10: Template removal profile of t-4MCA MIPs.....60
Figure 11: Template removal profile of PCM MIPs 59
Figure 12: Standard calibration curve of t-4MCA 60
Figure 13: Leaching of t-4MCA and PCM from MIPs. 60
Figure 14: Adsorption capacity of nine polymers and respective NIPs in chloroform or acetonitrile. Conditions: polymer mass = 5 mg, water/methanol 50:50% v/v as the eluent (n = 3, RSD) 62
Figure 15: FT-IR spectra for t-4MCA-based MIPs.....65
Figure 16: FTIR spectra for PCM-based MIPs..... 64
Figure 17: TGA curves for t-4MCA MIPs.....67
Figure 18: Derivative curves t-4MCA MIPs..... 66
Figure 19: TGA curves for PCM MIPs.....68
Figure 20: Derivative curves PCM MIPs 67
Figure 21: BET N_2 adsorption/desorption profiles of..... 68
Figure 22: BET N2 adsorption/desorption profiles of MIP (t), MIP (w) and NIP for t-4MCA... 68
Figure 23: BJH pore size distribution t-4MCA MIP, PCM MIP and NIP..... 69
Figure 24: XRD reflection patterns of washed PCM MIP, t-4MCA MIP and NIP..... 71
Figure 25: SEM image of unwashed t-4MCA MIP (a) and washed t-4MCA MIP (b) 72
Figure 26: SEM image of unwashed PCM MIP (a) washed PCM MIP (b)..... 73

© University of Venda

University of Venda
Creating Future Leaders

Figure 27: EDS spectra of NIP (a), washed t-4MCA (b) and washed PCM (c) 74
Figure 28: Effect of rebinding solvent on adsorption capacity. Conditions: polymer mass 10 mg, pH5, 10 mg L^{-1} 77
Figure 29: Effect of polymer mass used on adsorption capacity. Conditions: polymer pH = 5.6, concentration = 10 mg L^{-1}, H_2O/methanol 5:5 v/v as the eluent (n = 3) 78
Figure 30: pHPZC for NIP, t-4MCA and PCM MIPs 80
Figure 31: Effect of solution pH on adsorption capacity. Conditions, polymer mass = 10 mg, concentration = 10mg L^{-1}, H_2O/methanol 5:5 v/v as the eluent (n = 3). 80
Figure 32: Time effects on adsorption capacity. Conditions: polymer mass = 10 mg, H_2O/methanol 5:5 v/v as the eluent, sample pH 7 and concentration = 10 mg L^{-1} (n = 3)..... 82
Figure 33: Effect of initial concentration on adsorption capacity. Conditions: polymer mass = 10 mg, H_2O/methanol 5:5 v/v as the eluent, pH 7, time = 60 min (n = 3)..... 83
Figure 34: Langmuir linear plot of t-MCA MIP, NIP and PCM MIP 85
Figure 35: Freundlich linear plot of t-MCA MIP, NIP and PCM MIP 86
Figure 36: Calibration curve of trans-4-methoxy cinnamic acid 89
Figure 37: Selectivity of t-4MCA MIP and NIP for t-4MCA and its structural analogs 90
Figure 38: HPLC chromatograms showing the photoisomerization of t-4MCA to c-4MCA over time. 94
Figure 39: Graphical representation of the adsorbed percentage of t-4MCA in three *cis/trans* isomeric ratio mixtures 96
Figure 40: 3 h HPLC chromatogram of t-4MCA with MIP, NIP, and the control 98
Figure 41: 12 h HPLC chromatogram of t-4MCA with MIP, NIP, and the control 99
Figure 42: Effect of NIP on t-4MCA photoisomerization kinetics 100
Figure 43: Effect of MIP on t-4MCA photoisomerization kinetics 100
Figure 44: TLC visualization of Wittig reaction progress of the synthesis of ethyl (E)-3-4(-methoxyphenyl) acrylate from 4-methoxy benzaldehyde..... 102
Figure 45: ^{1}H NMR spectrum (a) aromatic expansion (b) of Ethyl (E)-3-(4-methoxyphenyl) acrylate as synthesized according to scheme 1..... 103
Figure 46: ^{13}C NMR spectrum (a) DEPT-135 NMR spectrum (b) of ethyl (E)-3-(4-methoxyphenyl) acrylate as synthesized according to scheme 1..... 105

© University of Venda

Figure 47: FTIR spectrum of ethyl (E)-3-(4-methoxyphenyl) acrylate 106
Figure 48: ^{1}H NMR spectrum (a) aromatic expansion (b) of Ethyl (E)-3-(4-methoxyphenyl) acrylate as synthesized according to scheme 2. 108
Figure 49: Calibration curve Et-MOPA using HPLC 109
Figure 50: ^{1}H NMR spectrum (a) aromatic expansion (b Ethyl (E)-3-(4-methoxyphenyl) acrylate as synthesized according to scheme 3.....110

© University of Venda

List of tables

Table 1: Contra-indications of *cis/trans* drugs available in the market 21
Table 2: The chemical composition of the synthesized MIPs and NIPs 38
Table 3: ΔE of t-4MCA, PCM with 4-VP and MAA in five different solvents 56
Table 4: BET surface area analysis and porosity 70
Table 5: Swelling percentage of MIPs in different solvents 75
Table 6: Imprinting efficiency of t-4MCA 78
Table 7: Imprinting efficiency of t-4MCA 80
Table 8: Imprinting efficiency of T-4MCA and PCM MIPs 82
Table 9: Imprinting efficiency of t-4MCA and 84
Table 10: Langmuir and Freundlich isotherm parameters for t-4MCA adsorption..... 87
Table 11: Parameters for the method validation of five phenolic acids 88
Table 12: HPLC analysis of *trans* and *cis* isomers in control, ... 108

© University of Venda

List of schemes

Scheme 1: Synthesis of ethyl (E)-3-(4-methoxyphenyl) acrylate 102

Scheme 2: Synthesis of ethyl (E)-3-(4-methoxyphenyl) acrylate using NIPs as a catalyst 107

Scheme 3: Synthesis of ethyl (E)-3-(4-methoxyphenyl) acrylate using MIPs as the catalyst... 109

© University of Venda

University of Venda
Creating Future Leaders

Chapter 1

Introduction

This chapter establishes the critical importance of *cis/trans* isomer control in pharmaceuticals, particularly cinnamic acids. It presents a problem statement outlining current limitations, defines the research aim and objectives centred on Molecularly Imprinted Polymers (MIPs), and poses key research questions**.** The chapter concisely frames the need and direction of the study, positioning MIPs as a potential solution to isomeric separation and synthesis challenges.

© University of Venda

1. Introduction

1.1 Background

The widespread use of chiral pharmaceuticals, including both enantiomers and diastereomers (not excluding *cis/trans* isomers), is a trait that is now defining modern medicine (Ceramella et al., 2022; Coelho et al., 2021). The exact three-dimensional structure of drug molecules determines how they interact with biological targets, from vital cancer treatments like paclitaxel, a single enantiomer (Munjal et al., 2019; Ryang et al., 2019) to life-saving cardiovascular drugs like the β-blocker propranolol, which exists as a racemate (Jinfeng Liu et al., 2022; DH Madsen et al., 2024; Saad et al., 2022). But there is a significant problem with this important relationship between structure and activity, one stereoisomer may be therapeutically beneficial, but its counterpart may be inactive, weaker, or even harmfully toxic (Ayudhya et al., 2022; Han et al., 2019; Ikeda et al., 2020; Sokka et al., 2021; Tchekalarova et al., 2024). A clear historical reminder of this inherent risk is the thalidomide tragedy, in which one enantiomer resulted in severe birth defects (Grünherz et al., 2022; Khanal et al., 2022; Newbronner & Wadman, 2021). Historically, limitations in synthetic and separation technologies, coupled with an incomplete understanding of stereochemical effects, led to the development and use of many drugs as mixtures of stereoisomers (Dong et al., 2020; R Kumar et al., 2016; Olbrycht et al., 2021).

This legacy persists in influencing contemporary drug development. Despite considerable advancements in asymmetric synthesis (Maestro et al., 2024; Zhang, 2023), numerous critical reactions, such as the multifaceted Wittig olefination, a fundamental method for carbon-carbon double bond formation and an essential step in the synthesis of various pharmaceuticals and fine chemicals (Khan et al., 2024; Masuda et al., 2023; Muralikrishna et al., 2019) frequently produce mixtures of *cis/trans* isomers (Dong et al., 2020; Edgar et al., 2019; Shipman et al., 2019). Significant challenges arise for chemical families such as cinnamic acid derivatives, which demonstrate varied biological activity and serve as important precursors in drug discovery (Chandra et al., 2019; Drakontaeidi & Pontiki, 2024; Zolfaghari et al., 2020). Cinnamic acid and derivative compounds, distinguished by an alkene functionality, rapidly undergo *cis/trans* isomerization, resulting in isomers that may exhibit significantly distinct pharmacological characteristics (Dong et al., 2020). The *trans* isomer is frequently the major product, and attaining high *cis* ratio production and separation can be challenging (Chen et al., 2021), and isolating the isomers post-formation poses a significant obstacle (Fjæstad et al., 2022; Fumagalli et al., 2020; Lin et al., 2020). Furthermore, these separation challenges are not exclusive to pharmaceuticals; they also affect the analysis and purification of

© University of Venda

stereoisomeric compounds in environmental samples (e.g., pesticides and other pollutants) (Wang et al., 2021), industrial effluents (e.g., byproducts of chemical manufacturing) (Kotowska et al., 2021; Nuro et al., 2022; Rulence et al., 2023; Sant'Ana et al., 2024), and natural product extracts (e.g., isolating specific isomers from botanical sources) (Le et al., 2023; Salem et al., 2020).

Conventional techniques for separating stereoisomeric mixtures, predominantly utilizing chromatography (HPLC, GC, SFC), frequently exhibit inefficiency, necessitating considerable method development, expensive specialty columns, and substantial quantities of potentially hazardous organic solvents (Gai et al., 2023; Madsen et al., 2019; Olbrycht et al., 2021; Song et al., 2021; Tang et al., 2022). Solid-phase extraction (SPE) employing traditional sorbents (e.g., C18-silica, polymeric resins) typically exhibits insufficient stereoselectivity, especially regarding the nuanced structural distinctions between *cis* and *trans* isomers (Castillo-Aguirre et al., 2019; Martinenghi et al., 2020; Murcia-Morales et al., 2019). Although sophisticated materials such as metal organic frameworks (MOFs), covalent organic frameworks (COFs) and immunoaffinity sorbents exhibit potential, they frequently encounter challenges related to synthetic complexity, stability, or cost constraints (Maciel et al., 2020; Mancera-Arteu et al., 2023; Vrobel & Tarkowski, 2023). The ongoing challenge and rigorous regulatory demands from agencies such as the FDA, EMA, and SAHPRA, which require comprehensive characterization of individual stereoisomers and justification for mixtures, constitute a substantial impediment to pharmaceutical development (Ghanem et al., 2023; Lythgoe et al., 2022; Mpanza et al., 2022; Pham et al., 2023).

The study addresses this critical unmet need by introducing a novel approach based on molecularly imprinted polymers (MIPs). MIPs are synthetic polymers with tailored recognition sites, created through a "lock-and-key" template polymerization process, offering exceptional selectivity, robustness, and cost-effectiveness compared to traditional separation methods (Chen et al., 2019; Jayasinghe & Moreda-Piñeiro, 2021; Xingbin Ma et al., 2022). Uniquely, this work explores the application of MIPs for selective separation and stereo-directing catalysis. Presented here, for the first time, the use of a (t-4MCA)-imprinted MIP to directly influence the stereochemical outcome of the Wittig reaction, a key reaction in the synthesis of cinnamic acid derivatives and other alkene-containing compounds. Furthermore, it is demonstrated that the MIP has the ability to manipulate photoisomerization equilibria, selectively sequestering the *trans* isomer and enriching the solution in the *cis* form.

© University of Venda

This dual functionality, stereoselective catalysis and selective adsorption, positions MIPs as a powerful new tool for achieving high *cis/trans* isomeric purity sustainably and efficiently. By demonstrating the potential of MIPs to address this persistent challenge, this research contributes to the advancement of both pharmaceutical synthesis and green chemistry, paving the way for developing safer and more effective medications. The specific objectives of this research were to synthesize and characterize t-4MCA MIPs, optimize their binding properties, evaluate their selectivity, and, most importantly, demonstrate their novel application in controlling the stereochemistry of both Wittig reactions and photoisomerization processes.

1.2. Problem statement

The pharmaceutical and fine chemical sectors encounter a continual and significant challenge, the efficient and selective synthesis of molecules that display *cis/trans* isomerism. The challenge is based on the idea that geometric isomers, although having identical chemical formulas, can exhibit significantly diverse biological activities, affecting medication efficacy, safety, and overall performance. The existence of an undesirable *cis* or *trans* isomer can reduce therapeutic efficacy, cause adverse effects, or potentially make a molecule poisonous.

Numerous significant chemical reactions, such as the extensively used Wittig olefination to produce carbon-carbon double bonds, frequently produce mixtures of *cis* and *trans* isomers. Additional separation and purification are required, which are often the most inefficient, expensive, and environmentally detrimental stages in the total synthetic process. Conventional chromatographic separations, although adaptable, frequently encounter difficulties in distinguishing minor structural variations between *cis/trans* isomers, necessitating considerable amounts of organic solvents and producing enormous waste. The dependence on unsustainable processes is progressively at odds with the principles of green chemistry and the rigorous regulatory standards for single-isomer medicines.

Derivatives of cinnamic acid, a category of chemicals with extensive medicinal promise, illustrate this problem. These compounds, along with numerous others possessing alkene functions, are susceptible to *cis/trans* isomerization, and the resultant combinations frequently necessitate arduous purification. The inefficiency and lack of selectivity in acquiring the desired isomer is a major impediment in the advancement of novel pharmaceuticals and other valuable commodities. The constraint encompasses not only cinnamic acids but also a diverse array of molecules featuring carbon-carbon double bonds, affecting various domains of chemical synthesis. Therefore, a significant unmet need persists for breakthrough technology capable of

© University of Venda

tackling this fundamental difficulty in two primary manners. 1) by improving the stereoselectivity of reactions that yield *cis/trans* isomers, hence promoting the creation of the preferred isomer, and 2) by offering effective and eco-friendly techniques for the separation of *cis/trans* isomers from reaction mixtures. Meeting this requirement would enhance the efficiency of new pharmaceutical and fine chemical development while promoting a more sustainable and accountable chemical sector. The existing deficiency of effective, selective, and environmentally friendly methods for managing *cis/trans* isomerism constitutes a significant barrier to advancement in various domains. The study presents an innovative strategy that may serve as a remedy.

1.3. Aim of the study

To drive the t-4MCA photoirradiation and Wittig reactions by characteristic and synthetic approach of molecularly imprinted polymers (MIPs) to selectively favor one diastereomer over the other in a short period.

1.3.1. Broad objective of the study

- To synthesize t-4MCA based molecularly imprinted polymers (MIPs) for selective enhancement and purification of the *trans* isomer in a mixture by a photoisomerization reactions and Wittig.
- To explore the potential of MIPs to increase the yield of the *trans* isomer and streamline the product purification process of these reactions.

1.3.2 Specific objectives of the study

Part A: MIP synthesis and evaluation

- Synthesize MIPs using t-4MCA as templates and non-imprinted polymers (NIP).
- Synthesize dummy molecularly imprinted polymers (MIPs) utilizing paracetamol (PCM) as a template to examine its potential as a structural analog of t-4MCA.
- Eliminate residual template compounds from MIPs and NIPs through an appropriate washing protocol.

© University of Venda

- Characterize the morphology, thermal stability, functional groups, and surface area of (MIPs) and (NIPs) through scanning electron microscopy (SEM), thermogravimetric analysis (TGA), Fourier-*trans*form infrared spectroscopy (FTIR), and Brunauer-Emmett-Teller (BET) analysis.
- Conduct swelling studies of the polymers with rebinding solvent.
- Optimize MIP adsorption parameters (rebinding solvent, contact time, sample pH, polymer mass, initial concentration) experimental, determine the point of zero charge (pH_{PZC}).
- Evaluate MIP selectivity using structural analogs, ferulic acid, t-4MCA, t-4HCA and (Et-MOPA).

Part B: Photoirradiation reaction, Wittig reaction and MIP application

- Conduct photoirradiation reactions to induce *cis/trans* isomerization of t-4MCA.
- Study the stereoselective effects of molecularly imprinted polymers on the induced mixture.
- Investigate the isomeric ratio produced by the photoirradiation reaction when run in the presence of t-4MCA MIPs and NIPs.
- Synthesize Wittig ylide starting materials.
- Perform Wittig reactions for t-4MCA and Et-MOPA.
- Analyze the product mixtures to determine the ratios of formed isomers.
- Characterize Wittig reaction products using spectroscopic techniques (^{13}C-NMR, ^{1}H-NMR and HPLC).
- Repeat the Wittig reactions in the presence of synthesized MIPs.
- Characterize the resulting Wittig reaction products.
- Quantify isomer ratios to assess the influence of MIPs on the yield of the isomers.

1.3.3 Research questions

- Can t-4MCA-based MIPs be synthesized successfully?
- Does a double bond in t-4MCA impact the MIP synthesis process?
- Are the synthesized MIPs capable of selectively extracting *trans* isomers from mixtures containing *cis* and *trans* isomers?
- How specific are the MIPs towards their template compounds compared to their analogues?

© University of Venda

- Do the Wittig and photoirradiation reactions produce the expected *trans* and *cis* isomers, and in what proportions?
- Can the synthesized MIPs significantly enhance the proportion of the *trans* isomer in the final product?

© University of Venda

Chapter 2

Literature review

This chapter provides a detailed study of the importance of pharmaceutical drugs particularly cinnamic acids and its derivatives. It highlights the challenges associated with chiral or isomeric drugs, provides current ways or techniques used to resolve the challenges and introduces MIPs as the most appropriate sorbents to be used in resolving these challenges.

© University of Venda

2. Literature review

Part A

2.1 Importance of cinnamic acid and its derivatives

Phenolic acids, a significant subclass of polyphenols abundant in human diets, are categorized into benzoic acids (C6-C1) and Cinnamic Acids (CA) (C6-C3) (Kumar & Goel, 2019). These compounds share a benzene ring, carboxylic group, and varying hydroxyl/methoxyl groups, with cinnamic acids uniquely possessing an alkene group as in Figure 1 (Lima et al., 2016). Research into these compounds, particularly cinnamic acid and its derivatives, has been extensive, exploring their diverse pharmacological properties (Ruwizhi & Aderibigbe, 2020; Wang et al., 2021) and potential therapeutic applications (Malekipour et al., 2023; Vaisnav et al., 2023), making them attractive targets for extraction and purification.

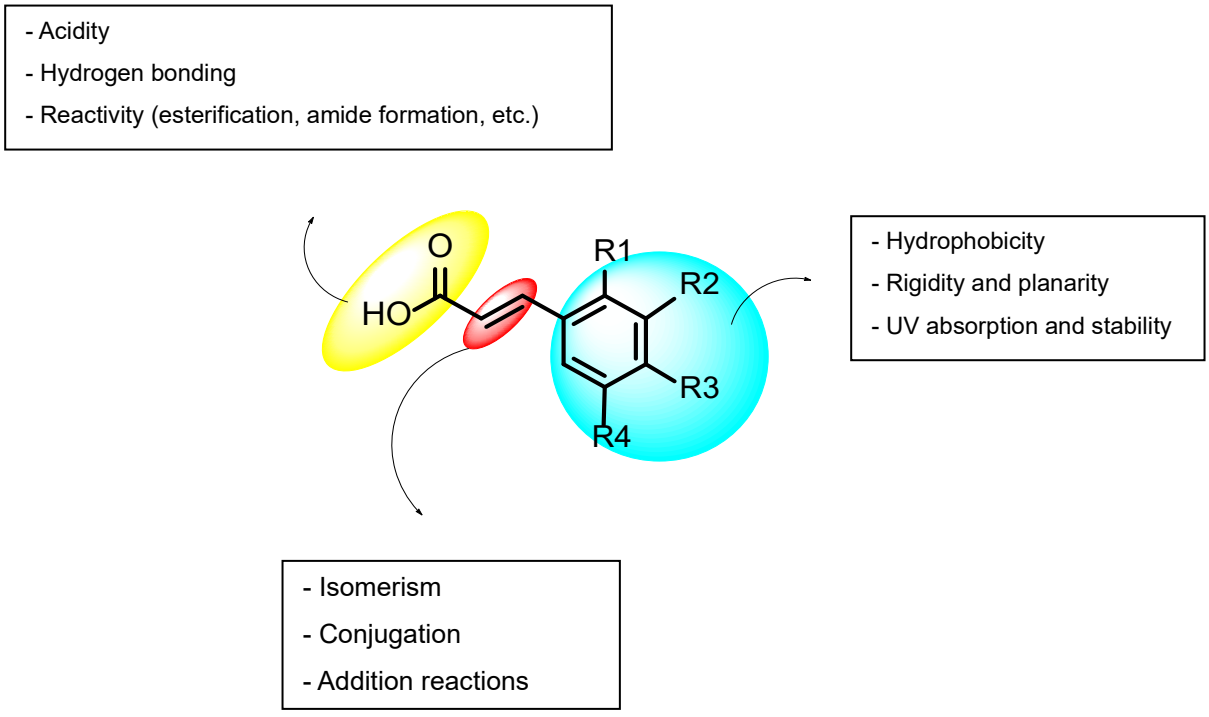


Figure 1: General structure of cinnamic acid, R_1, R_2, R_3 and R_4 are OCH_3/OH/H

Phenolic compounds are well-known antioxidants because of their high redox potential. They can act as reducing agents, scavengers of singlet oxygen, hydrogen donors, or metal ions chelators. CA, a naturally

© University of Venda

occurring phenylpropanoid, is a precursor to various specialized metabolites in plants, including flavonoids, lignins, and coumarins (Tsao, 2020). CA and its derivatives are essential components in plant biology, contributing to growth, development, and defense mechanisms (Nehela et al., 2023; Tani et al., 2019). Figure 2 below shows the structures of cinnamic acid **(1)** and its derivatives. They consist chiefly of p-coumaric acid **(2)**, ferulic acid **(3)**, caffeic **(4)**, sinapic acid **(5)** and methoxy cinnamic acid **(6)**.

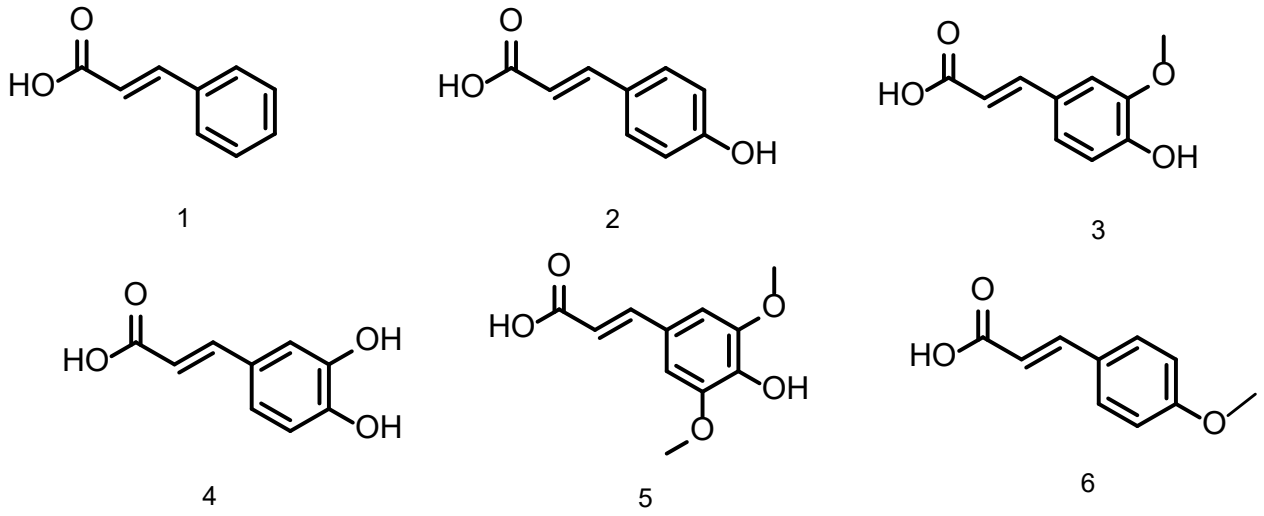


Figure 2: Structures of Cinnamic Acid (CA) and its derivatives.

2.1.1 Sources and abundance

CA and its derivatives are widely distributed in various plant species and plant-based products (Poonsri et al., 2019; Silva et al., 2019) One of the most abundant sources of cinnamic acid and its derivatives are cereal grains, particularly wheat, barley, and oats. These grains are rich in ferulic acid, with wheat bran being a particularly potent source (Schieber., 2018). Additionally, fruits and vegetables, for instance, apples, are a rich source of chlorogenic acid, while oranges are a good source of sinapic acid (Butkevičiūtė et al., 2020; Natić et al., 2024). Moreover, spices like cinnamon and cloves are rich sources of cinnamic acid and its derivatives. Caffeic acid, on the other hand, primarily comes from coffee in the human diet (Butt & Sultan, 2011). It is worth noting that trans-4-methoxy cinnamic acid is mostly found in coffee beans (Clifford., 2019), although it is also commonly found in medicinal plants such as Granny's Nightcap (*Aquilegia vulgaris L.)* (Bylka., 2004) and Buerger's Figwort (*Scrophularia buergeriana* Miq.) (Kim & Kim., 2000).

© University of Venda

2.1.2 Pharmacological activities

Research has demonstrated cinnamic acid's potential as an antioxidant, anti-inflammatory, and anticancer agent. The derivatives of cinnamic acid are also being investigated for therapeutic applications against various diseases, like diabetes and cardiovascular disorders (Anantharaju et al., 2017). Hadjipavlou-Litina & Pontiki, 2014 explored the induction of cancer cell death by cinnamic acid derivatives through Histone deacetylase (HDAC) inhibition. Additionally, the antioxidant properties of cinnamic acid and its potential health benefits have been emphasized by Barajas-Ramírez et al. (2022). Promkatkaew et al. (2023) discussed the host-guest interaction between 4-MCA and cyclodextrins, with the resulting complexes absorbing in both UVB and UVA regions, reinforcing 4-MCA's utility as a UV filter. The above investigations aim to unlock cinnamic acid's pharmaceutical potential and its derivatives, contributing significantly to drug discovery and therapeutic advancements.

2.1.3 Biosynthesis and structural diversity of cinnamic acid and its derivatives

The biosynthesis of cinnamic acid and its derivatives in plants involves multiple enzymatic pathways. The key pathway is the shikimate pathway, where the L-phenylalanine is deaminated by phenylalanine ammonia-lyase (PAL) to produce *trans*-cinnamic acid, a key precursor for a wide range of phenylpropanoids (Liu et al., 2024). Phenylpropanoid compounds include lignins, which provide structural integrity to plant cell walls, and various secondary metabolites like flavonoids, coumarins, and tannins (Kumar et al., 2016). The diversity of derivatives arises from modifications such as hydroxylation, methylation, and esterification, leading to compounds like ferulic acid and p-coumaric acid (Liu et al., 2024; Mutz et al., 2023). Phenylpropanoid derivatives can exist in both *cis* and *trans* isomeric forms, complicating their separation due to their structural similarities and the presence of conjugates with sugars, lipids, or other molecules (Wang et al., 2020).

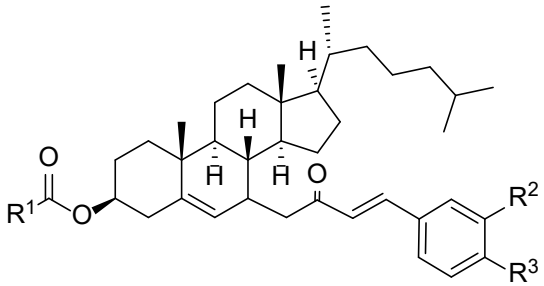
Numerous studies have emphasized this separation difficulty. For example, efforts to separate tetraalkynylbutatrienes' *cis* and *trans* isomers using high-performance liquid chromatography or gravity were unsuccessful (Auffrant et al., 2004). Evidence of the dynamic nature of isomeric transformations was demonstrated by an electrodynamic field ability to induce the *cis/trans* isomerisation of caffeoylquinic acids (Xie et al., 2011) making the separation of *cis/trans* isomers all that more difficult.

© University of Venda

2.1.4 Anthropogenic sources

Beyond their numerous beneficial effects and natural occurrences, they are increasingly observed in various environmental matrices due to human activities. Recent studies highlight their presence in environmental deposits, effluents of all kinds, including pesticides in agricultural runoff, and in both sewage (Wang et al., 2022) and industrial effluents (Speranza et al., 2020). The environmental persistence of these compounds, particularly the distinction between *cis* and *trans* isomers, raises concerns about their potential ecological and health impacts. They are now increasingly classified as emerging pollutants due to their widespread occurrence in the environment.

In reference to the above statement, derivatives of cinnamic, coumaric, caffeic, and ferulic acids are frequently found in olive mill wastewater, with concentrations ranging from 0.05-0.2 g/L to as high as 10 g/L, depending on factors such as the olive variety and the location of the mill (Stamatelatou et al., 2012). Research has shown that phenolic allelochemicals like cinnamic acid and its derivatives can significantly impact crop health and yield, causing substantial agricultural losses (Monisha et al., 2018). These compounds, known for their potent allelopathic effects, are released into the environment through various natural processes such as root exudation, leaching from plant tissues, and decomposition of plant material. (Lu et al., 2022) prepared new natural product-based pesticide candidates, a series of new cholesterol ester derivatives containing cinnamic acid-like fragments at the C-7 as observed in Figure 3.



I: R^1= Ph, R^2R^3=OCH_2O

II: R^1= Ph, R^2R^3=OCH_2O

Figure 3: Cholesterol esters derivatives I and II.

Gryko et al. (2021) studied the effects of natural cinnamic acid derivatives in wastewater and their findings suggested that caffeic acid, 4-hydroxycaffeic acid (4-HCA), 3,4-dihydroxycinnamic acid (3,4-dHCA) and 3,4,5-trihydroxycinnamic acid (3,4,5-tHCA) particularly under aerobic conditions, inhibited COD

© University of Venda

biodegradation. Resultantly, this negatively impacts key wastewater treatment processes like carbon degradation and nitrification. Furthermore, a varying degradation rate between the *cis* and *trans* isomers was observed (Gryko et al., 2021), implying that the *trans* isomers are less prone to degradation than *cis* isomers. The stability could potentially lead to a higher likelihood of bioaccumulation. Which has implications for water treatment technology and the need to develop methods specifically targeting the removal of these more persistent isomers.

The studies collectively underscore the necessity for continued research into the environmental behavior and impacts of these compounds, particularly focusing on isomer selective separation methods which stem from the distinct properties and effects resulting from their *cis* and *trans* geometrical isomers, where very little or no research has been done.

2.2 Challenges in cinnamic acid and derivatives production and separation

The production and separation of cinnamic acid isomers present significant challenges brought about by current natural and synthetic methodologies (Huang et al., 2021). Recent advancements have addressed these issues; however, as highlighted in a study by Baeza et al. (2016), the inherent complexities in achieving high-purity isomers hinder scalable production processes. Moreover, research by Durndell et al. (2019) and Zhang et al. (2020) underscores the efficiency constraints in traditional separation techniques, prompting the exploration of innovative approaches such as enzyme-assisted synthesis (Xie et al., 2024; Zhao, 2024) and molecularly imprinted polymers for improved selectivity and yield (Konzock et al., 2023; Riedel et al., 2023; Zhang et al., 2020). The studies emphasize the pressing need for continued development to overcome barriers in cinnamic acid production and separation.

© University of Venda

2.3 Techniques for stereoisomer separation

2.3.1 Chiral high-performance liquid chromatography

Chiral chromatography, especially High-Performance Liquid Chromatography (HPLC) with a chiral stationary phase (CSP), is a specific type of liquid chromatography intended for the separation of enantiomers, which are non-superimposable mirror copies. In contrast to traditional HPLC, which separates substances based on variations in physicochemical attributes like polarity, size, or charge, chiral HPLC operates on the idea of differential interaction between enantiomers and a CSP. It is fundamental to stereochemical analysis and purification. Chiral HPLC depends on the distinct interactions of stereoisomers with a chiral selector fixed on the chromatographic medium (Ao et al., 2022; Y Li et al., 2023; Zeng et al., 2024). Commonly utilized classes of CSPs include polysaccharide-based phases (e.g., cellulose and amylose derivatives) (Wang et al., 2022), cyclodextrin-based phases (Shi et al., 2021; Zeng et al., 2024), Pirkle-type phases, which employ small chiral molecules (Guarducci et al., 2024; Seog et al., 2023), and macrocyclic glycopeptide phases (Papp et al., 2019). The selection of CSP is contingent upon the distinct structures of the stereoisomers undergoing separation, and technique development frequently entails the evaluation of several columns and mobile phase compositions to attain optimal resolution (Hancu et al., 2022; Yan et al., 2022). Chiral HPLC, while exceptionally efficient for analytical separations, can be modified for preparative scale separations; however, this typically necessitates specialized and costlier instrumentation (Yuying Wang et al., 2019).

Chiral HPLC is also used to separate *cis/trans* isomers. Jurkovičová et al., (2024) synthesized two new chiral photosensitive mesogens derived from cinnamic acid. They used HPLC with a Daicel CHIRALPAK AD-3 column with silica gel particles coated with amylose tris(3,5-dimethylphenylcarbamate) as the chiral selector to assess the chiral purity of these compounds by separating their enantiomers. Importantly, they also optimized the conditions for enantioselective HPLC to achieve baseline separation for all studied materials and effectively separated the *cis* and *trans* isomers.

Cervantes-Díaz et al. (2024) successfully separated four diastereoisomers of a profoxydim, demonstrating the high resolving power of polysaccharide-based CSPs for complex mixtures of stereoisomers. The

© University of Venda

separation was achieved by the development and validation of a chiral HPLC method for the separation and determination of these stereoisomers in rice matrices. The separation was achieved using a Chiralcel OJ-3R column, a type of polysaccharide-based CSP where the chiral selector is cellulose tris(4-methylbenzoate). The optimization of the mobile phase composition was crucial to achieve adequate separation of all four isomers within a reasonable timeframe and with good peak shapes.

Seibert et al., (2025) investigated Ketamine, a general anesthetic, and its numerous derivatives that possess a single chiral center, thus existing as enantiomeric pairs. The researchers evaluated the performance of four distinct polysaccharide-based chiral stationary phases. Among these, a CSP designated as AMY-3, which is likely based on amylose, consistently exhibited the best separation capabilities for the tested compounds under normal phase conditions. It is noteworthy that this study achieved the first-time enantioseparation for some of the novel ketamine derivatives. Furthermore, the HPLC system was coupled with an optical rotation detector, enabling the determination of the elution order of the enantiomers, a critical step in the characterization of chiral compounds. The systematic screening of multiple CSPs underscores the importance of this approach in chiral method development to identify the most suitable stationary phase for a particular set of analytes.

2.3.2 Gas chromatography with chiral columns

Chiral gas chromatography (GC) is a highly selective analytical technique employed to determine the enantiomeric composition of volatile and semi-volatile samples. The technique utilizes chiral stationary phases (CSPs) within a GC column, enabling the separation of enantiomers based on their differential interactions with the chiral environment. For volatile compounds, chiral GC offers a complementary approach, utilizing chiral stationary phases within a GC column (Betzenbichler et al., 2022). While primarily used for enantiomeric separations, chiral GC can also effectively resolve *cis/trans* isomers in specific cases, particularly when the molecule is chiral. Cyclodextrin derivatives are frequently used as CSPs in chiral GC, A notable type of CSP employed in chiral GC is based on cyclodextrin derivatives, known for their ability to form complexes with chiral molecules, thus facilitating their separation. The inclusion of cyclodextrins can enhance chiral discrimination of target compounds, as demonstrated in relevant studies (Nessiem et al., 2024) enabling the separation of enantiomers and, in some cases, *cis/trans* isomers of volatile organic compounds.

© University of Venda

To facilitate analysis by GC, which requires analytes to be in the gaseous phase, cinnamic acid derivatives might need to be converted into more volatile and thermally stable derivatives. Common derivatization techniques for carboxylic acids include esterification (e.g., forming methyl esters) or silylation (e.g., forming trimethylsilyl esters). The choice of the derivative would depend on the specific functional groups in the chiral cinnamic acid derivative. Because chiral GC, in general, requires optimization of the analytical method and involves the use of specialized, potentially more expensive, chiral columns, achiral methods for the separation of *cis/trans* isomers have been predominantly employed.

The enantiomeric purity of amphetamine derivatives is important in pharmaceutical analysis and forensic toxicology. Hubner et al. (2024) used two cyclodextrin-based chiral GC columns to investigate the enantioseparation of trifluoro acetylated amphetamine derivatives, including novel psychoactive substances (NPS). The columns were Astec® CHIRALDEX™ G-PN and LIPODEX™ D, containing different cyclodextrin chiral selectors. A temperature gradient method (140°C to 200°C at 1°C/min) with GC-MS detection was used. The CHIRALDEX™ G-PN column achieved baseline separation for seven and partial separations for sixteen derivatives, while the LIPODEX™ D column provided six baseline and nine partial separations. The maximum operating temperature of the columns (200 - 220°C) was a limitation. The study highlighted the different selectivity of the columns for the amphetamine derivatives

Shi et al. (2021) identified specific CD stationary phases suitable for GC enantioseparation and optical purity determination of a subset of 2-bromopropionates, while highlighting limitations for cycloalkyl derivatives. They investigated the enantioseparation of various alkyl and cycloalkyl 2-bromopropionates using gas chromatography (GC) with seven different cyclodextrin (CD) derivatives as chiral stationary phases. Baseline enantioseparation (allowing for optical purity determination) was achieved for methyl, ethyl, 2-bromoethyl, and prop-2-yn-1-yl 2-bromopropionates on specific CDs (e.g., 2,3,6-tri-O-methyl-β-CD). Isopropyl, isobutyl, tert-butyl, and 3-methylbut-2-en-1-yl 2-bromopropionates showed only partial separation, unsuitable for purity analysis. Cycloalkyl 2-bromopropionates generally showed poor enantioseparation, with only partial separation for some and no separation for phenyl 2-bromopropionate.

© University of Venda

Chiral 2-arylcarboxylic acid esters are important intermediates in preparation of enantioenriched 2-arylpropionic acids type Non-steroidal anti-inflammatory drugs (NSAIDs). Shi et al. (2016) investigated the enantiomeric separation of 17 pairs of 2-arylcarboxylic acid ester enantiomers using capillary gas chromatography (CGC) with seven different β-cyclodextrin derivatives (CDs) as chiral stationary phases. The type of CD significantly impacted separation efficiency. For 2-phenylpropionates, CDs with both alkyl and acyl substituents (especially 2,6-di-O-pentyl-3-O-butyryl-β-cyclodextrin) were most effective. For 2-(4-substituted phenyl)propionates: 2,3,6-tri-O-methyl-β-cyclodextrin performed best. A key challenge identified is the potential for inaccuracies in indirect methods due to the derivatization step. Future directions must likely focus on the development of more versatile and robust chiral stationary phases for direct enantioseparation by GC which MIPs fit this criteria.

2.3.3 Super critical chromatography

Supercritical Fluid Chromatography (SFC), employing supercritical carbon dioxide as the mobile phase, represents a greener alternative to traditional HPLC and can also be coupled with chiral stationary phases for stereoisomer separations (Avigo et al., 2023; Zhao et al., 2019). SFC often provides faster separations and reduced solvent consumption compared to HPLC (Jurin et al., 2024).

Pandya et al. (2020) successfully separated four luliconazole stereoisomers (RZ(+), SZ(-), RE(+), and SE(-)) using SFC with a Chiralpak IH column based on amylose tris as the chiral selector. Separation of enantiomeric pairs was achieved within 5 minutes. CO_2:isopropanol (80:20, v/v) mobile phase provided optimal selectivity and resolution. The separation was primarily entropy-driven, with retention time increasing with temperature and decreasing with pressure.

Havnen et al. (2020) developed and validated a fast, robust method using supercritical fluid chromatography (specifically, ultra-high performance supercritical fluid chromatography, UHPSFC) coupled with tandem mass spectrometry (MS/MS) for separating and quantifying R/S-amphetamine enantiomers in human serum. UHPSFC-MS/MS with a Chiralpak AD-3 column was used. Supercritical CO_2 is utilized as the primary mobile phase component. Supercritical CO_2 and 0.1% ammonium hydroxide in 2-propanol/methanol (50/50, v/v) was used as a modifier. Successfully applied to analyze patient serum

© University of Venda

samples, distinguishing between R- and S-amphetamine intake. The method provides a rapid, sensitive, and reliable tool for enantiomeric amphetamine analysis in serum, crucial for forensic toxicology and therapeutic drug monitoring (differentiating legal/illicit use). The use of supercritical fluid chromatography offers advantages in speed and efficiency, further enhanced by the semi-automated sample preparation.

Segawa et al. (2018) developed a supercritical fluid chromatography-tandem mass spectrometry (SFC-MS/MS) method for the simultaneous chiral analysis of methamphetamine (MA) and its precursors (e.g., ephedrine and pseudoephedrine). The SFC-MS/MS method used was utilizing a polysaccharide-based chiral stationary phase. The method allowed determination of synthetic routes and origins of seized methamphetamine samples by analyzing stereoisomeric ratios of both the drug and its precursors. The method showcases SFC-MS/MS's utility in forensic drug profiling. The simultaneous chiral analysis of both methamphetamine and its precursors provides crucial information for tracing the source and manufacturing methods of seized samples, enhancing forensic investigations.

Lipka et al. (2023) investigated the chiral separation of salmeterol xinafoate and salmeterol base isomers using SFC in both analytical and preparative settings using a Chiralpak IG column. The optimal conditions (mobile phase, temperature, pressure) for salmeterol base enantiomer separation were, CO_2 modified with 0.2% triethylamine in methanol. The examined salmeterol xinafoate behaviour suggested scalability. The research demonstrated SFC's versatility for chiral separation of salmeterol (a β2-adrenergic receptor agonist for asthma treatment). The study covered analytical (quality control) and preparative aspects, highlighting SFC's potential for producing enantiomerically pure pharmaceuticals.

(Berger & Berger, 2013) showcased the separation of *cis*- and *trans*-isomers of vitamin K1 using SFC with pure carbon dioxide as the mobile phase. The separation was achieved in approximately 6 minutes with a resolution of 3.4, which was reported to be significantly faster than existing HPLC methods and utilized more environmentally benign solvents. The early work underscores the feasibility of employing SFC for the separation of geometric isomers in pharmaceutical-related compounds.

© University of Venda

2.3.4 Solid phase extraction

Solid-phase extraction (SPE) is a widely used sample preparation technique in analytical chemistry, but conventional SPE sorbents, such as C18-silica or polymeric resins, lack the stereoselectivity required to separate enantiomers or *cis/trans* isomers (Bernhardt et al., 2022). These sorbents primarily rely on non-specific hydrophobic interactions, which are generally insufficient to distinguish between the subtle structural differences of stereoisomers (Hroboňová & Špačková, 2020). The inherent limitation of traditional SPE highlights the need for more specialized approaches, such as the use of molecularly imprinted polymers (MIPs) (Hroboňová & Špačková, 2020).

Part B

2.4 Stereoisomerism in drug development

Stereoisomers are molecules with identical molecular formulas but distinct three-dimensional arrangements of atoms, which significantly impacts their properties, particularly in pharmaceuticals (Chieffi et al., 2020a). Enantiomers, or optical isomers, are non-superimposable mirror images that often exhibit divergent biological activities due to chiral centers (Janicki et al., 2023), impacting pharmacokinetic profiles due to stereo-selective metabolic enzyme preferences (Chieffi et al., 2020b; Janicki et al., 2023), Diastereomers, including *cis/trans* isomers, which result from restricted rotation around double bonds or rings, also display differing physical and chemical characteristics (Grenet et al., 2021).

According to Camunas-Alberca et al. (2023), pharmaceutical isomers include stereoisomers of optical and geometrical isomerism (*cis/trans* configuration). *Cis/trans* isomerism is a type of stereoisomerism that is highly stable and reactive, thus posing difficulties with separating the isomers (Feng et al., 2022) and effectiveness and patient safety for pharmaceutical purposes (Wei et al., 2013). The significance of stereoselectivity in drug synthesis is acknowledged, as achieving control over stereoisomer production can enhance therapeutic efficacy and reduce adverse effects (Phillips & Pombeiro., 2023). Distinguishing between stereoisomers is particularly crucial in drug development, as these variations may influence protein-ligand interactions and bioavailability (Pan & Kong., 2024), Pre*cis*e characterization and quantification of stereoisomers necessitate sophisticated analytical techniques, with regulatory agencies

© University of Venda

mandating rigorous stereochemical analysis to ensure drug safety and efficacy. Robust synthetic methodologies, capable of producing single stereoisomers or desired isomeric ratios, are essential for consistent drug quality.

2.4.1 Effects of *cis/trans* isomerism in drug development

It is crucial to ensure that the *cis/trans* isomer drugs, which are included in the SAHPRA CPP (South African Health Products Regulatory Authority Critical Path Process) / Biowaiver, meet the necessary standards for effectiveness and safety (SAHPRA, 2024). *Cis/trans* isomer drugs can interact differently with enzymes in the body (Zhang et al., 2024). The difference in interaction is due to their distinct 3D structures influencing their pharmacokinetic activities, i.e., ((ADME) how they are absorbed, distributed, metabolized, and excreted) leading to differences in how well they work and their potential side effects (Xu et al., 2022). While some drugs may benefit from one isomer not being metabolized (Reddy & Dubey., 2023), removal of inactive isomers will reduce metabolic drug load, avoid *cis/trans* interconversion, and reduce unwanted drug interactions (Sokka et al., 2021).

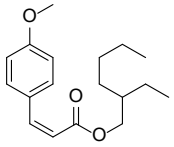
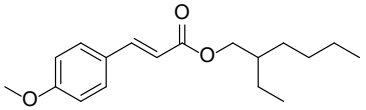
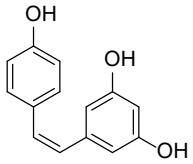
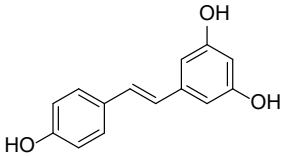
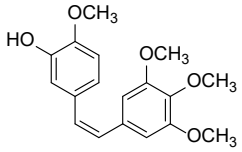
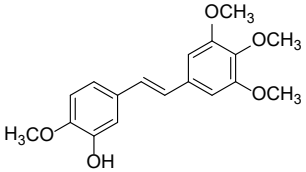
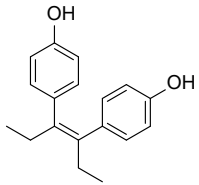
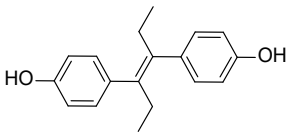
Research demonstrated that drug isomerism can have varying therapeutic effects and adverse toxicological effects (Leicach & Chludil., 2014). Miliovsky et al. (2015) found that *trans*-cinnamic acid was more effective at reducing inflammation in rats than *cis*-cinnamic acid. Intraperitoneal injections in a pleurisy model (an injection site and model used in animal studies) were used to demonstrate the aspect. Animal studies don't always predict human reactions (Tukker & Westerink., 2021), and some seemingly non-harmful compounds have shown harmful effects in humans (Pali-Schöll et al., 2017). The stated findings only emphasizes the need for careful testing and following safety guidelines when using these substances.

In *in-vitro* studies by Leischner et al. (2021) investigated resveratrol in human cancer cells with different p53 statuses, and they reported that the *trans*-resveratrol exhibited stronger antitumor activity compared to *cis*-resveratrol in most of the tested cancer cell lines. Table 1 lists some molecules with *cis/trans* isomers configuration that results in different biological activities.

© University of Venda

University of Venda
Creating Future Leaders

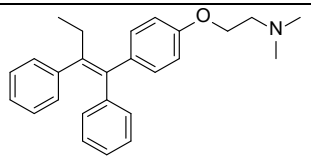
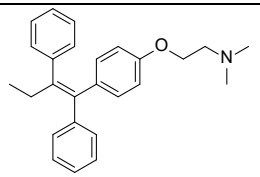
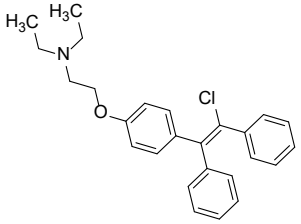
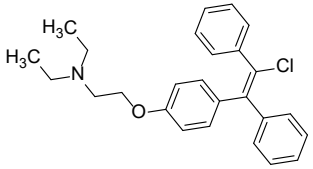
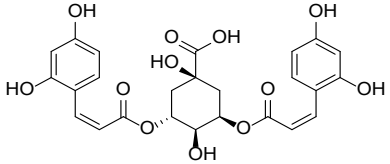
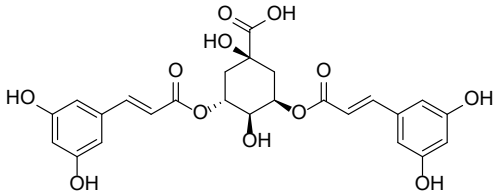
Table 1: Contra-indications of *cis/trans* drugs available in the market

Drug name	*Cis*-isomer structure and activity	*Trans*-isomer structure and activity	Reference
Octinoxate	 -Genotoxic effects on human liver cells. -Less photostable UV filters	 Less photostable UV filters	(Lorigo et al., 2024)
Resveratrol	 Low antitumor activity	 High antitumor activity	(Leischner et al., 2021)
Combretastatin A-4	 Cancer therapy	 Less active	(Gaspari et al., 2017)
Diethylstilbestrol	 Estrogenic activity	 Weak estrogenic	(Lorigo et al., 2024)

© University of Venda

University of Venda
Creating Future Leaders

Table 1: Contraindications of *cis/trans* drugs available in the market…….*Continued*

Drug name	*Cis*-isomer structure and activity	*Trans*-isomer structure and activity	Reference
Tamoxifen			(Shagufta et al., 2020) (Robertson et al., 1982)
	Antiestrogenic (breast cancer)	Estrogenic (uterine cancer)	
Clomiphene			(Gupta & Khanna, 2018; Saffati et al., 2024)
	Fertility treatment	Weak estrogenic activity	
3,5-Dicaffeoylquinic acid			(Zheng et al., 2017)
	Different binding affinity to HIV-integrase to the *trans*	Different binding affinity to HIV-integrase to the *cis*	

© University of Venda

2.4.2 The importance of early isomer separation in drug development

In pharmaceutical development, the historical practice of marketing drugs as *cis/trans* mixtures or racemic mixtures, which contain both enantiomers, has resulted in significant issues (Sokka et al., 2021; Urbańska, 2024). The approach, although convenient, neglects the essential principle that various isomers of a molecule can function as separate chemical entities in a biological system (Madaraboina et al., 2023; Urbańska, 2024). The neglect has led to cases where drugs were subsequently recalled or subjected to restrictions due to adverse effects linked to a particular isomer (Perry et al., 2019). The case of thalidomide, in which one chiral enantiomer, the (S)-enantiomer, was found to be teratogenic, meaning it caused birth defects, specifically phocomelia (shortened limbs) in children born to mothers who took the drug during pregnancy. Whilst the (R)-enantiomer was responsible for the sedative effects of the drug resulted in significant birth defects, serves as a critical lesson in the pharmaceutical sector (Willey & Calip, 2019; Yu, 2023).

Recent studies have demonstrated that the selective separation of isomers can improve therapeutic efficacy and reduce the risk of adverse effects linked to other isomer forms (Niaei et al., 2024; Vadagam et al., 2023). The economic and safety implications of developing single-isomer drugs illustrate a broader trend towards pre*cis*ion medicine, with tailored therapeutic solutions increasingly sought by healthcare providers and patients (Petrusová et al., 2021). The emphasis on isomer purity resonates with regulatory requirements that demand comprehensive characterization and validation of drug products, underscoring the critical importance of targeted isomer development for pharmaceutical innovation (M Liu et al., 2023). The trend indicates a significant transition towards personalized therapy, potentially addressing public health issues related to drug safety and improving overall treatment outcomes (B Zheng et al., 2022).

The use of isomeric drugs as individual entities is likely more advantageous than their use in combination. Consequently, the development of single-isomer variants of *cis/trans* drugs represents a significant research focus, particularly in the context of chiral switching for chiral pharmaceuticals. Resultantly, this guarantees the presence of the correct isomeric form in suitable proportions while adhering to established purity standards. The synthesis of complex molecules, including cinnamic acid derivatives and their hybrids, presents further challenges, as in the following examples.

© University of Venda

Treatment with the anti-rheumatic drugs gold thioglucose and aurothiomalate, which are a mixture of *cis*- and *trans*-isomers of aurothioglucose, causes the side effect aurothioglucose retinopathy (eye problem) in humans (Eisler., 2003; Gunatilleke & Barrios, 2008).

Hydroxyphenyl stilbenes E- and Z-piceatannol and the hydroxyphenyl stilbene polydatin structures similar to cinnamic acids have minimum lethal doses in mice of (343.33 mg/kg body weight) and (476.19 mg/kg body weight) respectively, which differs to resveratrol ((E)-5-(4-hydroxystyryl)benzene-1,3-diol) with an LD10 of 2000 mg/kg body weight mice and LD50 of 3000 mg/kg body weight rats. These differences are very important from a regulatory point of view and cannot be ignored. Therefore, cinnamic acid *cis/trans* isomers and their derivatives have to be controlled and tested according to the World Health Organization (WHO) guidelines.

The *cis* and *trans* isomers of flupentixol exemplify the need for stereoselective therapeutic drug monitoring. Research indicates that these isomers display unique pharmacokinetic profiles, influencing their absorption, distribution, metabolism, and excretion. Early consideration of these differences facilitates the development of tailored dosing regimens, thereby maximizing therapeutic benefits and minimizing adverse effects (Baumann et al., 2012).

These compounds demonstrate diverse biological activities, including anticancer, antidiabetic, antimicrobial, hepatoprotective, and neuroprotective effects, positioning them as promising drug candidates. For example, *p*-MCA has shown enhanced *in vitro* antiplasmodial activity. However, common synthetic reactions, like olefinations used to link cinnamic acids, often produce mixtures of geometrical isomers. This necessitates the development and implementation of stereoselective synthesis

© University of Venda

2.5 Molecular imprinting technology

Molecularly imprinted polymers (MIPs) are a class of synthetic polymers that are designed to have highly specific recognition capabilities towards a target molecule or an analyte, the selectivity is a result of the introduction of specific functional groups between the target analyte and the complementary binding sites within the MIP by the imprinting technology process (Hu et al., 2023; Zhan et al., 2019). The process in three steps involve the formation of a stable template-monomer complex were an appropriate functional monomer forms a complex with the template through various non-covalent bonding interactions (Hydrogen, electrostatic, van der Waals etc) in a suitable solvent (Cabaleiro-Lago et al., 2023; Jiang et al., 2022). The complex is then polymerised in place by an appropriate crosslinking agent to form a polymer, this is guided by the functional groups that are present around the complex. When the template is removed, the MIP can selectively and efficiently rebind the template through chemical functionality, size and shape (Bagheri et al., 2019; Barsbay & Mehrnia, 2020). Figure 4 illustrates the molecular imprinting process with the template extraction and recognition of the analyte.

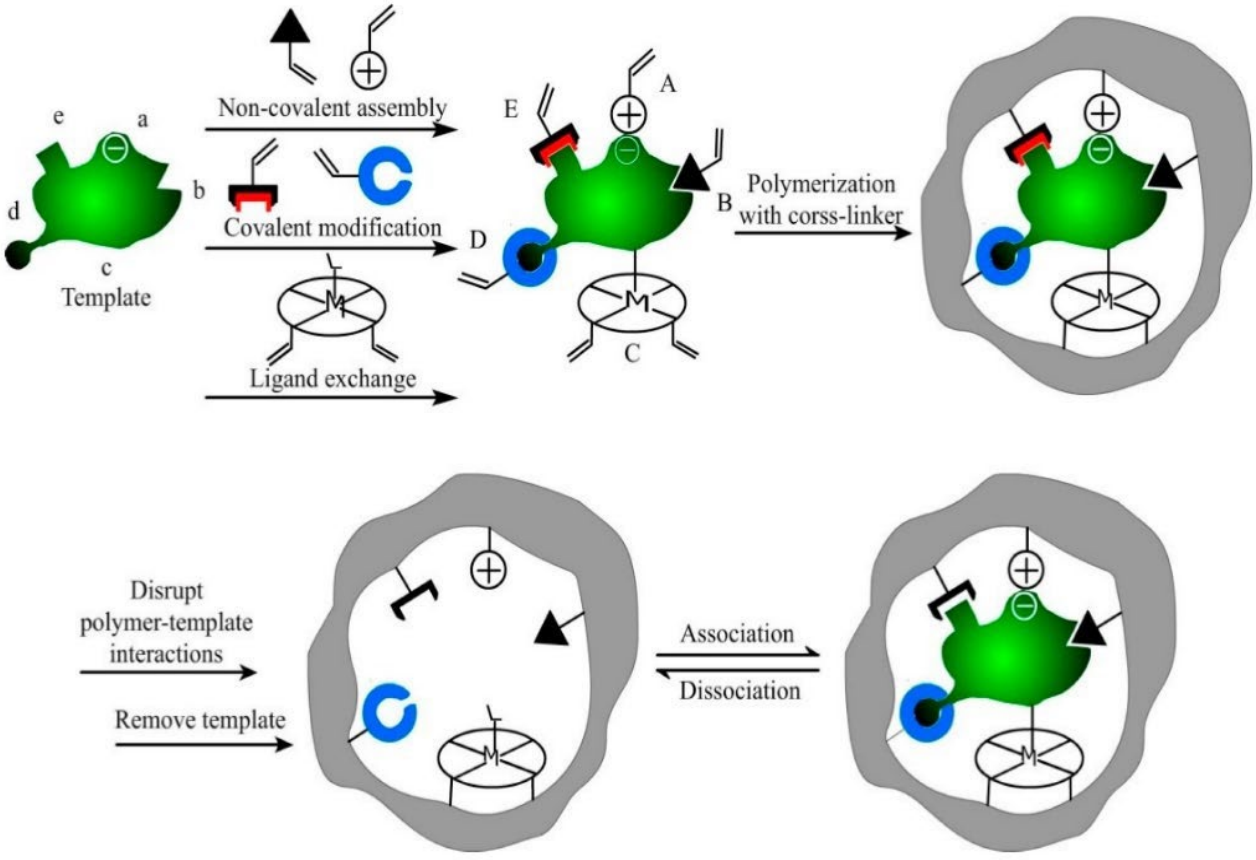


Figure 4: The three-step molecular imprinting process.

© University of Venda

The process not only enhances the selectivity of the MIPs but also allows for the development of materials that can mimic biological recognition systems such as antibodies (Lafuente Gonzalez et al.,2023; Batista et al., 2022). MIPs have been successfully utilized in various applications, including solid-phase extraction, sensor development, and environmental monitoring, demonstrating their versatility and effectiveness in selectively capturing target molecules from complex mixtures (Sharifi et al., 2023; Zare et al., 2022; Sijam et al., 2021; Zuo et al., 2022). Recent advancements in MIP technology have focused on improving their performance through innovative synthesis methods and the incorporation of functionalized materials. For instance, the use of magnetic nanoparticles in conjunction with MIPs has enhanced their applicability in solid-phase extraction and sensor applications, allowing for easier separation and recovery of the target analytes (Lafuente-González et al., 2023; He et al., 2023; Gallegos-Tabanico et al., 2022). Furthermore, the integration of computational approaches in MIP design has facilitated the optimization of their binding properties, leading to enhanced analytical performance (Suryana et al., 2021; Zuo et al., 2022). Overall, the development of MIPs continues to evolve, with ongoing research aimed at expanding their functionality and application across various fields, including biomedicine, environmental science, and food safety (Li et al., 2022; Gao et al., 2020).

2.5.1 Pre-polymerization reagents

2.5.1.1 Template

The selection of appropriate template molecules is a crucial step in the synthesis of highly selective MIPs. Various types of template molecules have been explored, including drugs, hormones, proteins, pesticides and other small organic compounds (Amarh et al., 2024; Gkika et al., 2024; Koesdjojo et al., 2007). Template molecules should be chemically inert and stable during free radical polymerisation, but some tend to be unstable, expensive or difficult to remove from the polymer matrix. New trends are emerging in template molecule selection and design. Researchers are exploring the use of "dummy templates" that are structurally similar to the target molecule but easier to obtain or remove from the polymer matrix (Danylec et al., 2015; Yoshimi et al., 2023).

Alkene-based templates, although primarily offer pi(π)-bonds for interaction with functional monomers, may limit the types of interactions and the selectivity of the resulting MIP, or they might not. The double bond can potentially interfere with the polymerisation process, leading to unwanted side reactions or affecting the

© University of Venda

polymer structure. In these instances, the “dummy template” approach might be particularly valuable because of the potentially unstable nature of these templates (Sellergren, 2000).

The use of cinnamic acids and their derivatives as template molecules has also been explored (Fathi et al., 2020; Joke Chow & Bhawani, 2016; Til et al., 2020). These compounds possess alternative desirable structural properties that can effectively be imprinted into the polymer matrix when the alkene bond is stable (Koesdjojo et al., 2007).

2.5.1.2. Functional monomer

The choice of functional monomer is a crucial factor in the successful synthesis of polymers, as it dictates the strength and stability of the monomer-template complex formation, which in turn affects the selectivity and binding affinity of the final imprinted material (Gkika et al., 2024; Hasanah et al., 2021; Mwanza et al., 2024). Figure 1 indicates some typical functional monomers, but three types are most commonly used. Type I is acidic-like MAA and AA, Type II are alkaline based such as the pyridines and Type III have neutral pH such as styrene (Gkika et al., 2024).

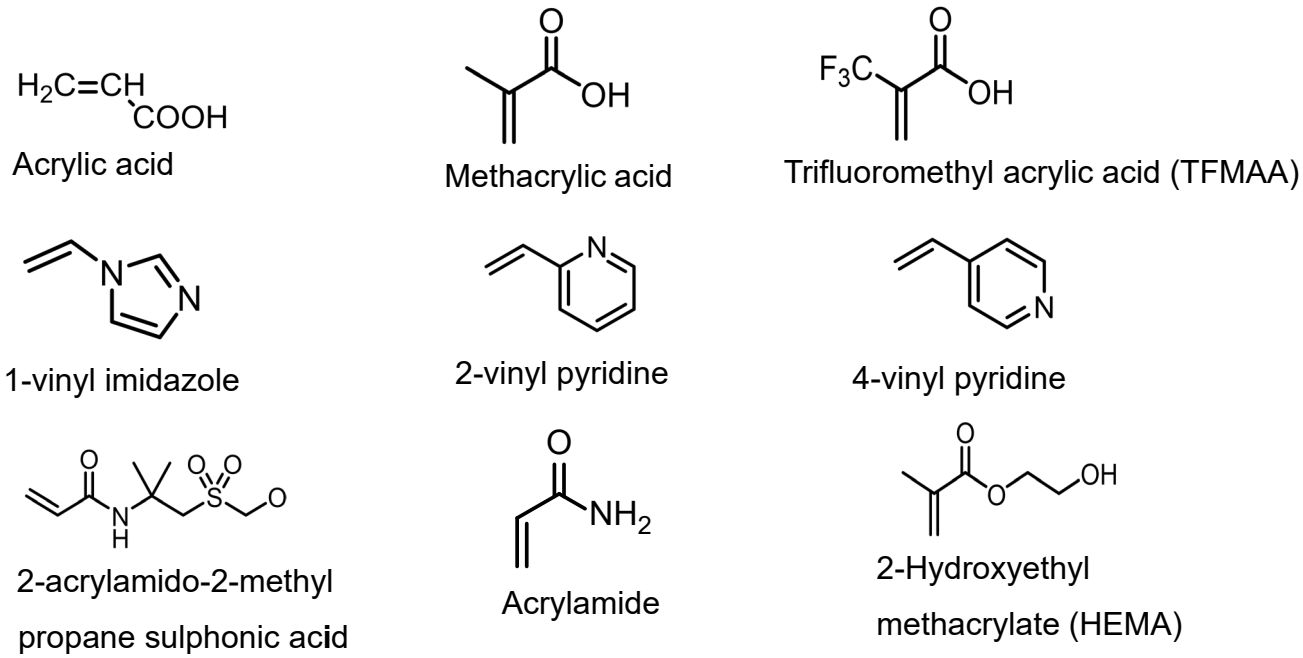


Figure 5: Commonly used functional monomers in the non-covalent approach of MIP synthesis

© University of Venda

The interaction between the functional monomer and the template molecule is typically non-covalent, such as hydrogen bonding, ionic interactions, or hydrophobic interactions. Molecular modelling and docking studies can be employed to determine the optimal functional monomer-template ratio by evaluating the binding energy of the pre-polymerization complex (Z Liu et al., 2021; Suryana et al., 2021). The approach allows for selecting the most suitable functional monomer and the appropriate stoichiometric ratio, essential for ensuring stable, high-affinity binding cavities within the imprinted polymer. Additionally, the excess of the monomer to template ratio during the polymerization process can significantly impact the selectivity of the imprinted polymer, as it can influence the distribution and accessibility of the imprinted binding sites. The effect of monomer amount on MIP was studied by (Thach et al., 2021). The research proved that the adsorption performance of a MIP would reach its highest point at a certain monomer concentration, and increasing the concentration after reaching the optimum point caused a decreased adsorption capacity (Thach et al., 2021).

Various other strategies have been explored to improve the molecular imprinting polymers specificity, including using multi-functional monomers (Niu et al., 2024), UV-VIS (Hasanah et al., 2019), FTIR (L Xie et al., 2020), and NMR (Quaglia et al., 2001) have been some of the other methods used but recent strategies include Isothermal Titration Calorimetry (ITC) (Decompte et al., 2020), Quartz Crystal Microbalance (QCM) (Tiwari & Pattanayek, 2024) and Surface Plasmon Resonance (SPR) (Maria et al., 2024). which can enhance the stability and selectivity of the resulting MIPs. Common functional monomers for cinnamic acid and its derivatives include methacrylic acid (MAA) and acrylic acid (AA). The monomers are chosen due to their ability to form hydrogen bonds with the carboxyl group present.

© University of Venda

2.5.1.3 Cross-linker

Cross-linkers are vital elements in polymer synthesis, significantly influencing the shape and stability of the resultant materials. In addition to their structural function, cross-linkers play a crucial role in stabilizing the imprinted binding sites, thereby preserving their structural integrity and enhancing the selectivity and affinity of the MIP for the target molecule (Liu et al., 2022). The cross-linker comprises up to 90 mol% of the polymerization mixture in conventional MIP procedures (Aminnezhad et al., 2024). In nanoMIPs, which are molecularly imprinted polymers with nanoscale dimensions generated via solid-phase polymerization, the cross-linker is often present in a significantly lower concentration, generally around 2 mol%.

The ratio of cross-linker to functional monomer is a critical parameter in controlling the morphology and binding characteristics of MIPs. In traditional MIPs and nanoMIPs (Jin Liu et al., 2022), a high cross-linker ratio 10–20 mol% generally leads to a more rigid and porous polymer structure with enhanced binding capacity and rigidity that prevents polymer chain entanglement and agglomeration during synthesis (Z Zhang et al., 2023). A study by Li et al. (2022) demonstrated that a high cross-linker ratio resulted in a more rigid and porous polymer structure with enhanced binding capacity for bisphenol (Liu et al., 2022). On the other hand, excessively high cross-linking >20 mol% can also hinder MIP performance (Jin Liu et al., 2022; Mukasa et al., 2023). While it enhances structural stability, it can reduce binding affinity by making the polymer too rigid for the binding sites to rearrange around the target molecule (Mukasa et al., 2023). Strong covalent interactions resulting from high cross-linking can also lead to slow binding and re-binding kinetics and make it difficult to remove the template from the polymer matrix (Adeleke et al., 2024). Therefore, a careful balance is necessary to achieve optimal cross-linking density for desired MIP performance.

The choice of cross-linker can affect the intermolecular forces and interactions within the complex, ultimately influencing the final structure and performance of the MIP (Hasanah et al., 2021; Zuo et al., 2022). Cross-linking can *trans*form the properties of polymers, making them more suitable for various applications. For instance, cross-linking polymethyl methacrylate (PMMA) improves heat performance, mechanical strength, chemical resistance, and abrasion resistance (Goff et al., 2020). Figure 6 presents some commonly used cross-linkers.

© University of Venda

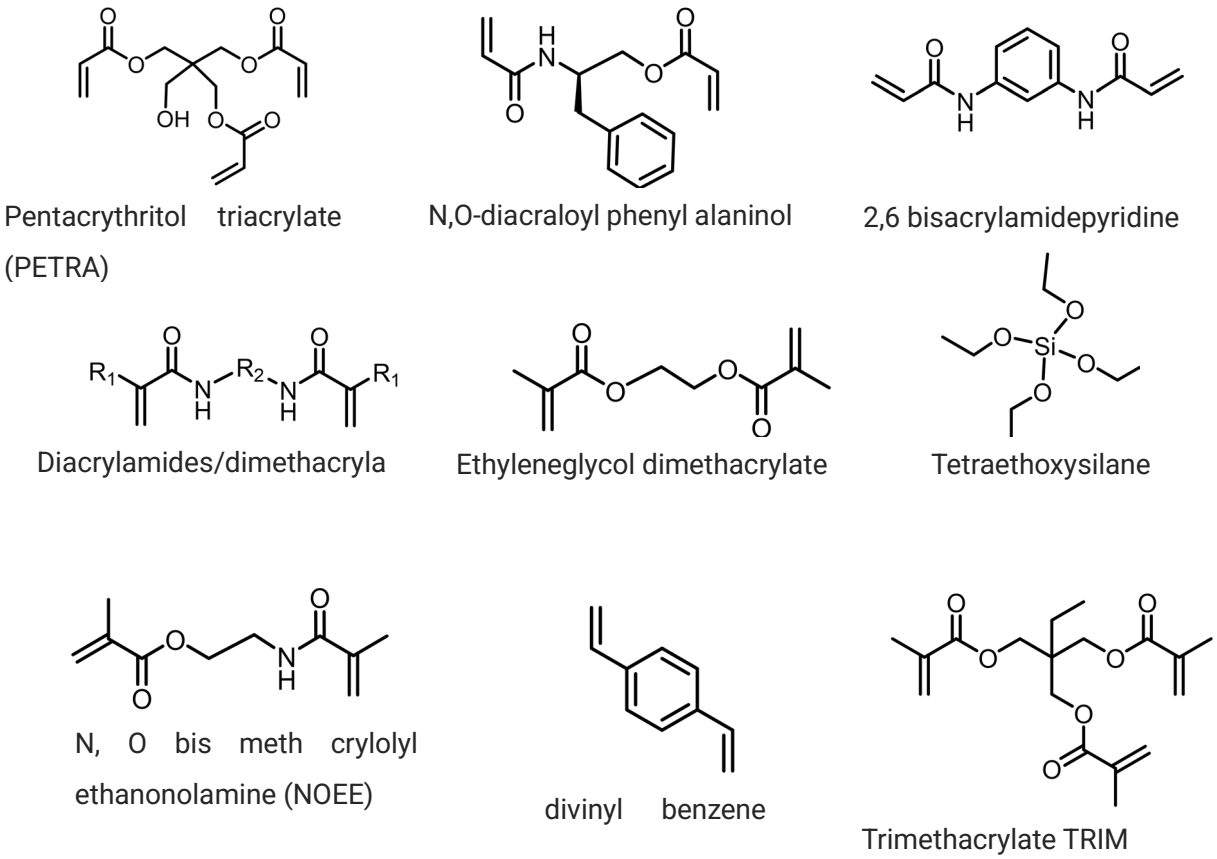


Figure 6: Commonly used cross-linkers

EDGMA, while known to be more hydrophobic than, say, BIS (N, N'-Methylenebisacrylamide, commonly used in hydrogels), the presence of the ether linkages (-O-) in its structure introduces some degree of hydrophilicity. This allows for better interaction with and recognition of pharmaceutical templates with this mixed character.

Swelling tests are commonly used to measure the degree of cross-linking in a polymer (Mrówka et al., 2020). The cross-linked sample is placed into a good solvent at a specific temperature. The change in mass or volume of the sample is then measured. The more cross-linking present in the polymer, the less swelling will occur, this is because the cross-links restrict the movement of the polymer chains and prevent them from absorbing as much solvent.

© University of Venda

University of Venda
Creating Future Leaders

Chapter 3

Materials and Methods

This chapter details the chemicals, instrumentation, and methodologies utilized in the synthesis of molecularly imprinted polymers (MIPs) and organic compounds. Optimization experiments and characterization processes for the synthesized products are also described.

© University of Venda

The research plan is outlined as follows

Method Development

Specification of chemicals, solutions, equipment, and instrumentation employed throughout method development.

Part 1

- Synthesis of MIPs using E-4-methoxy cinnamic acid (t-4MCA) and corresponding NIPs, Synthesis of analogues of the template molecule.
- Preparing dummy MIPs using paracetamol (PCM) as the template and corresponding NIPs.
- Wash protocols: Washing the t-4MCA MIPs, PCM MIPs and NIPs.
- Characterization of all polymers, including swelling studies.
- Optimize adsorption parameters: Rebinding solvent, polymer mass, sample pH (point of zero charge), contact time (kinetic modelling) and initial concentration (adsorption modelling).
- Assessment of the ability of t-4MCA MIPs and NIPs to selectively extract t-4MCA from a binary mixture with each analogue.

Part 2

- Perform Photoirradiation studies on t-4MCA to obtain both the product ratio and the time when a stable mixture of *cis*-4methoxy cinnamic acid (c-4MCA) and t-4MCA are produced.
- Investigation of extraction efficiency of t-4MCA MIPs, PCM MIPs and NIPs in a mixture of c-4MCA and t-4MCA produced in three different isomer concentration ratios.
- Conduct photoirradiation experiments in the presence of the polymers to study the stereoselective effect of polymers on the ratios of the isomers.
- Synthesis of the Wittig reagent, then synthesize Et-MOPA using the Wittig reaction. The synthesis and product will serve as a baseline for comparison with further reactions with MIPs as catalysts. The same synthesis outcome was used to analyse the t-4MCA catalyzed reaction.
- Investigation of total isomeric ratios produced by the Wittig reaction of Et-MOPA and t-4MCA in the presence of MIPS.

© University of Venda

3.1 Chemicals and reagents

The following chemicals were utilized in this research. For the synthesis and washing of MIPs, ethylene glycol dimethacrylate (98%), methacrylic acid (≥ 99%) and 1,1'-azobis (cyclohexanecarbonitrile) (98%) were sourced from Sigma-Aldrich (Darmstadt, Germany). Paracetamol synthesis employed p-nitrophenol (≥ 99%), acetic anhydride (≥ 99.5%) and sodium borohydride (≥ 99%) from Sigma-Aldrich (Darmstadt, Germany). Synthesis of (E)-Para-methoxy cinnamic acid involved commercially available (E)-para-methoxy cinnamic acid (≥ 98%), para-anisaldehyde (≥ 98%) form (Fluka, South Africa), triphenylphosphine (99%) and ethyl bromoacetate (98%) were purchased from Sigma-Aldrich (Darmstadt, Germany). Various solvents (acetonitrile, methanol, ethanol, dichloromethane, ethyl acetate, hexane) and other reagents (potassium hydroxide, potassium chloride, hydrochloric acid, glacial acetic acid, sodium hydroxide, sodium chloride, magnesium sulfate) were obtained from (Merck, South Africa) and Rochelle Chemicals (Johannesburg, South Africa). All LC-MS solvents ultrapure water, methanol and acetonitrile were obtained from Stargate SA (Johannesburg, South Africa).

All chemicals were utilized as received without further purification unless otherwise specified. Solutions were prepared using deionized (DI) water obtained from a Purite Analyst Fusion 160/320 distillation system (Lasec, South Africa). The system utilizes carbon pre-treatment, reverse osmosis, and deionization. Stock solutions (500 mg/L) of paracetamol and 4-methoxycinnamic acid were prepared by dissolving the appropriate amounts in 10 mL of methanol. These stock solutions were stored in a cool, dark location when not in use. Fresh working solutions were prepared daily by diluting the stock solutions.

3.2 Equipment and instruments

pH measurements measurements were performed with an edge® Multiparameter pH Meter - HI2020 equipped with a HI11310 digital glass body pH electrode with a 3.5 mm connector and 1 m cable, all from (Hanna Instruments, South Africa)

Reaction progress was monitored using thin-layer chromatography (TLC) on silica gel 60 F254 plates acquired from Merck (Johannesburg, South Africa). The mobile phase consisted of ethyl acetate and

© University of Venda

petroleum ether in a 50:50 (v/v) ratio. Flash column chromatography was used to purify most crude reaction products, employing a mobile phase gradient ranging from 10:90 to 30:70 (v/v) ethyl acetate: petroleum ether. The remaining products were purified by recrystallization from methanol.

Fourier-transform infrared (FTIR) spectroscopy, a highly sensitive technique was employed to investigate the local environment within the synthesized polymer materials. The technique provides an infrared absorption spectrum of the sample, offering simultaneous collection of high-resolution data across a broad spectral range. The resulting spectra allowed for the identification of changes in the vibrational modes and bond types associated with the functional groups of the polymer. The information is crucial for differentiating between template-inserted and template-extracted MIPs, as well as non-imprinted polymers (NIPs). A Bruker Alpha FTIR spectrometer (Alpha Platinum ATR Diamond) from Bruker Optics South Africa was utilized for the characterization of the synthesized samples' bond structures. The analysis covered a frequency range of 400-4000 cm^{-1}. The instrumental parameters included a resolution of 4 cm^{-1}, 24 scans for both sample and background measurements, and a sample temperature of 20 °C. All samples were analyzed in their solid state.

UV-Vis absorption spectral data were collected using a photoLab® 7600 UV-VIS spectrophotometer from Xylem (Johanessburg, South Africa). The instrument features OptRF technology for reagent-free measurements, a wavelength range of 190 - 1100 nm, a grating monochromator with step motor/reference beam, a Xenon flash lamp, and a spectral bandwidth of 4 nm.

Thermogravimetric analysis (TGA) was performed to monitor the mass of synthesized MIP samples as a function of temperature and time. A TGA Q500 V20.13 was utilized for this analysis. Experiments were conducted under a high-purity nitrogen atmosphere with a flow rate of 40 mL/min and a heating rate of 20 °C/min across a temperature range of 0-1000 °C. TGA allows for the investigation of weight changes in the sample associated with dehydration or decomposition processes triggered by increasing temperatures. Approximately 0.05 g of each sample was used for the analysis.

A Scanning electron microscopy with integrated energy-dispersive X-ray spectroscopy (SEM-EDX) model JSM-7500F from (JEOL, Japan) was used to characterize the surface morphology and elemental composition of MIP particles before (unwashed) and after (washed) template extraction. In SEM, a focused electron beam (originating from a tungsten filament and accelerated at 10 kV) scans the sample surface. Interactions with the sample generate emitted electrons, which are collected by a detector and used to create images revealing

© University of Venda

the surface morphology. Simultaneously, the EDX module analyzes characteristic X-rays emitted from the sample, allowing for the determination of elemental composition. The combined analysis provides insights into potential morphological and compositional changes resulting from the template extraction process.

For the Brunauer Emmett Teller (BET) surface area analysis, a Tristar II 3020 version 3.2, serial number 215 was used to analyse the surface area, pore volume and pore size of the synthesised MIPs. Dry MIP samples with a minimum of 0.3 g were degassed at 100°C for a degassing duration of 4 h.

^{1}H and ^{13}C Nuclear Magnetic Resonance (NMR) spectroscopy is a technique used to analyze the structure and properties of organic compounds by observing the interaction of atomic nuclei with a magnetic field. In this analysis, a Bruker 400 MHz instrument from Bruker, (Massachusetts USA) was employed. The sample is placed in a strong magnetic field, causing the nuclei of certain atoms (like hydrogen-1 and carbon-13) to align themselves with the field. Radio frequency radiation is then applied, and when the frequency matches the resonance frequency of a specific nucleus, it absorbs energy and flips its orientation. As the nuclei relax back to their original state, they emit signals that are detected by the spectrometer. Tetramethylsilane (TMS) served as the internal reference (0.00 ppm), and spectra were obtained in either chloroform ($CDCl_3$) or dimethyl sulfoxide (DMSO) solvents.

3.3 LC-MS analysis

A Shimadzu 9030 LC instrument (Shimadzu, Japan) equipped with an autosampler, a thermostated column compartment, and a binary pump was used. Chromatographic separation utilized an Evosphere C18 column (100 × 2.1 mm, 1.7 µm particle size (Shimadzu) (Honeydew, South Africa) with a gradient elution of water (A) and methanol (B), each containing 0.1% formic acid, at a flow rate of 0.4 mL min^{-1}. The gradient is presented, 5% B was held for 1 min, increased to 95% B over 1 min, held at 95% B for 1 min, returned to 5% B in 1 min, and re-equilibrated at 5% B for 1.5 min

Detection via mass spectrometry was conducted utilizing a q-TOF high-resolution mass spectrometer equipped with an ESI source in positive ionization mode. The analyte was quantified using MRM *trans*itions of 179.070 – 161.059 and 179.070 – 133.064. Key MS parameters included an interface voltage of 4.0 kV, interface temperature of 300°C, nebulization and dry gas flow of 3 L min^{-1}, heat block temperature of 400°C,

© University of Venda

DL temperature of 280°C, detector voltage of 1.8 kV, and flight tube temperature of 42°C. Mass accuracy was preserved at 1 ppm through sodium iodide calibration. Argon served as the collision gas, utilizing a collision energy of 20 eV with a spread of 5 eV. Data analysis was conducted utilizing Lab Solutions software on the Shimadzu platform (Shimadzu, Japan).

3.4 HPLC analysis

High-performance liquid chromatography (HPLC) was employed to quantify the isomer ratio of operational solutions throughout photoirradiation and following MIP application. An LC2030 3D Plus Premium-i HPLC system (Shimadzu, Japan) facilitated the analysis. The system incorporates an LC-40B XR dual pump, enabling binary gradient separations up to 70 MPa. The flow rate ranged from 0.1 µL min^{-1} to 10 mL min^{-1} with exceptional accuracy (±2 µL min^{-1}) and pre*cis*ion (< 0.06%). Detection was achieved using an SPD-20 3D UV-Vis photodiode array detector, capable of wavelengths between 90 and 800 nm. A CTO-40 column oven maintained a constant temperature of 40°C. Sample introduction was performed using a SIL-40C autosampler with an injection volume range of 0.1-100 µL at a flow rate of 1 mL min^{-1}. Separation of the isomers occurred on a Shimpack C18 HPLC column (2.1 x 100 mm, 2.7 µm particle size). The optimized method utilized a 15-min runtime with a gradient elution starting at 60/40 9/v/v) methanol/water (5 min), followed by a shift to 5/95 (v/v) methanol/water (5-12 min), and concluding with a return to 60/40 (v/v) methanol/water (12-15 min). Data acquisition and chromatogram collection were managed by Shimadzu's LC Lab-Solutions software.

© University of Venda

Part A

3.5 Synthesis of molecularly imprinted polymers MIPs and respective NIPs

Procedure A: Polymers were synthesized by the precipitation polymerization process, with an appropriate functional monomer, cross-linker and porogen according to the ratios chosen as shown in Table 2. 1,1'-Azobis cyclohexanecarbonitrile (ACHN) was used as a radical initiator. A modified procedure based on Fathi Til et al. (2020) was employed. For the synthesis, t-4-MCA (178 mg, 1 mmol) analyte and (344 g, 4 mmol) MAA were dissolved in 5 mL of ethanol, followed by the addition of 55 mL of acetonitrile or chloroform in a 100 mL round-bottom flask. The solution was purged with nitrogen gas for 2 min and subsequently sonicated for 20 min at room temperature. Thereafter, 2.83 mL of EGDMA (15 mmol) and 51 mg of ACHN (0.31 mmol) as the radical initiator were added to the solution. The reaction mixture was purged with nitrogen gas for an additional 10 min before being submerged in an oil bath equipped with a thermometer, initially set at 60°C and then gradually increased to 65°C for 24 h. Since the polymerization initiation releases nitrogen gas, the round bottom flask was loosely fitted with a polypropylene stopper wrapped in parafilm. The same procedure was repeated for the non-imprinted polymers (NIP), but without adding the template. All other polymers were synthesized in the same manner but according to the reagents and mole equivalents presented in Table 2.

© University of Venda

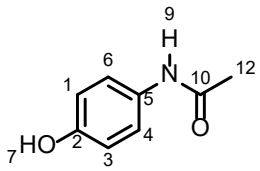
Table 2: The chemical composition of the synthesized MIPs and NIPs

Polymer	Template molecule (T)	Functional monomer (FM)	Crosslinker (CL)	Molar ratio (T: FM: CL)	Porogen
MIP 1	4-MCA	MAA	EGDMA	1:4:20	$CHCl_3$
NIP 1	------	MAA	EGDMA	1:4:20	$CHCl_3$
MIP 2	PCM	MAA	EGDMA	1:4:20	$CHCl_3$
NIP 2	------	MAA	EGDMA	1:4:20	MeCN
MIP 3	4-MCA	MAA	EGDMA	1:4:20	MeCN
NIP 3	------	4-VP	EGDMA	1:4:20	$CHCl_3$
MIP 4	PCM	MAA	EGDMA	1:4:20	MeCN
NIP 4	------	4-VP	EGDMA	1:4:20	MeCN
MIP 5	4-MCA	4-VP	EGDMA	1:4:20	$CHCl_3$
MIP 6	PCM	4-VP	EGDMA	1:4:20	$CHCl_3$
MIP 7	4-MCA	4-VP	EGDMA	1:4:20	MeCN
MIP 8	PCM	4-VP	EGDMA	1:4:20	MeCN
MIP 9	4-MCA	MAA	EDGMA	1:3:15	MeCN

© University of Venda

3.6 Synthesis of analogs of trans-4-methoxy cinnamic acid

3.6.1 Paracetamol (7)



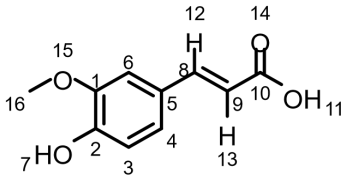
7

The synthesis followed a method by Barter et al. (2005). To begin with 7.0 g (0.05 mol) of nitrophenol was reduced to 11 g (0.1 mol) of aminophenol. Sodium borohydride, sodium hydroxide, and palladium on carbon were used as the reducing agent and catalyst. 11 g (0.1 mol) of p-aminophenol was then suspended in 30 mL of water in a 250 mL beaker. To this mixture, 12 mL (0.1 mol) of acetic anhydride was added and warmed to above room temperature while stirring vigorously. The mixture was then heated in a water bath until the solid dissolved. After 10 min, the solution was cooled, filtered, and the precipitate was washed with cold water. In the current work recrystallization from hot water and air-drying on filter paper yielded para-acetylaminophenol with a melting point of about 168°C and a 93% yield.

^{1}H NMR (400 MHz, DMSO): δ_H (ppm) 9.67 (s, 1H, H-9), 9.19 (s, 1H, H-7), 7.33 (d, J = 8.8 Hz, 2H, H-6, H-4), 6.67 (d, J = 8.8 Hz, 2H, H-1, H-3), 1.97 (s, 3H, H-12). **^{13}C NMR (101 MHz, DMSO)**: δ_C (ppm) 167.70 (C10), 153.22 (C-2), 131.08 (C-5), 120.95 (C-6, C-4), 115.09 (C-1, C-3), 23.80 (C12). **IR ν_{max} (cm^{-1})**: 3324 cm $^{-1}$ for O-H stretching, 3162 cm^{-1} for C-H stretching, 1656 cm^{-1} for C=O stretching, 1609 cm $^{-1}$ for C=C stretching, 1565 cm $^{-1}$ for N-H bending, and 1507 cm^{-1} for asymmetrical C-H bending.

© University of Venda

3.6.2 Ferulic acid (3)

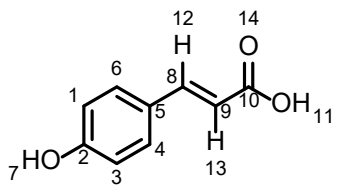


Procedure B: Ferulic acid was synthesized through a condensation reaction by Xia et al. 2008. Vanillin (9.9 g, 65 mmol) and malonic acid (7.3 g, 70 mmol) were added to a mixture of toluene (15 mL), pyridine (100 mmol), and aniline (0.7 mL). The reaction mixture was stirred at a reflux temperature for 2 h, upon cooling to room temperature, a yellow precipitate formed. The precipitate was isolated by filtration and washed with 50 mL portions of 3 M hydrochloric acid (HCl) and water, repeated twice each. In the current work, the crude product was recrystallized from ethanol (EtOH) to yield a light beige powder (3.8 g) with a melting point of 189-200 °C.

^{1}H NMR (DMSO, 400 MHz): δH (ppm) 9.54 (1H, s, H-7), 7.27 (1H, s, H-6), 7.07 (1H, d, J = 8.2 Hz, H-3), 6.79 (1H, d, J = 8.2 Hz, H-4), 6.36 (1H, d, J = 15.9 Hz, H-13), 7.46 (1H, d, J = 15.8 Hz, H12), 3.80 (3H, s, H-16). **^{13}C NMR (101 MHz, DMSO):** δ H (ppm) 168.46 (C-10), 149.54 (C-1), 148.36 (C-2), 144.98 (C-8), 130.55 (C-6, C-4), 116.19 (C-9), 115.77 (C-1.C-3), 125.72(C-5). **IR ν_{max} (cm^{-1}):** 3438 cm^{-1} (O-H stretch, carboxylic acid and phenolic), 1688 cm^{-1} (C=O stretch, carboxylic acid), 1274 cm^{-1}, 1216 cm^{-1}, and 1113 cm^{-1} (C-O stretches vibrations, phenolic and carboxylic acid), 1630 cm^{-1} and 1598 cm^{-1} (C=C stretch, aromatic and alkene), 900 cm^{-1} (C-H bending (out-of-plane), Aromatic).

© University of Venda

3.6.3 4-hydroxy cinnamic acid (2)



The compound was synthesized using **procedure B** with a mass of 4-hydroxy benzaldehyde at 7.9 g. The product was a light-yellow compound of mass 4.5 g with a melting point of 200-210ºC.

IR ν_{max} (cm^{-1}): 3200-3500 cm^{-1} (O-H stretch, carboxylic acid and phenolic), 1680 cm^{-1} (C=O stretch, carboxylic acid), 1250 cm^{-1} and 1170 cm^{-1} (C-O stretch vibrations, phenolic and carboxylic acid), 1600 cm^{-1} and 1510 cm^{-1} (C=C stretch, aromatic and alkene), 900 cm^{-1} (C-H bending (out-of-plane), aromatic)

The synthesized compounds (ferulic acid, 4-hydroxycinnamic acid, and ethyl (E)-3-(4-methoxyphenyl) acrylate except paracetamol) were used in conjunction with commercially available 4-methoxycinnamic acid for selectivity studies. These studies aim to evaluate the extraction efficiency of molecularly imprinted polymers (MIPs) within a binary system where t-4MCA will be paired with the above-mentioned compounds. The experimental approach provided insights into the MIPs' ability to adsorb t-4MCA from a binary mixture selectively.

3.7 Synthesis of control MIPs using a dummy template

The MIPs for the synthesis of the dummy template were synthesized using the same procedure A, except that 151 mg of paracetamol as the template was used.

3.8 Template removal protocol of MIPs

t-4MCA is a moderately polar aromatic compound that likely forms hydrogen bonds and other non-covalent interactions with the functional groups within the MIPs. The methanol:acetic acid (9:1) v/v mixture is a common washing solvent for MIPs. Methanol acts as a general solvent, while acetic acid can disrupt hydrogen bonding, promoting template removal. To ensure that the template and any unreacted monomer species was

© University of Venda

fully removed from the molecularly imprinted polymers (MIPs), 2 g of MIPs were placed in a 50 mL centrifuge tube, and a solvent mixture of 90% methanol and 10% acetic acid was added until the volume reached 20 mL. The tube was then shaken at 150 rpm for 20 min and centrifuged for 3 min. A 2 mL sample of the supernatant was then analyzed with UV-Vis. The washing cycle was repeated ten times. It should be noted that non-imprinted polymers (NIPs), were also subjected to the same washing process. After the completion of the washing cycles, the MIPs and NIP materials were then washed with MeOH to remove any traces of AcOH. Both MIPs and NIPs were dried overnight at 90°C to remove any remaining solvent. The removal of porogen molecules establishes crucial diffusion channels within the polymer. These channels are vital for the efficient re-absorption of analytes and their subsequent release from the created cavities. All the polymers synthesized, t-4MCA MIP, PCM MIP and their respective NIPs (washed MIP (w) and unwashed MIP (t)), were characterized using the methods mentioned in section 3.2.

3.9 Swelling behavior of polymers

Swelling analysis was conducted using various solvents. The polymers were tested in methanol, ethanol, acetonitrile, and ethanol-acetonitrile (5:5 v/v). Approximately 20 mg of each polymer was accurately weighed and placed into individual 2 mL microtubes. Each microtube was then filled with 2 mL of the respective solvent, sealed, and vigorously shaken for 2 min. The tubes were subsequently left undisturbed for 24 h to allow for equilibration. Following equilibration, the excess solvent was removed, and the weight of the swollen polymer sample was measured. The percentage swelling ratio was calculated using equation (1):

$$\% \text{ Swelling} = \left[\frac{\text{mw} - \text{md}}{\text{md}}\right] * 100 \ldots\ldots\ldots\ldots\ldots\ldots\ldots\ldots (1)$$

where mw represents the mass of the swollen polymer, and md represents the mass of the dry polymer. Each experiment was repeated three times to ensure accuracy.

3.10 Optimisation of adsorption parameters affecting the adsorption of the template to the MIPs.

The adsorption properties of the MIPs synthesised were first evaluated. The parameters studied were pH, contact time, mass of polymer used and initial concentration of template that affect the individual isomer

© University of Venda

extraction efficiency of the MIPs. Experiments were performed in triplicate by varying one parameter while keeping the others constant.

3.10.1 The effect of adsorption solvent

The choice of rebinding solvents is a crucial factor influencing the adsorption efficiency of the polymers. The solvent affects the physical and chemical properties of the MIPs and plays a significant role in the interactions between the MIPs and the target analytes during the rebinding process. The effect of adsorption solvent on the adsorption capacity of t-4MCA MIP and the NIP was undertaken in this study. A mass of 10 mg of each polymer were placed in five separate 4 mL centrifuge tubes. Methanol, acetonitrile, water, 5/5 v/v methanol: water and 5/5 v/v acetonitrile: water solutions were put in the tubes with each polymer and sealed tightly. The solutions were spiked with an appropriate volume of analyte to make 10 mg L^{-1} solutions. The binding was allowed to equilibrate at room temperature for 1 h by shaking the tubes on a benchtop shaker at 150 rpm. The difference between the initial concentration and the equilibrium concentration was calculated, after which the adsorption capacity, which is the amount adsorbed per unit mass, was calculated using equation (2):

$$q = \frac{(Ci - Cf)V}{m} \dots\dots\dots\dots\dots\dots\dots\dots\dots (2)$$

q is the adsorbed amount of each template per unit mass of the MIP (mg g^{-1}), Ci is the initial concentration of each template (mg mL^{-1}), Cf is the final equilibrium concentration of each template after adsorption (mg mL^{-1}), V is the volume of the solution used (mL) and m is the mass of the MIP (mg).

3.10.2 Effect of polymer mass

Adsorption of t-4MCA onto the t-4MCA MIPs, PCM MIPs and NIPs was carried out in 4 mL of 10 mg L^{-1} of a 50:50 v/v methanol/water solution. Each 15 mL vial was filled with varying masses of polymer 5 mg, 10 mg, 20 mg, 30 mg, 40 mg, and 60 mg. The binding was allowed to occur at room temperature for 1 h by shaking the tubes on a benchtop shaker at 150 rpm, the experiment was carried out in triplicate. The solutions were then analysed using LC-MS MRM methods for detection and quantification of t-4MCA in solution after

© University of Venda

adsorption, from which the amount adsorbed on the polymer was calculated. Then, from that, the adsorption capacity was calculated.

3.10.3 Point of zero charge pH_{pzc}

The pH_{pzc} refers to the specific pH value at which the overall surface charge of MIPs becomes neutral. The pH_{pzc} helps predict the MIP's adsorption behavior towards charged analytes. Adsorption is favored when the analyte has an opposite charge to the MIP surface. By controlling the pH of the solution, you can tune the MIP's selectivity for specific analytes based on their charge. MIPs surface charge in water is generated from interactions between ions in solution and the surface functional groups of the adsorbent. Surface charge and pH_{pzc} point of zero charges are essential features in adsorbent surface science and play a key role in the adsorption process. The pH of the surrounding solution significantly impacts the surface charge, particularly concerning acidic and basic groups, and the interaction between the adsorbent surface and electrolytes defines the pH_{pzc} (Madrakian et al., 2013).

A series of 10 mL 0.1 M KCl solutions were prepared in 20 mL centrifuge tubes at initial pH ranges 2, 4, 7, 9 and 11. The pH was adjusted using 0.1 M HCl and 0.1 M NaOH to achieve the desired pH values. A mass of 20 mg of the MIP samples were introduced into each of the prepared KCl solutions. The resulting mixtures were then subjected to continuous shaking at 100 rpm on a benchtop shaker for a duration of 24 h at a controlled temperature of 25°C. The containers were tightly sealed throughout the equilibration period to prevent evaporation and potential contamination. Following equilibration, the final pH of each solution was carefully measured using a calibrated pH meter. The final pH levels were graphed alongside their respective initial pH values. The intersection point between this graph and the line where initial pH equals final pH (represented by the line $y = 0x$) was identified as the MIPs pH_{pzc}

© University of Venda

3.10.4 Effect of sample pH

The pH at which adsorption capacity of t-4MCA MIPs, PCM MIPs and NIPs will be optimum and give the highest adsorption capacity was investigated. Centrifuge tubes that are 15 mL were charged with 4 mL of 10 mg L^{-1} of a 5:5 v/v methanol/water solution at room temperature. Each 15 mL vial was filled with varying pH solutions of pH 2, 4, 7, 9 and 11. The binding was allowed to occur at room temperature for 1 h by shaking the tubes on an elliptical benchtop shaker at 150 rpm, the solution was then analysed with the LC-MS MRM method from which the amount adsorbed on the polymer was calculated then further the adsorption capacity. The analysis was performed in triplicates.

3.10.5 Effect of contact time

The time taken by t-4MCA MIPs, PCM MIPs and NIPs to have the optimum adsorption capacity with the highest adsorption capacity was investigated. The experiments were carried out in triplicate in 15 mL volume centrifuge tubes with a 4 mL volume of 10 mg L^{-1} of a 5:5 v/v methanol/water solution at room temperature. Each 15 mL vial was filled with 10mg of polymer mass. The binding was allowed to occur at room temperature for the chosen times of 30 min, 60 min, 90 min, 120 min and 270 min. The tubes were shaken on an elliptical benchtop shaker at 150 rpm, the solution was then analysed with the LC-MS MRM method, from which the amount adsorbed on the polymer was calculated, then further the adsorption capacity.

3.10.6 Effect of initial concentration

The effect of the initial concentration of t-4MCA on adsorption capacity of t-4MCA MIP, PCM MIP and respective NIP was investigated in triplicates by adding 10 mg of each polymer to five 4 mL solutions containing 10 mg/mL of a 5:5 v/v methanol/ water mixture. The setup was necessary because all the templates were found to be partially soluble or insoluble in water. The binding was allowed at room temperature for 1 h by shaking the tubes on a benchtop shaker at 150 rpm. The amount of template adsorbed by the MIP was calculated as the difference between the initial amount and the amount remaining in the solution after adsorption.

© University of Venda

3.10.6.1 Adsorption isotherms

Adsorption isotherms are graphical representations or mathematical models that describe the relationship between the amount of an analyte adsorbed onto the MIPs and the concentration of the analyte in solution at constant temperature. In other words, they show how the adsorption of an analyte into a polymer material changes with varying concentrations of that polymer in solution. There are several types of adsorption isotherms, and they are typically used to characterize and understand the adsorption behavior of different materials. The most encountered adsorption isotherms are the Langmuir and the Freundlich isotherms.

The Langmuir isotherm as seen in equation (3) assumes that adsorption occurs at specific sites on the polymer and that there is a monolayer of adsorbed molecules. It suggests that the adsorption process is a reversible, single-step process with no interaction between adsorbed molecules. The Langmuir isotherm is often used for physisorption or when adsorption sites are limited.

$$\frac{Ce}{qe} = \frac{1}{b * qm} + \frac{Ce}{qm} \dots\dots\dots\dots\dots\dots\dots\dots (3)$$

The Freundlich isotherm in equation (4) is an empirical model that describes non-ideal adsorption behavior. It suggests that adsorption is a multilayer process, allowing for interactions between adsorbed molecules. The Freundlich isotherm equation is expressed as:

$$qe = KF * Ce^{\frac{1}{n}} \dots\dots\dots\dots\dots\dots\dots (4)$$

where Ce is the equilibrium concentration (mg L^{-1}), qe is the amount adsorbed at equilibrium (mg g^{-1}), qm is the maximum adsorption capacity (mg g^{-1}), b is a constant related to the energy of adsorption (L mg^{-1}), K_F is the equilibrium constant (mg g^{-1}). 1/n, and n is the adsorption intensity.

The IF (imprinting factor) value helps evaluate the adsorption effectiveness of the MIP. The imprinting factor was calculated as the ratio of equilibrium adsorption capacity values of the MIP and the NIP using equation (5).

© University of Venda

$$\mathrm{IF} = \frac{\mathrm{qMIP}}{\mathrm{qNIP}} \ldots\ldots\ldots\

3.11 Selectivity studies

Investigations to determine the selectivity of the synthesized t-4MCA MIPs and NIPs on the analogues, ferulic acid, t-4HCA, Et-MOPA individually and in competition with the t-4MCA analyte as a binary solution were conducted. In triplicate, 10 mg L^{-1} of 4 mL volume of each analyte was incubated for 60 min with 10 mg each of polymer with an adjusted pH to 7 in a 5:5 v/v methanol:/water solution. The polymers were allowed to equilibrate for 60 min after which they were centrifuged at 5000 rpm for 15 min. The supernatant was extracted, filtered and sent for HPLC analysis. The measured values gave the concentration of the unextracted compounds, from which concentration percentages were evaluated.

Part B

3.12 Procedure for photoisomerization to generate *cis/trans* mixtures

A stock solution of (t-4MCA) was created by dissolving 10 mg of the compound in 1 L of methanol, yielding a 10 mg L^{-1} concentration. In the photoisomerization experiments, 8 mL aliquots of the t-4-MCA solution were placed into separate 30 mL quartz tubes, which were then sealed with rubber stoppers. The tubes were subsequently positioned within a designed UV lamp enclosure containing a 254 nm UV lamp. The total duration of irradiation was 12 h. Samples were extracted from the quartz tubes at specified intervals, 0 h (initial), 3 h, 6 h and 12 h, to assess the progress of photoisomerization and identify the optimal irradiation duration. The samples underwent analysis via HPLC to determine the relative quantities of *cis* and *trans* isomers. The HPLC spectra collected at each time point were analyzed and compared to the spectrum of the unirradiated t-4MCA solution to evaluate the degree of conversion. The analysis assessed potential degradation or dimer formation resulting from extended UV exposure.

© University of Venda

3.12.1 Selective extraction of t-4MCA from a *cis/trans* mixture using MIPs - Batch binding method

Following the photoisomerization experiments, the (MIPs) were employed to selectively extract the t-4MCA isomers (*trans*-isomers) from the reaction mixture of *cis/trans* isomers using a batch binding method. The approach involves incubating the MIPs directly with the sample solution, allowing for equilibrium binding to occur. A mass of 10 mg of individual t-4MCA MIPs, PCM MIP and NIP was added to a measured 4 mL of 10 mg L^{-1} photoisomerized reaction mixture containing a mixture of t-4MCA and c-4MCA in 15 mL separate centrifuge tubes. The mixture was incubated at room temperature in an elliptical benchtop shaker at 150 rpm to allow for equilibrium binding between the MIPs and the isomer. The experiment was performed in triplicates and three different isomer ratios, 40:60 *cis/trans* mixture, 60:40 *cis/trans* mixture and 50:50 *cis/trans* mixture. After the incubation period, the MIPs were centrifuged at 5000 rpm, and then the supernatant was extracted and sent for HPLC analysis. The batch binding method is relatively simple and requires less specialized equipment compared to SPE. It allows for greater flexibility in adjusting the MIP-to-sample ratio and incubation conditions to optimize the extraction process.

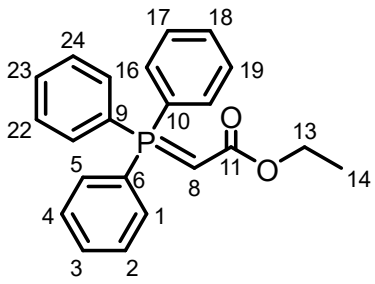
3.12.2 Photoirradiation experiment in the presence of t-4MCA MIPs - Batch binding method

To further explore the potential of MIPs to manipulate photoisomerization equilibria, a series of photoirradiation experiments were conducted in the presence of t-4MCA-imprinted MIPs with respective NIPs using a batch binding method. The investigation aimed to assess the ability of MIPs to selectively sequester the *trans*-isomer during photoirradiation reaction, thereby influencing the *cis/trans* isomeric ratio. A volume of 8 mL aliquots of the t-4MCA were placed into separate 20 mL quartz tubes with 10 mg t-4MCA MIP NIP and control with no MIP, then sealed with rubber stoppers. The tubes were subsequently positioned within a designed UV lamp enclosure containing a 254 nm UV lamp inside a bench-top shaker for 3 h. The suspension was centrifuged at 5000 rpm for 15 min, then the supernatant was drawn and underwent analysis via HPLC to determine the relative quantities of *cis* and *trans* isomers. The HPLC spectra collected were then analyzed and compared to the spectrum of the control irradiated t-4MCA solution to evaluate the degree of conversion.

© University of Venda

3.13 Synthesis of ethyl (E)-3-(4-methoxyphenyl) acrylate Et-MOPA) (8) Wittig reaction

3.13.1 Synthesis of ethyl 2-(triphenylphosphoranylidene) (ylide) acetate, a substrate in the Wittig reactions

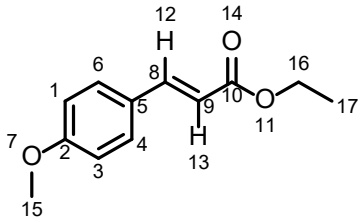


Triphenylphosphine (35.0 g, 130 mmol) was dissolved in 200 mL of ethyl acetate. Ethyl bromoacetate (12.0 mL, 100 mmol) in 50 mL of ethyl acetate was added, and the mixture was stirred for 24 h at room temperature. The resulting white solid was filtered, rinsed with cold ethyl acetate, and dried under vacuum. The solid was redissolved in 200 mL dichloromethane, followed by 200 mL of 4% aqueous sodium hydroxide solution (8 g, 200 mmol). After 15 min of vigorous stirring, the organic layer was separated, washed with saturated sodium chloride solution, dried ($MgSO_4$), filtered, and evaporated under reduced pressure. The product was dissolved in 50 mL of diethyl ether, filtered, and vacuum dried with stirring for 16 h, yielding 28 g (84% yield).

^{13}C NMR (101 MHz, DMSO): δ_C (ppm) 30.8 (C8),171.3 (C-11), 57.7 (C-13), 14.95 (C-14). **IR ν_{max} (cm^{-1}):** 1638 cm^{-1} (C=O stretch, ester), 1310 cm^{-1} (P=C stretch), 1180 cm^{-1} (C-O stretch, ester), 3000-3100 cm^{-1} multiple sharp peaks (C-H stretch, aromatic), 1430-1500 cm^{-1} (C=C stretch, aromatic), 900 cm^{-1} (C-H bending (out-of-plane), Aromatic).

© University of Venda

3.13.2 Synthesis of (Et-MOPA) (8) using the Wittig reaction



Procedure C: A modified method by Speed et al. 2004 was carried out. In a 50 mL round-bottomed flask equipped with a magnetic stir bar, 4-methoxy benzaldehyde (0.64 g, 4.7 mmol) was suspended in dichloromethane (20 mL). The mixture was cooled in an ice bath for 10 min before slowly adding (carbethoxymethylene) triphenylphosphorane (2.0 g, 5.7 mmol). After stirring for an additional 45 min in the ice bath, the reaction was allowed to warm to room temperature. The solvent was removed using a rotary evaporator, and the residue was then quenched with 20 mL of hexanes. The suspension was stirred and filtered by vacuum filtration through a Büchner funnel. In this current synthesis, the filtrate was collected in a pre-weighed round-bottomed flask and concentrated using a rotary evaporator. A 0.8 mL pale-yellow liquid product was obtained, which resulted in 97% t-4MCA and 3% c-4MCA.

^{1}H NMR (400 MHz, DMSO): δ H (ppm) 7.68 (2 H, d, J 8.5,H-6, H-4), E isomer 7.60 (1 H, d, J 16.0, H12), Z isomer 5.8 (1H, d, J 12.71), 6.97 (2 H, d, J 8.6, H-1 ,H-3), E isomer 6.48 (1 H, d, J 16.0, H13), Z isomer 6.9 (1H, d, J 12.79), 4.02 (2 H, s, H-16), 3.79 (3 H, s, H-15), 1.17 (3 H, s, H-17). **IR ν_{max} (cm-1):** 3000-3100 cm^{-1} (C-H stretch (sp^2), aromatic), 1718 cm^{-1} (C=O stretch, ester), 1600-1680 cm^{-1} (C=C stretch, aromatic), 1635 cm^{-1} (C=C stretch, alkene), 1174 cm^{-1} (C-O stretch, ester), 1250 cm^{-1} (C-O stretch, ether), 900 cm^{-1} (C-H bending (out-of-plane), aromatic) 2850-2950 cm^{-1} (C-H stretch, aliphatic).

3.13.3 Synthesis of t-4MCA using Wittig reaction

The synthesis of t-4MCA using **Procedure C** was the same as synthesizing the Et-MOPA except that in real-life applications, the resulting Et-MOPA would undergo hydrolysis to introduce the hydroxyl group in the carboxylic acid functional group.

© University of Venda

3.14 Wittig reactions in the presence of synthesized MIPs

To investigate the potential of molecularly imprinted polymers (MIPs) to influence the stereochemical outcome of the Wittig reaction, a modified procedure by Speed et al. (2004) as the previously described Wittig reactions for Et-MOPA analogue was repeated in the presence of the synthesized t-4MCA-imprinted MIPs and newly synthesized Et-MOPA MIP. The novel approach aimed to explore the ability of MIPs to act as stereoselective catalysts, favouring the formation of specific isomers.

A mass of 20 mg of the t-4MCA and Et-MOPA MIPs were added to the reaction flask containing the (4.7 mmol) 4-methoxybenzaldehyde 20 mL in dichloromethane, the mixture was gently stirred for 10 min in the ice bath. After that, (5.7 mmol) (carbethoxymethylene)triphenylphosphorane was slowly added to the flask. After stirring for an additional 45 min in the ice bath, the reaction was allowed to warm to room temperature. The solvent was removed using a rotary evaporator, and the residue was then quenched with 20 mL of hexanes. The suspension was stirred and filtered by vacuum filtration through a Büchner funnel to remove the triphenylphosphine oxide by-product and the MIPs. The filtrate was collected in a pre-weighed round-bottomed flask and concentrated using a rotary evaporator. A pale-yellow liquid product was obtained. The isolated crude product was analyzed using ^{1}H NMR ^{18}C-NMR and HPLC to determine the isomeric ratio of the Et-MOPA and t-4MCA analogue. The ratios obtained from the Wittig reactions with MIPs were compared to those from the control experiments (without MIPs). The comparison allowed for the evaluation of the MIPs' ability to alter the stereoselectivity of the Wittig reaction.

© University of Venda

University of Venda
Creating Future Leaders

Chapter 4

Results and discussion

This chapter details the results obtained from the synthesis of polymers and elution of the analytes from the MIPs, characterization using FTIR, TGA, SEM, EDX, powder XRD of the synthesized polymers. Results from the optimization experiments of adsorption capacity are analyzed and discussed, selectivity studies of the synthesized polymers are undertaken and application of the polymers on the Wittig reaction investigated is reported.

© University of Venda

4. Results and discussion

Part A characterization

4.1 Chemical computational analysis

The optimization of the three-dimensional ground state molecular configurations for t-4MCA, PCM, and the monomer MAA was conducted employing the density functional theory (DFT) and Becker-style variant of the three-parameter Lee-Yang-Parr (B3LYP) correlation function. The optimisation was accomplished within a 6-31+G (d, p) basis set utilizing the Gaussian 2 software. The optimized structures are presented in Figure 7. Subsequent to structure optimization, the energy differences (ΔE) of t-4MCA, PCM, and MAA when dissolved in acetonitrile, methanol, ethanol, tetrahydrofuran, and chloroform were calculated.

The computational process was carried out in stages. First, structural conformations of t-4MCA, PCM, and MAA were optimized in a vacuum, then in each of the five solvents, acetonitrile, methanol, ethanol, tetrahydrofuran and chloroform. Secondly, the energies of these molecules, in their optimal conformations, in both vacuum and solvent environments were determined. Lastly, equation (8) below was used to calculate the ΔE for t-4MCA, PCM, and MAA

.

$$\Delta E = E(\text{vacuum}) - E(\text{solution}) \dots\dots\dots\dots\dots\dots (8)$$

This approach helped gauge the affinity of t-4MCA, PCM, and MAA for the various solvents, with a higher ΔE indicating a stronger solvent affinity.

© University of Venda

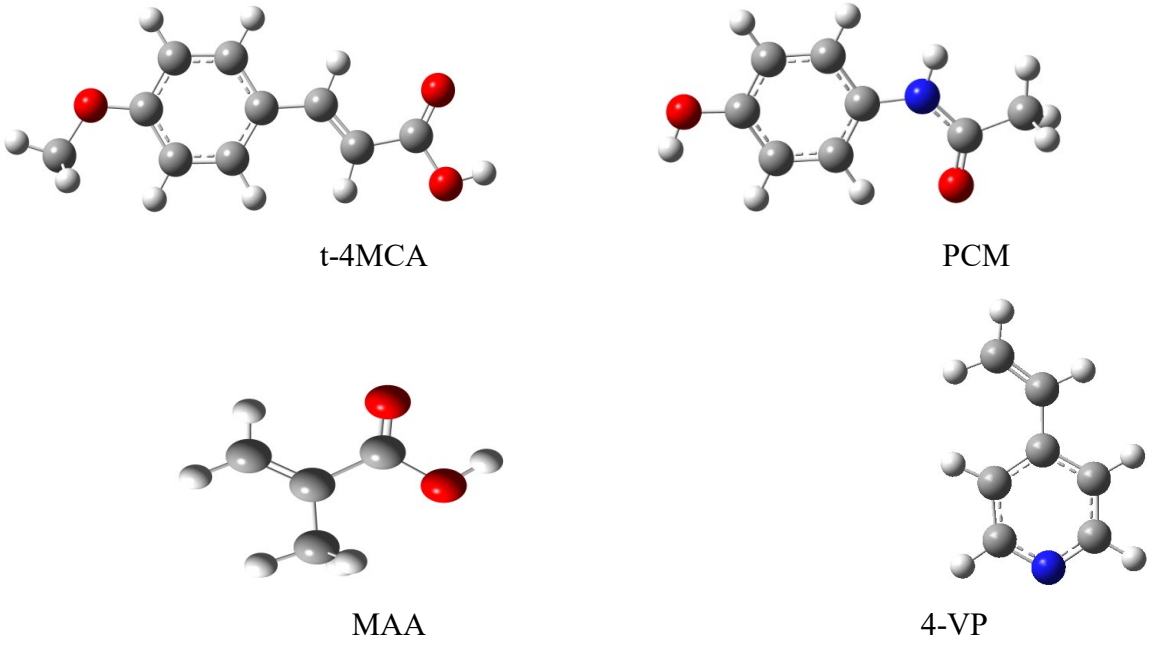


Figure 7: Optimized structures of t-4MCA, PMC, 4-VP and MAA

The energy difference (ΔE) between t-4MCA and PCM was calculated in five different solvents using equation 1. The results, in Table 3, indicate a decrease in ΔE for both t-4MCA and PCM in the following order of solvents: acetonitrile > methanol > ethanol > THF > chloroform. The results suggested that acetonitrile had the strongest interaction, while chloroform has the weakest. The ΔE of MAA and t-4VP in same solvents showed a similar interaction trend, with acetonitrile being the strongest and chloroform being the weakest. The findings suggested that acetonitrile demonstrated the highest attraction towards the template molecule, with values of 31.70 kJ mol^{-1} for t-4MCA and 39.71 kJ mol^{-1} for PCM, along with monomer values of 18.90 kJ mol^{-1} for MAA and 16.71 kJ mol^{-1} for 4-VP. The strong attraction was not beneficial as it diminished or lessened the interactions among t-4MCA, PCM, and the monomers MAA and 4-VP, a critical step for forming the template-monomer complex interaction before the polymerization process. Conversely, chloroform displayed minimal influence on the creation of the complex, as shown by its lowest ΔE value of 24.99 kJ mol^{-1} for t-4MCA and 31.00 kJ mol^{-1} for PCM, along with monomer values of 14.93 kJ mol^{-1} for MAA and 11.86 kJ mol^{-1} for 4-VP. Thus, it was anticipated that the MIP created using chloroform as the porogen and 4-VP as the functional monomer will exhibit superior selectivity, attributed to the solvent's minimal disruption of the interactions between the template and the functional monomer.

© University of Venda

Table 3: ΔE of t-4MCA, PCM with 4-VP and MAA in five different solvents

	Functional monomers (kJ/mol)		Templates (kJ/mol)	
	MAA	4-VP	t-4MCA	PCM
Acetonitrile	18.90	16.71	31.70	39.71
Methanol	18.84	16.63	31.60	39.58
Ethanol	18.63	16.63	31.24	39.11
Tetrahydrofuran	16.58	13.74	27.77	34.58
Chloroform	14.93	11.86	25.00	31.00
Vacuum	0.00	0.00	0.00	0.00

4.2 Mechanism of synthesis of MIPs

Figure 8 shows the general mechanism of molecularly imprinted polymer synthesis. The figure describes the binding interactions between the t-4MCA template molecule, methacrylic acid as one of the functional monomers and ethylene glycol dimethacrylate as the cross-linker. The process eventually led to the formation of MIPs with specific binding sites. Because of this, the FT-IR spectrum presented in Figures 15 and 16 showed peaks corresponding to these chemical compounds.

© University of Venda

University of Venda
Creating Future Leaders

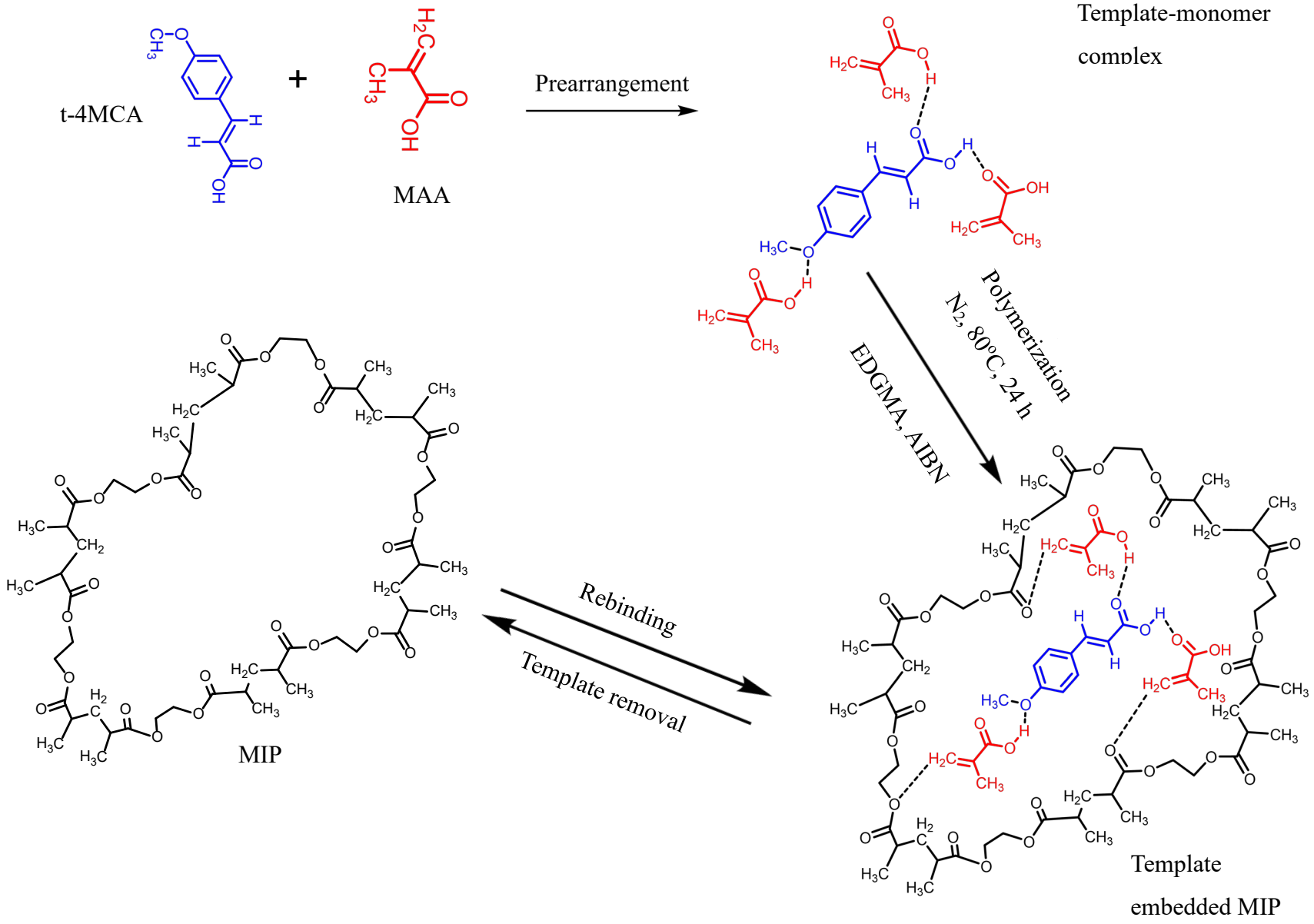


Figure 8: Proposed reaction mechanism for the polymerization

© University of Venda

4.3 Synthesis and characterization of MIPs

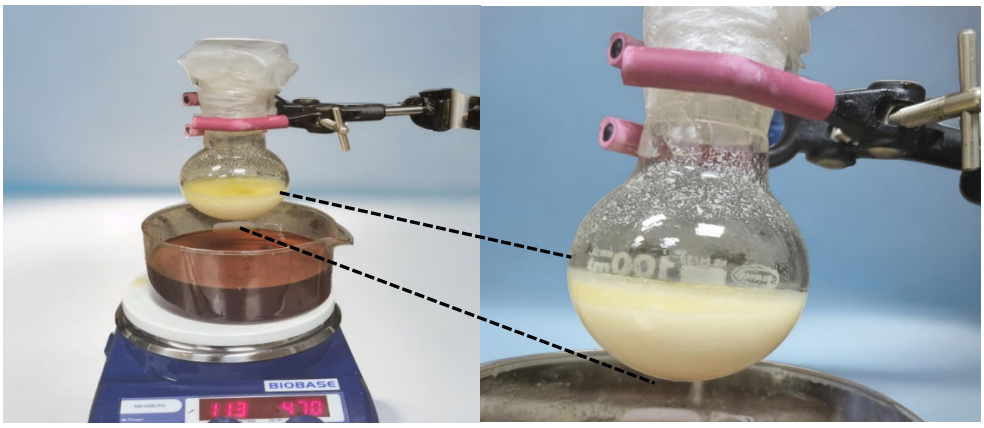


Figure 9: Synthesis of t-4MCA polymers and respective NIPs

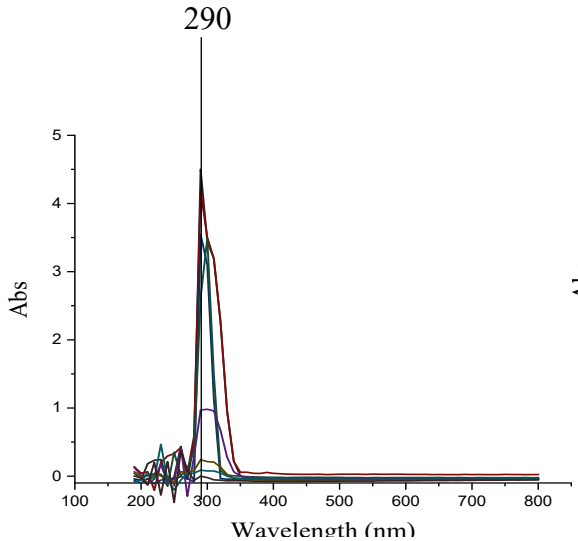
Nine polymers of different templates, functional monomer, porogen and molar ratio compositions and their respective non-imprinted polymers were synthesized using the precipitation polymerization method of synthesis. Table 2 in the methodology section indicates the different compositions and ratios that were investigated. Figure 9 above shows the specific synthesis of t-4MCA and their NIP in chloroform. The figure showed a clear separation of the polymers from the solvent, they gradually settled at the bottom of the round bottom flask, which pointed out to precipitation polymerization, signifying a possibility of a successful synthesis of the polymers. Most of the polymers exhibited a similar qualitative observation.

© University of Venda

4.4 Removal profile of t-4MCA and PCM templates from MIPs synthesized with MAA and chloroform.

The MIP materials were eluted in 20-min intervals using a 10% (v/v) methanol (MeOH) and acetic acid (AcOH) solution, followed by washing with methanol to remove any residual acetic acid.

UV-Vis spectroscopy was performed on t-4MCA and PCM across 190 nm to 800 nm, revealing maximum absorbance at 290 nm for both templates, as shown in Figures 10 and 11. The absorbance decreased with each elution cycle, indicating the progressive removal of the template from the pores. Complete removal was achieved after eight cycles, as evidenced by an absorbance close to zero for both templates, confirming successful template extraction from the MIPs.



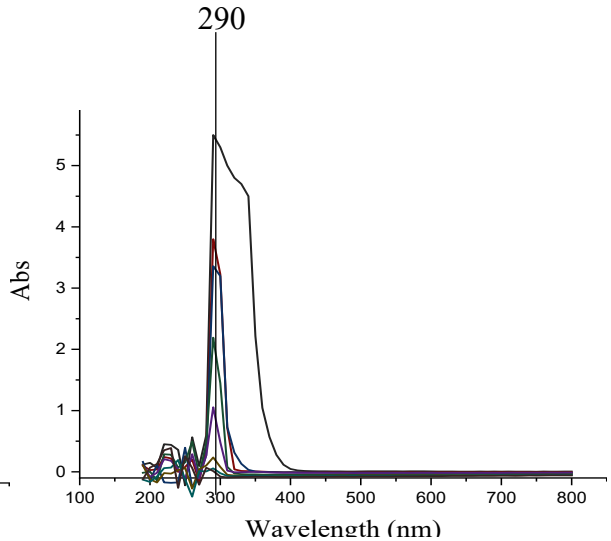


Figure 10: Template removal profile of t-4MCA MIPs **Figure 11:** Template removal profile of PCM MIPs

The concentrations of the templates eluted during each wash were calculated using the calibration equations $y = 0.1156x - 0.0598$, where $R^2 = 0.9967$ for t-4MCA, which was found from the standard calibration curve in Figure 12 which is the absorbance of the analyte read with increases in concentration.

© University of Venda

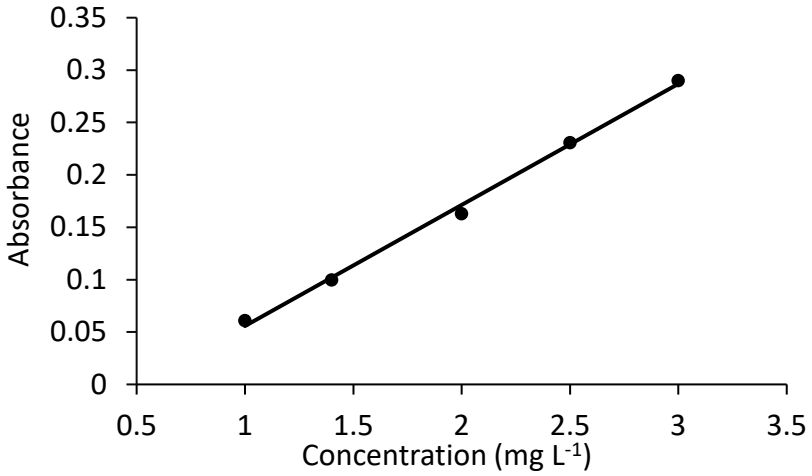


Figure 12: Standard calibration curve of t-4MCA

For the dummy templated PCM MIPs, the concentration eluted out was calculated using the following linear equation $y = 0.0235x - 0.4692$, where $R^2 = 0.9966$. The standard calibration graph is in the appendix.

Near exponential decay curves in Figure 13 were obtained when the concentration eluted was plotted against the number of elutions. Elutions 1-5 for both templates showed a significant decrease in concentration, which corresponds to the removal of loosely bound templates due to non-specific binding molecules on the surface of the polymer. In contrast, the later elutions 5-8 exhibited a levelling off with a more gradual decrease in eluent concentration, which can be attributed to the extraction of tightly bound template molecules within the polymer pores.

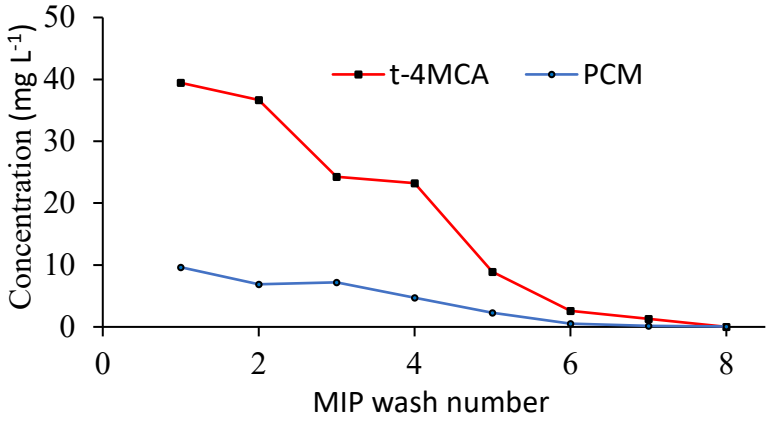


Figure 13: Leaching of t-4MCA and PCM from MIPs.

© University of Venda

PCM's gradual and low-concentration elution indicates that it was never strongly bound to the MIP in the first place. It was primarily washed out from the polymer matrix during filtration of the porogen from the MIPs after the synthesis; very little was released from specific binding sites, indicating that very few binding sites were created. In a similar study by Zheng et al. (2022), it was observed that there was an MAA:template equivalence range that promoted a stable formation of the template-monomer complex above which was unassembled monomer residues not interacting with the PCM but forming clusters of MAA-MAA which might have led to a false template pore formation and high surface area. It was observed that with the PCM MIP, the 1:4 ratio used for the monomer and template, might have been the case.

© University of Venda

4.5 Batch binding studies for all MIPs and NIPs synthesized

Batch-binding studies of t-4MCA and PCM for the nine different compositions of MIPs and their respective NIPs were conducted. Figure 14 shows the adsorption capacity obtained with each of the eight MIP compositions and their corresponding NIPs using a UV-VIS spectrophotometer.

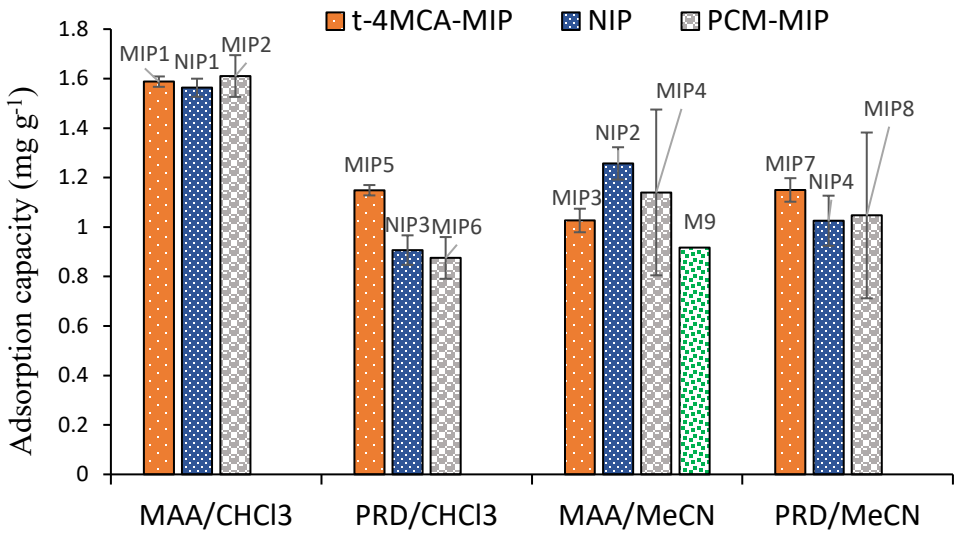


Figure 14: Adsorption capacity of nine polymers and respective NIPs in chloroform or acetonitrile. Conditions: polymer mass = 5 mg, water/methanol 50:50% v/v as the eluent (n = 3, RSD)

When 4-VP is utilized as a functional monomer, the MIPs exhibited higher adsorption than their corresponding NIPs (e.g., NIP3 vs MIP5 AND NIP4 vs MIP7). The increased adsorption capacity can be attributed to the extra interaction between the basic monomer and the acidic template. The pyridine ring of the monomer could promote adsorption because it can form both acid-base interactions and strong hydrogen bonds (Li et al., 2013). Similar studies by Zhang et al. (2001) demonstrated that when salicylic acid was imprinted using 4-VP and acrylamide as functional monomers, 4-VP showed a superior imprinting effect than acrylamide (Zhang et al., 2002). Computational theoretical studies earlier carried out also corroborated this, as 4-VP gave the lowest ΔE of 11.86 kJ/mol. The results demonstrated that the composition of the MIPs, particularly the type and ratio of functional monomers as seen with lower adsorption capacity for MIP 9 compared to MIP 3 of the same constituents, played a crucial role in the binding efficiency and selectivity towards the target analytes (Shafqat et al., 2023).

© University of Venda

Comparing MIPs with the same template and MAA as a functional monomer but prepared in different solvents (e.g., MIP 1 vs MIP 3; MIP 2 vs MIP 4), it was observed that chloroform generally led to higher adsorption capacities than acetonitrile. The results suggested that chloroform may facilitate better interactions between the MAA and template during imprinting. The experimental results agree with the computational theoretical results obtained in Table 3.

When MAA was used as a functional monomer, the NIPs mostly exhibited higher adsorption than their corresponding MIPs (e.g., NIP2 vs MIP3). Baggiani et al. (2012) directly addressed this phenomenon and investigated the underlying reasons. The author highlighted that the traditional view in molecular imprinting, where MIP binding sites are solely attributed to the imprinting process, might be incomplete. The authors propose that the imprinting effect enhances pre-existing NIP binding properties. Thus, if an NIP demonstrates an affinity for the target molecule, its MIP counterpart may not necessarily offer a marked increase in adsorption effectiveness. In certain instances, the NIP could surpass the MIP in performance. Becskereki et al. (2021) also investigated this phenomenon where selectivity assessment involves comparing the binding of the target analyte to both MIPs and NIPs. The researchers isolated the specific binding contribution that arises solely due to the imprinting process. The authors cautioned against solely relying on the ratio of binding affinities between the target analyte and interferents as the sole measure of selectivity. The article advocated for a more nuanced approach considering factors like binding site heterogeneity and potential competition between molecules.

Therefore, both articles suggested that it was not always the case that MIPs would have superior adsorption capacity compared to NIPs. The relative performance depends on various factors, including the NIP's inherent binding properties, the imprinting process's effectiveness, and the specific experimental conditions. For this reason and the observation that MIP 1, NIP 1 and MIP 2 had the highest adsorption capacity, 1.59 mg g^{-1}, 1.56 mg g^{-1} and 1.6 mg g^{-1} respectively. It was interesting to continue with the assessment of the MIP 1, NIP 1 and MIP 2 performance, but using very sensitive detection method such as the LC-MS to assist with the very nuanced differences that occur between the MIPs.

© University of Venda

4.6 Characterization of synthesized MIPs

4.6.1 Functional group analysis

Characterizing synthesized MIPs and NIPs through FTIR is crucial for understanding their functional group composition, the polymer structural integrity after template removal and the impact of template presence on the polymer matrix. Specific functional groups were observed, such as C=O, C-H, C=C, and O-H, which are essential for assessing the successful synthesis and functionality of MIPs compared to NIPs. The presence of these functional groups was confirmed by analyzing the characteristics of absorption bands in the spectra.

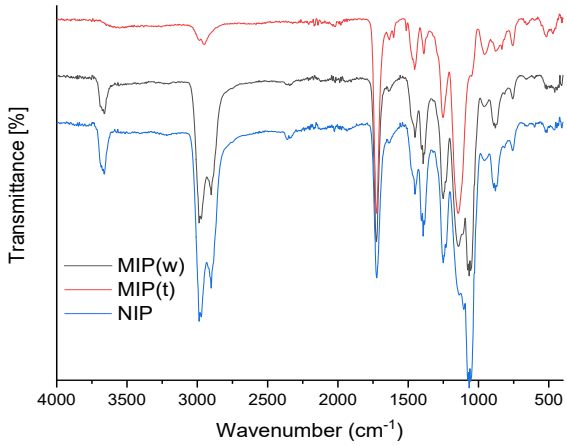


Figure 15: FTIR spectra for t-4MCA-based MIPs

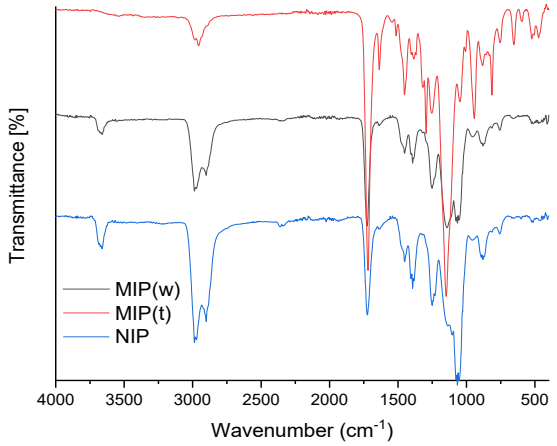


Figure 16: FTIR spectra for PCM-based MIPs

Figures 15 and 16 present the overlaid FTIR spectra for MIPs before and after they are washed, and the NIPs of t-4MCA and PCM, respectively. The FTIR spectra for all the polymers were almost identical and this is consistent with other studies (Til et al., 2020). The peaks around ~1635 cm^{-1} for t-4MCA MIPs have been attributed to the C=C stretching vibration of the template molecule aromatic ring. The comparison between the washed MIPs, unwashed MIPs and NIPs reveals an absence of these absorption bands. Results indicate the successful template removal during the washing process, consistent with findings in the

© University of Venda

literature (Espinoza-Torres et al., 2023). The bands at ~1600 cm^{-1}, 845 $cm^{-1}$and 750 cm^{-1} for PCM MIPs may be due to unreacted MAA (Suwanwong et al., 2014). MAA and EDGMA vinyl bands are typically found at about 1630 - 1640 cm^{-1} (Ariani et al., 2024). The absence of these peaks from the polymers confirm a successful polymerization.

The broad band at wavelengths 3380 cm^{-1} is due to bonded O-H of the carboxylic group of the polymer. In the washed MIPs and NIP the bonded O-H band is obscured by the sharp band that has shifted slightly higher to 3475 cm^{-1} for free O-H from the residual methanol/acetic acid wash or residual water from the atmosphere. In both figures the frequencies at ~2980 cm^{-1} and ~1451 cm^{-1} are the methylene groups' stretching and s*cis*sors C-H vibrations in the polymer materials from the EGDMA cross-linker backbone, this was consistent with the literature (Mpupa et al., 2021). At approximately 1720 cm^{-1}, a C=O vibration from the EDGMA and MAA carbonyl group is observed, this is shifted to slightly higher wave numbers than that of the functional monomer MAA and EDGMA indicating a bond formation of monomer and crosslinker. The intensity of this band for the washed polymers is reduced, evident from the intensity of the unwashed polymers, which overlaps with the blue NIP spectrums. The phenomenon can be explained by the template molecule being assembled with the monomer via hydrogen bonding with C=O during the preparation of the MIP prior to washing. The intense C-O stretch at 1135 cm^{-1} is attributed to the aliphatic ether in EDGMA, this also corroborates the successful synthesis of MIPs. It was noted that the peak intensities for the identified hydroxyl and methylene groups were lower in the MIP(t) compared to both the MIP(W) and NIP of t-4MCA and PCM. The reduction in intensity could be due to the presence of the template in MIP(t).

© University of Venda

4.6.2 Thermogravimetric analysis of polymers

The thermostability of the imprinted polymer particles for MIP(t), MIP(W) and NIP is shown through the TGA curves of t-4MCA in Figure 17. The thermograms indicate an initial mass loss of about 0.08 mg (0.77%), 0.2 mg (2.3%) and 0.45 mg (4.67%), respectively. The lost initial mass was thought to be the decomposition of volatile compounds, such as the solvents trapped in the pores. The MIP(w) and NIP samples were stable between 100 and 300°C with no change in mass, but MIP(t) had a steady mass change in this temperature range, indicating that it was the least stable polymer material. The instability was attributed to the degradation of t-4MCA molecules and the decrease in active sites of MIP functional groups bound to the template surface.

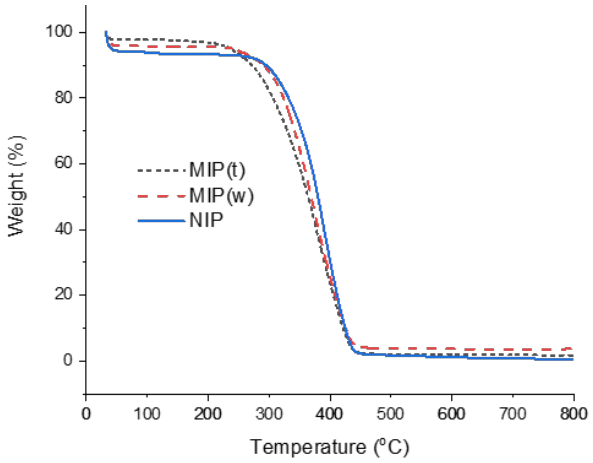


Figure 17: TGA curves for t-4MCA MIPs

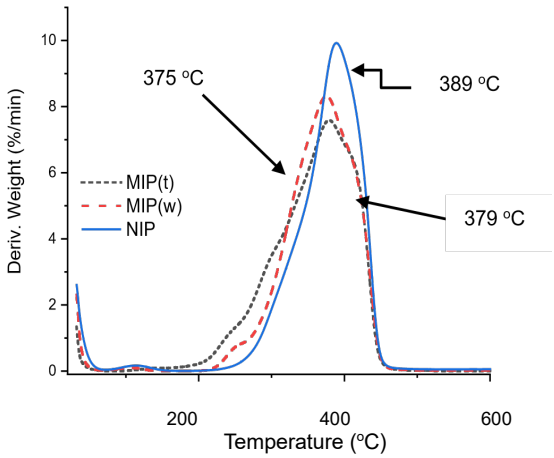


Figure 18: Derivative curves t-4MCA MIPs

Figure 18 is the curve for temperatures where the most decomposition occurs for MIP(t), MIP(w), and NIP. According to these curves, the maximum decomposition temperatures were found to be 379°C for the unwashed MIP, where 39.76% which is 3.85 mg of the total mass of 9.93 mg was lost. The 375°C temperature was for the washed MIP with 44.26% which is 3.73 mg weight loss from a total of 8.43 mg and 389°C for the NIP with 41.2% weight loss equivalent to 3.93 mg from 9.53 mg total weight. At this temperature is where polymer structure and material degradation like the cross linker EDGMA happened. At temperatures above 450°C, all polymer materials were completely decomposed. The results were consistent with the findings by Zahedi et al. (2017).

© University of Venda

Figure 19 illustrates the thermostability of imprinted polymer particles for MIP(t), MIP(w), and NIP through the TGA curves for PCM. The thermograms indicate an initial mass loss of about 0.05 mg (0.51%), 0.06 mg (0.67%) and 0.45 mg (4.67%), respectively. This was attributed to the decomposition of volatile compounds. The NIP and MIP(w) samples remained stable between 100°C and 300°C without any change in mass, while MIP(t) began to show a gradual mass change starting around 250°C. The trend was attributed to the PCM molecules degradation along with diminishing MIP functional group active sites linked to the template surface.

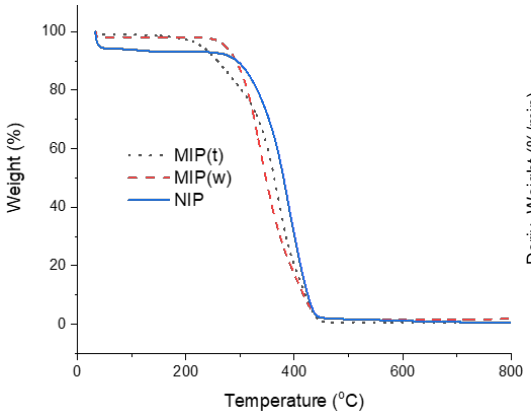


Figure 19: TGA curves for PCM MIPs

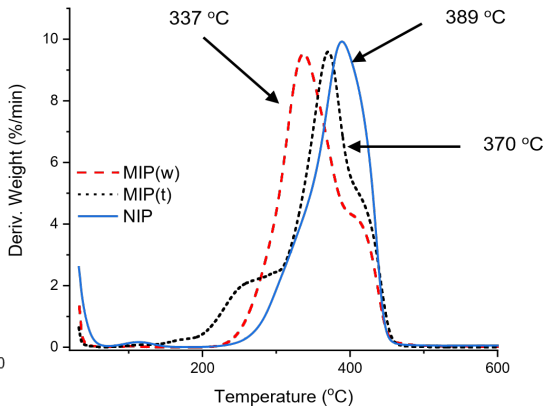


Figure 20: Derivative curves PCM MIPs

Figure 20 presents the first derivative curve for MIP(t), MIP(w), and NIP. According to these curves, the maximum decomposition temperatures were found to be 370°C for the unwashed MIP, where 42.96%, which was 4.08 mg of the total mass of 9.5 mg was lost. The degradation temperature of 337°C was for the washed MIP with 59.54% which was 5.56 mg weight loss from a total of 9.33 mg and 389°C for the NIP with 41.2% weight loss equivalent to 3.93 mg from 9.53 mg total weight.

The differences in polymer material decomposition temperatures between the washed and unwashed MIPs was attributed to structural variations that occurred during the template removal process because the washed polymers showed a slower thermal degradation than the unwashed MIPs. Above 430°C, all polymer materials underwent complete decomposition.

© University of Venda

4.6.3 Nitrogen gas adsorption analysis

The results for nitrogen gas adsorption are shown in Figure 22 for t-4MCA MIPs and Figure 21 for PCM MIPs together with the NIP. The isotherm exhibits a type IV isotherm according to the IUPAC classification (Madhu et al., 2023). The observation is characteristic of mesoporous material indicating pores in the range of 2-50 nm, this is confirmed by the average pore size values in the range 4.3-6.371 nm obtained for all polymers as in Table 2 (Cheng & Qi, 2020). The Type H4 hysteresis loop observed further indicated the mesoporous nature of all the polymers. It suggested the presence of aggregates of plate-like particles with narrow slit-like pores that favor the adsorptive properties of the template. The hysteresis loop for MIP (W) is not closed from the relative pressure at around 0.3 this is consistent with the constricted microporous character (Lanfredi et al., 2020).

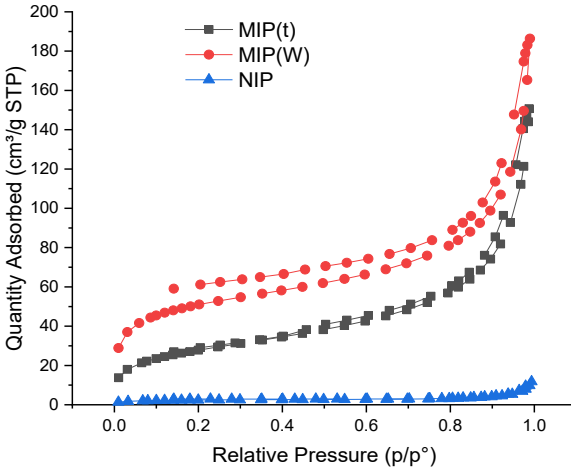


Figure 22: BET N2 adsorption/desorption profiles of MIP (t), MIP (w) and NIP for t-4MCA

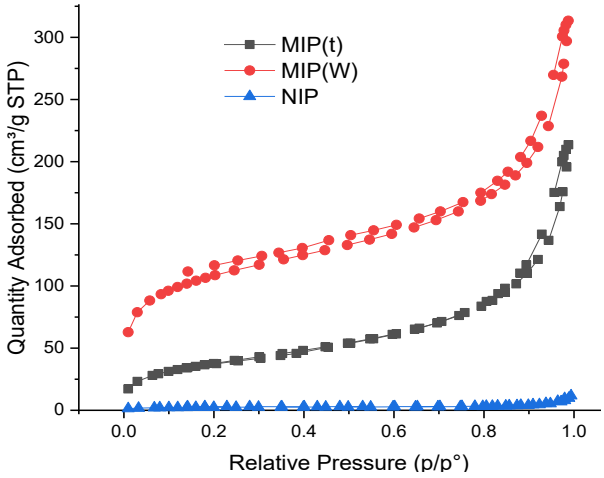


Figure 21: BET N_2 adsorption/desorption profiles of MIP (t), MIP (w) and NIP for PCM

© University of Venda

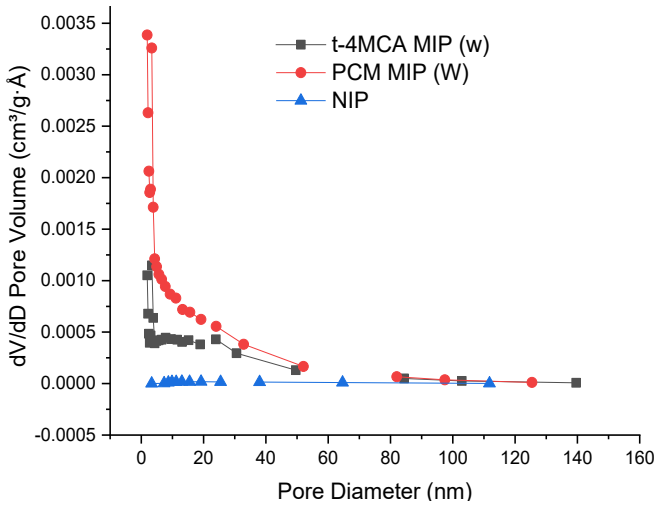


Figure 23: BJH pore size distribution t-4MCA MIP, PCM MIP and NIP

Figure 23 displays the pore size distribution isotherms of MIPs that have been washed for both the templates and NIPs. The isotherms reveal a bimodal distribution with the second smaller peak around 30 nm for all the polymers, indicating a variation in pore size populations (Li et al., 2022). Most pores are concentrated in the 10 to 20 nm range, classifying them as mesopores. The greater pore volume observed in the MIPs compared to the NIPs suggested that the imprinting process led to the forming of a more porous structure.

Table 4 presents the surface area, pore volume, and pore diameter of washed and unwashed polymer materials for t-4MCA and PCM obtained from BET analysis. The results indicated that the surface area of the MIPs ranged from 100.1 to 374.8 $m^2 g^{-1}$, significantly higher than the 7.84 $m^2 g^{-1}$ observed for the NIPs. Additionally, the pore volume for the MIPs ranged from 0.149 to 0.363 $m^2 g^{-1}$, compared to just 0.0085 $m^2 g^{-1}$ for the NIPs. These results suggested that cavities were formed from the template during the synthesis, and the shrinkage of the pores from the unwashed polymer to the washed polymer provides evidence of the template's removal. Consequently, the synthesized MIPs exhibited greater pore size and pore volume than the NIPs, indicating the formation of a complementary spatial structure for the MIPs' selective recognition of the template. The analysis also supports the notion that the presence of the template during synthesis was advantageous. Similarly Zhi et al. (2023) emphasized that the imprinting process significantly enhances both the specific surface area and pore volume of MIPs.

© University of Venda

Table 4: BET surface area analysis and porosity

Polymers	Surface area (m^2 g^{-1})	Pore volume (cm^3 g^{-1})	Pore diameter (nm)
t-MCA MIP (w)	175.165	0.190	4.345
t-MCA MIP (t)	100.067	0.149	5.999
PCM MIP (w)	374.729	0.363	3.876
PCM MIP (t)	137.976	0.220	6.371
NIP	7.837	0.0085	4.300

The MIP (w) isotherms in Figures 21 and 22 for all MIPs showed a higher adsorption capacity than the MIP (t), indicative of a higher surface area and pore volume, as could be observed in Table 4. The NIP showed the lowest adsorption capacity, which is in correspondence with what is expected of NIPs as they lack template-induced structural modifications that are present in the MIPs as a result of imprinting and the presence of binding sites complementary to the t-4MCA and PCM.

© University of Venda

4.6.4 Morphology analysis of polymers

4.6.4.1 XRD analysis

The phase purity of washed PCM MIP, t-4MCA MIP and NIP were demonstrated with XRD spectroscopy and are presented in Figure 24. PCM analyte in literature usually displays a characteristic peak around 2θ = 25-26 degrees, along with other prominent peaks typically observed at 2θ values of 12, 17, 21, and 24 degrees (Akhiani et al., 2015). Both MIPs and NIPs exhibit a similar diffraction profile, characterized by the absence of the analyte peaks and crystallinity, indicating that both polymers are amorphous materials and are devoid of template material (P Huang et al., 2024). The amorphous behavior is typical for polymers. In the case of the synthesized NIPs, which were produced without any template, no changes in crystallinity were observed.

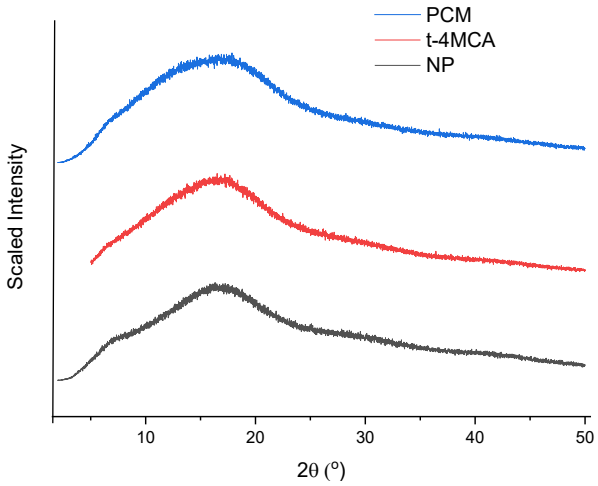


Figure 24: XRD reflection patterns of washed PCM MIP, t-4MCA MIP and NIP

© University of Venda

4.6.4.2 SEM analysis

Scanning electron microscopy (SEM) was used to assess the variations in the surface morphology of the MIPs. Figure 25 shows SEM images of washed MIPs in image A and unwashed MIPs of t-4MCA in image B. Image B's surface appears smoother than image A's, with fewer visible protrusions and indentations. The softer surface and less extensive agglomeration in the washed MIPs could be beneficial for the binding of target molecules, as it allows for better access to the binding sites within the MIPs.

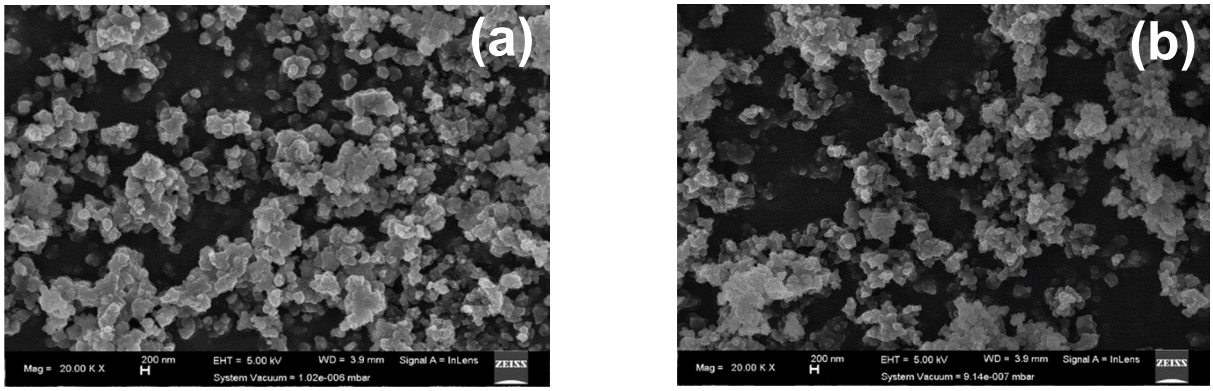


Figure 25: SEM image of unwashed t-4MCA MIP (a) and washed t-4MCA MIP (b)

The washed MIPs show less extensive agglomeration than the unwashed MIPs, with particles appearing more loosely packed. The washed MIPs appear to have a more uniform particle size distribution, with particles that appear more sheet-like or plate-like with irregular edges. In contrast, the unwashed MIPs exhibited more irregular, angular shapes. The changes in morphology likely resulted from the removal of the t-4MCA template molecules during the washing process.

© University of Venda

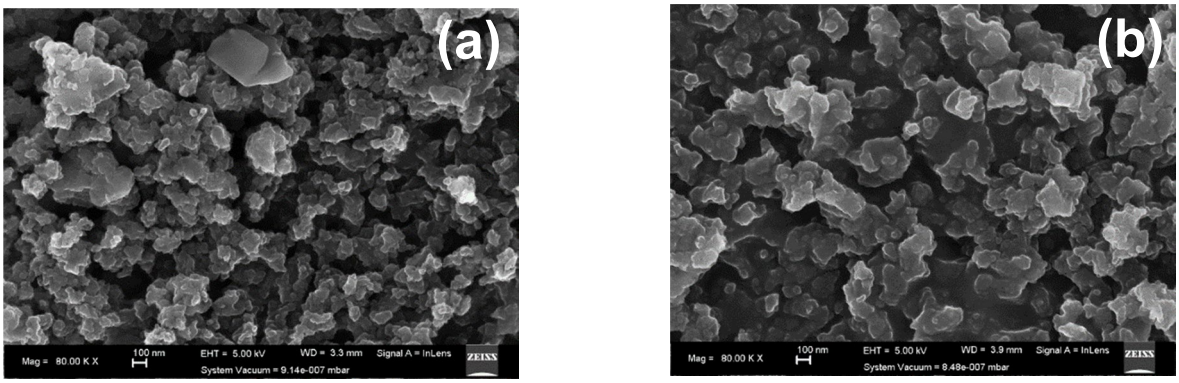
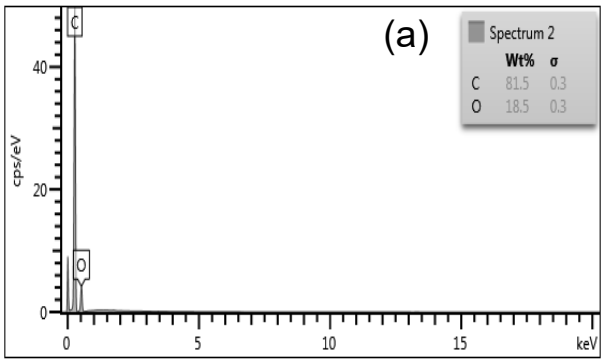


Figure 26: SEM image of unwashed PCM MIP (a) washed PCM MIP (b)

Figure 26 illustrates the surface morphology of synthesized polymers of PCM washed and unwashed with the image taken at 80.00 kX. The surface of the particles appears extremely rough, with numerous small protrusions and indentations. The results suggests a high degree of surface area and potentially high porosity. The particles in image A exhibit irregular shapes, with some appearing more angular and others more rounded. Image B's washed MIP particles appear more sheet-like or plate-like with irregular edges.

4.6.4.3 EDX analysis

EDX analysis is another important study to determine the elemental compositions in the synthesized polymers. The EDX spectra in Figure 27 for washed MIP of t-4MCA, washed MIP of PCM and NIP, showed that both polymers had similar elemental composition due to the removal of the template from the MIP, resulting in the MIP and NIP having relatively similar elemental compositions.



© University of Venda

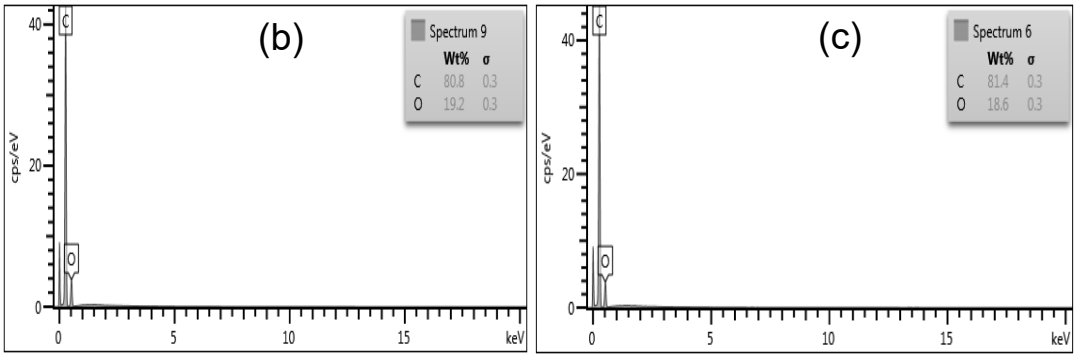


Figure 27: EDS spectra of NIP (a), washed t-4MCA (b) and washed PCM (c)

The EDX analysis of all polymers demonstrated the mass percentage of the main chemical elements, namely carbon (C) and oxygen (O). Based on Figure 27, the percentage of the C element was in the 80% range and around the 20% range for oxygen. These results indicated that the MIPs and NIP were made up of C as the main element in the polymer backbone.

© University of Venda

4.7 Swelling studies

The swelling behavior of the NIP and the two molecularly imprinted polymers (t-4MCA and PCM) was investigated in four different solvents: methanol, ethanol, acetonitrile, and a 1:1 (v/v) mixture of ethanol and acetonitrile. The swelling percentage, calculated as the percentage change in mass, was determined for each polymer-solvent combination. The results are presented in Table 5.

Table 5: Swelling percentage of MIPs in different solvents

	Swelling % of polymers in various solvents			
	Methanol	Ethanol	Acetonitrile	Ethanol-Acetonitrile (5:5 v/v)
NIP	92.57	389.05	29.70	76.24
t-4MCA MIP	175.12	208.42	457.71	197.51
PCM MIP	505.97	231.03	338.61	367.49

The thermodynamic compatibility between the polymer network and the solvent molecules governs the swelling behavior of polymers in different solvents (P Huang et al., 2024). The NIP showed the highest swelling in ethanol (389.05 %) and the lowest in acetonitrile (22.70%), indicating a stronger affinity of the MAA-co-EGDMA backbone for ethanol due to hydrogen bonding and favorable van der Waals interactions. PCM MIP had the highest swelling in methanol (505.97 %), indicating strong interactions within its polymer matrix. In contrast, t-4MCA MIP showed greater swelling in acetonitrile (457.71 %). Since all three polymers NIP, t-4MCA MIP, and PCM MIP share the same fundamental MAA-co-EGDMA matrix, the differences in their swelling behavior can be attributed to the presence and nature of the imprinted cavities in the MIPs, and the resulting differences in the overall polymer network structure (Singh & Singh, 2022).

The swelling in the ethanol-acetonitrile mixture for NIP (76.24 %), t-4MCA MIP (197.51 %), and PCM MIP (367.49 %) was generally intermediate between the values in the pure solvents, consistent with a combined effect of the individual solvent interactions. While sufficient swelling is necessary to allow the target analyte to access the imprinted sites, excessive swelling can disrupt the shape complementarity of the cavities, leading to reduced selectivity and increased non-specific binding. The optimal rebinding solvent often

© University of Venda

represents a compromise between these two opposing effects. A combination of solvents like this one fits the criteria for the synthesised MIPs and NIP composition.

4.8 Enhancing the parameters that influence adsorption capacity

Parameters influencing the adsorption of t-4MCA were optimized. Because the aim was to enhance primarily binding efficiency then selectivity, the MIPs adsorption studies were optimized for maximum imprinting effect, rather than the optimum value. The result was effectively achieved by focusing on the differences in performance between MIPs and NIPs. The selection of the adsorption solvent was the first parameter to be optimized. Methanol, acetonitrile, water, and various combinations of organic solvents with water were tested. It was observed that trans-4-methoxy cinnamic acid was not soluble in pure water. Other optimized parameters included polymer mass, pH, adsorption time, and the initial concentration of the analyte, all conducted at ambient temperature.

4.8.1 Solvent effects on adsorption capacity of t-4MCA imprinted polymers

The adsorption capacity of the t-4MCA MIP and its corresponding NIP was evaluated in various solvent systems of methanol, acetonitrile, water, and 5:5 v/v combinations of organic solvents with water, as depicted in Figure 28. The highest adsorption capacities for the MIP were observed in pure acetonitrile (MeCN) and pure methanol, both reaching approximately 3.1 mg g^{-1} for the MIP. The strong binding in pure organic solvents aligns with previous findings where optimal rebinding often occurs in solvents similar to the porogen used during MIP synthesis.

© University of Venda

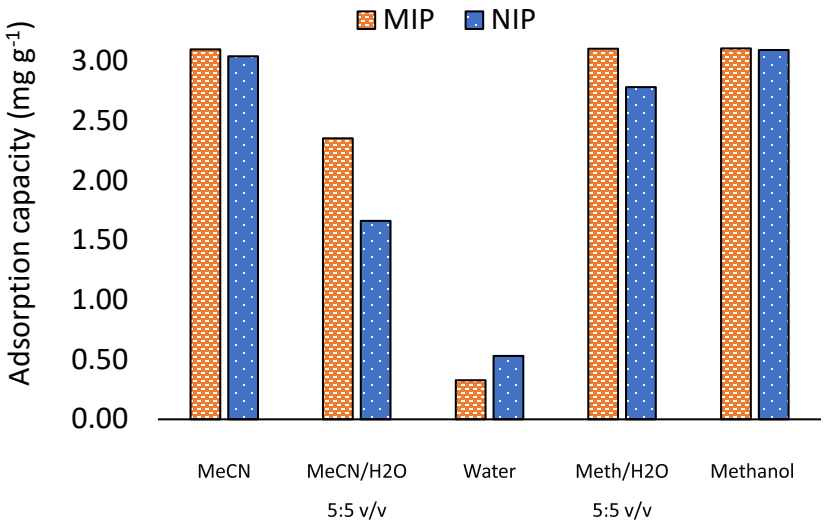


Figure 28: Effect of rebinding solvent on adsorption capacity. Conditions: polymer mass 10 mg, pH5, 10 mg L^{-1}

Conversely, when pure water was used as the solvent, the MIP and NIP exhibited significantly reduced binding, likely due to the poor solubility of t-4MCA in water, hindering its interaction with the binding sites. The methanol/water 5:5 v/v solvent mixture was, however, the one that was used for further optimization due to the evident difference in the adsorption capacity between the MIP and NIP, which unmasked the imprinting effect but still maintained the highest adsorption capacity in most of the solvents tested.

4.8.2 Effect of polymer mass on adsorption capacity of *t*-4MCA imprinted polymers

The influence of polymer mass on the adsorption capacity of the t-4MCA MIP, NIP and PCM MIP was investigated, as shown in Figure 29. The figure shows a MIP, NIP and PCM adsorption capacity from 5 mg to 60 mg polymer mass. With more polymer mass, the template molecule has a greater surface area and more active binding sites, leading to higher adsorption capacity. Generally, increasing the polymer mass from 5 mg to 60 mg resulted in a higher adsorption capacity

© University of Venda

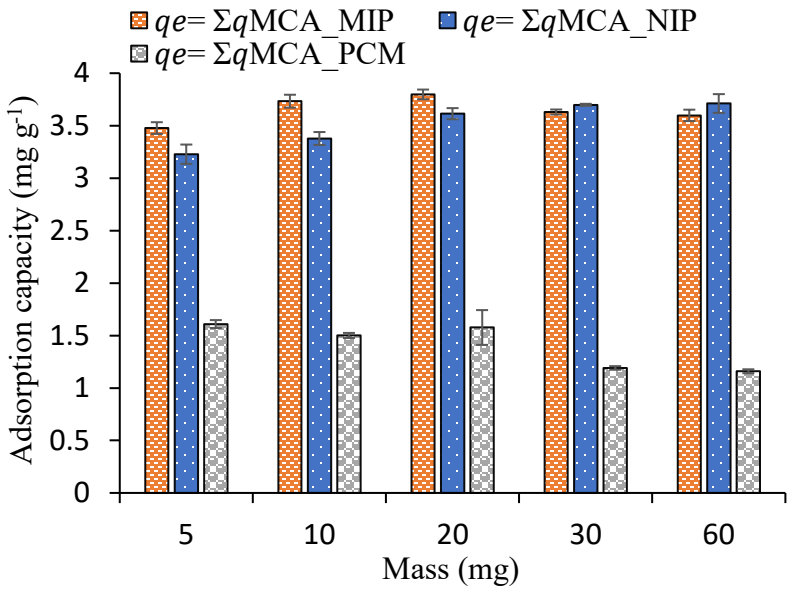


Figure 29: Effect of polymer mass used on adsorption capacity. Conditions: polymer pH = 5.6, concentration = 10 mg L^{-1}, H_2O/methanol 5:5 v/v as the eluent (n = 3)

Table 6: Imprinting efficiency of t-4MCA and PCM MIPs per mass of polymer

	Imprinting factor	
Mass (mg)	t-4MCA_MIP	PCM_MIP
5	1.08	0.50
10	**1.11**	0.40
20	1.05	0.42
30	0.98	0.33
60	0.97	0.32

The MIP shows an increase in adsorption capacity from 5 to 20 mg then slightly decreased. The result suggests that 20 mg might be close to the saturation point for the MIP under the given conditions. A similar trend, although less pronounced, was found by Anene et al. (2024) studying how the mass of the cationic polymer (PANI@MIP) affects extraction recovery of the a MIP. Although it increases throughout, the NIP adsorption capacity is consistently lower than the MIP adsorption capacities across all polymer masses. The analysis indicated that the imprinting process in MIPs effectively enhanced adsorption, as expected. PCM MIP had a different behavior. It showed a relatively small increase in adsorption capacity from 5 to 10 mg,

© University of Venda

followed by a slight decrease in higher polymer masses. The observation suggests that PCM has a much lower adsorption efficiency than MIP and NIP, and its performance is not as influenced by changes in polymer mass. Although the optimum mass seemed to be at 20 mg, the mass that was further used as optimum was 10 mg, as it showed an imprinting factor of 1.11 as shown in Table 6, indicating the most pronounced imprinting effect, and therefore, the highest selectivity.

4.8.3 Investigating the impact of pH on polymer adsorption capacity and determining the point of zero charge pH_{PZC}

This study aimed to explore the impact of sample pH on the adsorption capacity of NIP, t-4MCA, and PCM MIPs. To evaluate this effect, experiments to determine adsorption capacity using solutions of t-4MCA analyte at a concentration of 10 mg L^{-1}, adjusting the pH levels from 2 to 11 were conducted. The results of these experiments are illustrated in Figure 31. Additionally, it was crucial to understand the electrostatic interactions between polymers and target molecules. Hence the pH_{PZC} of the polymers using the pH drift method, as outlined by Díaz de León-Martínez, et al. (2022) was determined. The findings in Figure 30 indicated that the pH_{PZC} for all polymers was 4. At this specific pH, the positive and negative charges reach equilibrium. By combining these analyses, the aim was to understand the charge characteristics of MIPs better so that we can better optimize the pH under which binding occurs.

© University of Venda

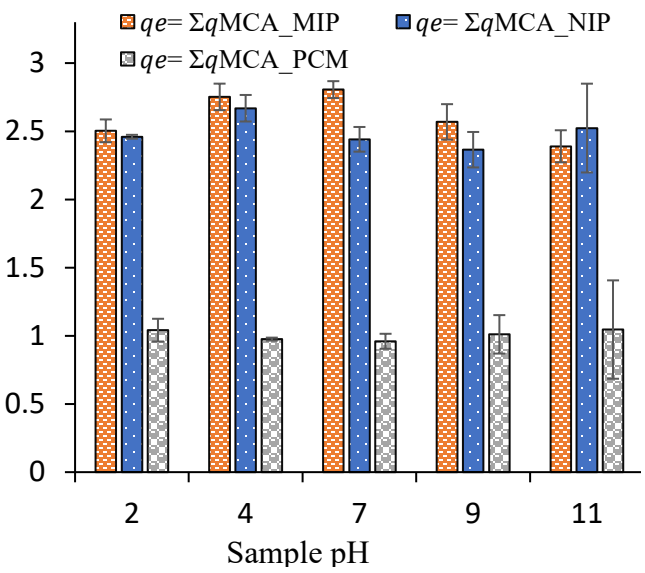


Figure 31: Effect of solution pH on adsorption capacity. Conditions, polymer mass = 10 mg, concentration = 10mg L^{-1}, H_2O/methanol 5:5 v/v as the eluent (n = 3).

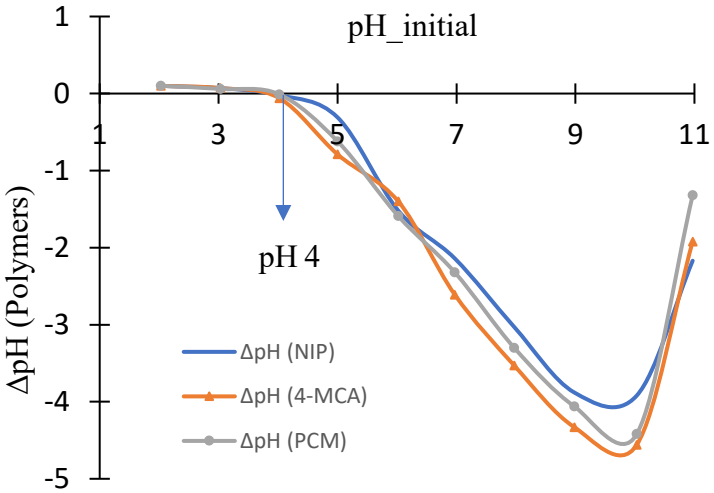


Figure 30: pHPZC for NIP, t-4MCA and PCM MIPs

Table 7: Imprinting efficiency of t-4MCA and PCM MIPs per solution pH

	Imprinting factor	
pH	t-4MCA_MIP	PCM_MIP
2	1.02	0.70
4	1.03	0.60
7	**1.15**	0.72
9	1.09	0.66
11	0.95	0.64

When the pH is below the pH_{PZC} = 4, a dominant net positive charge is observed, and the polymers are likely to adsorb negatively charged species more readily. In contrast, a net negative charge is prevalent above the pH_{PZC}, which is 4, where the polymers would absorb positively charged species. The study's findings can be linked to the choice of methacrylic acid as the monomer in polymer synthesis, notable for its weak acid properties with a pKa value of 4.7 (Meléndez et al. 2022).

The general trend in Figure 30 was an increase in capacity from pH 2 to pH 7, which was the highest for the t-4MCA MIPs at 2.72 mg g^{-1}. A decrease in pH value from pH 7 was observed after that. Electrostatic interactions and hydrogen bonding were likely the dominant forces governing adsorption in the MIPs, as

© University of Venda

they contributed to the selectivity and specificity of the binding sites. In the absence of specific binding sites, adsorption onto NIPs and dummy polymers was mainly driven by non-specific interactions, for example, van der Waals forces and hydrophobic forces. Depending on the pH level of the solution and the charged nature of the polymers' surfaces, electrostatic forces could also play a role.

The pKa of t-4MCA in water is 4.7, in a 50/50% water/methanol solution, the range shifts even higher, likely about 5.5 - 6, due to the increased pKa and the slight acidic nature of the methanol component of the solvent. The pH range is well above the calculated pH_{PZC} found for all polymers in the study, which was 4. At pH < pH_{PZC} the surface of this MIP is positively charged, and t-4MCA is likely to be neutral (pKa ~ 5.5-7.0), hindering adsorption. At pH > pH_{PZC} the MIP surface is negatively charged, and t-4MCA at 5.5 < pH < 7 has an increase in anionic form favoring adsorption. At pH > 7, t-4MCA is predominantly anionic, leading to strong electrostatic repulsion and disfavoring adsorption. Similar studies conducted by Fathi Til et al. (2020) where MAA, EDGMA and sinapic acid were used also revealed the different ionization forms of the template in solution and Alsudir et al. (2012) binding essay results for Bisphenol A indicated an optimal pH at 7.5 using the same monomer and crosslinker. At pH 7 the MIP also exhibited the highest imprinting factor of 1.15 as shown in Table 7.

4.8.4 Effect of contact time on the adsorption capacity of the polymers

Varying equilibration time versus adsorption capacity was investigated for the polymers between 30 min and 270 min. Figure 32 illustrates a distinct difference in the adsorption behavior of the three polymer types. For the t-4MCA MIP and the NIP an exponential increase in adsorption capacity is observed up to 90 min. The trend is attributable to the progressive filling of available adsorbent sites on the polymer surface by the t-4MCA analyte adsorbate as contact time increases (Sellergren, 2000). After 90 min, a decline in adsorption capacity is observed for both MIP and NIP, signifying the saturation of available binding sites and the approach towards equilibrium. In contrast, the PCM MIP exhibited significantly lower adsorption capacity and reached its saturation point much earlier, within 30 min. The observation suggested a far lower density of binding site conformations on the PCM MIP surface capable of interacting with t-4MCA. Following this rapid saturation, the PCM MIP's adsorption capacity gradually decreases until equilibration. However, the optimum contact time for highest imprinting factor 1.83 was observed at 60 min for the t-4MCA MIP and NIP as indicated in Table 8.

© University of Venda

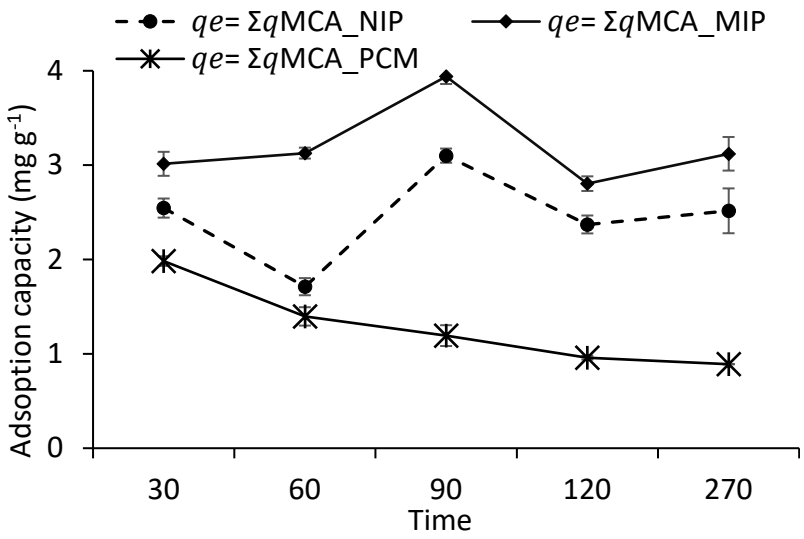


Figure 32: Time effects on adsorption capacity. Conditions: polymer mass = 10 mg, H_2O/methanol 5:5 v/v as the eluent, sample pH 7 and concentration = 10 mg L^{-1} (n = 3).

Table 8: Imprinting efficiency of T-4MCA and PCM MIPs with increasing time

	Imprinting factor	
Time (min)	t-4MCA_MIP	PCM_MIP
30	1.18	0.78
60	**1.83**	0.82
90	1.27	0.38
120	1.18	0.40
270	1.24	0.35

Similar studies by Fahri et al. (2024) investigated the synthesis of MIPs with magnetite cores for ibuprofen adsorption. The results indicated an optimal contact time of 90 min for maximum adsorption. The results align with the general observation that MIPs often exhibit a rapid initial uptake of the target molecule, followed by a slower approach to equilibrium, which is critical for maximizing adsorption efficiency. The faster saturation of PCM MIPs suggests a difference in the binding site accessibility or affinity compared to the t-4MCA MIPs, this might have been caused by a limited number of binding sites possibly created.

© University of Venda

4.8.5 Effect of initial concentration on t-4MCA adsorption

Figure 33 indicates the adsorption capacity of the t-4MCA MIP, NIP, and PCM in relation to the increasing initial t-4MCA concentration of 0.3 - 10 mg L^{-1} in a 5:5 v/v methanol/water solution. The adsorption capacity increased with rising t-4MCA concentration for both the MIP and NIP. The result is anticipated, as elevated starting concentrations create a stronger force for analyte adhesion to the polymer. Nonetheless, the MIP consistently showed superior adsorption capability than the NIP throughout the full concentration spectrum. The higher adsorption of the MIP verifies the existence of distinct binding sites formed by the imprinting process, which improves t-4MCA absorption relative to the non-specific interactions in the NIP. Table 9 indicates a decrease in the imprinting factor with an increase in concentration, indicating saturation of binding sites. Similar studies by Nadim et al. (2021) highlight this finding. Their study revealed a decline in the response of the imprinted polymer with elevated concentrations of recombinant human erythropoietin, implying that increased concentrations may induce saturation effects that diminish the imprinting factor.

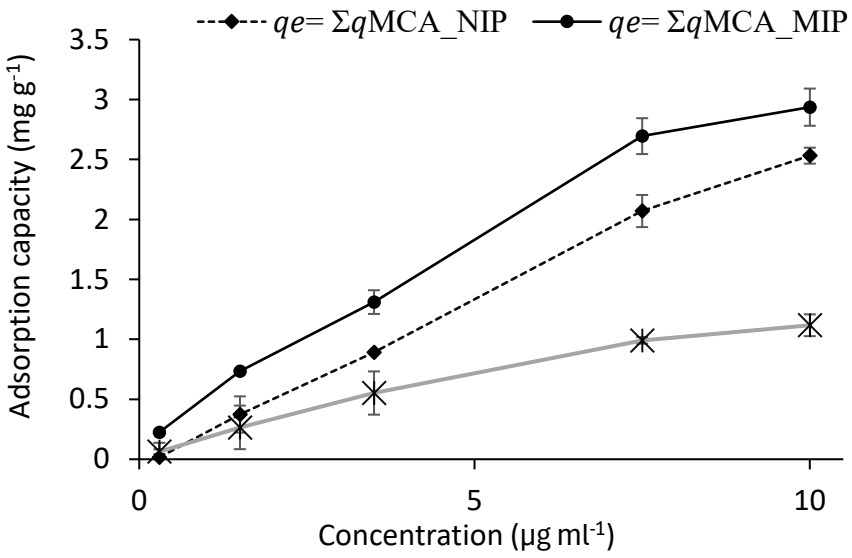


Figure 33: Effect of initial concentration on adsorption capacity. Conditions: polymer mass = 10 mg, H_2O/methanol 5:5 v/v as the eluent, pH 7, time = 60 min (n = 3)

© University of Venda

Table 9: Imprinting efficiency of t-4MCA and PCM MIPs with increasing initial concentration

Concentration (mg g^{-1})	t-4MCA_MIP	PCM_MIP
0.3	----	----
1.5	1.97	0.71
3.5	1.47	0.62
7.5	1.30	1.15
10	1.16	1.07

The PCM exhibited a negligible adsorption capacity, with a slight rise over the concentration range. The result indicated that the PCM lacked the particular binding sites found in the MIP, with its adsorption predominantly influenced by weak, non-specific interactions. Recent research efforts have found a similar trend of enhanced adsorption capability correlating with elevated analyte concentration for MIPs. Qiu et al. (2020) showed that the adsorption capacity of MIPs for sulfamethoxazole significantly increased with increasing analyte concentration, signifying a strong affinity of the imprinted sites for the target molecule. The results correspond with the Langmuir isotherm model, indicating that adsorption occurs at distinct homogenous locations within the polymer matrix. Li et al. (2022) similarly observed that hollow magnetic molecularly imprinted polymers demonstrated a saturation adsorption capacity for gallic acid, which increased with elevated analyte concentrations. The trend highlights the success of MIPs in selectively isolating target molecules from complex matrices.

4.8.5.1 Adsorption isotherms of *t*-4MCA on MIP, NIP, and PCM

The adsorption of t-4MCA onto the synthesized t-4MCA MIP, NIP, PCM was investigated to determine the nature of the binding interactions. The experimental data were fitted to both the Langmuir and Freundlich isotherm models, as the results are shown in Figures 34 and 35 and are summarized in Table 10.

The Langmuir isotherm model, was represented by the linearized equation equation (6):

$$\frac{1}{qe} = \frac{1}{qm} + \frac{1}{KL * qm} * \frac{1}{Ce} \ldots\ldots\ldots\ldots\ldots\ldots\ldots\ldots\ldots\ldots\ldots\ldots (6)$$

© University of Venda

The model makes several assumptions, it assumes a monolayer adsorption on a homogeneous surface with a fixed number of identical binding sites, where qe is the amount of t-4MCA adsorbed (mg g^{-1}), Ce is the equilibrium concentration (mL µg-^{1}), qm is the maximum adsorption capacity (mg g^{-1}) and KL is the Langmuir constant related to binding affinity (mL μg^{-1}) (An et al., 2019). A plot of 1/qe versus 1/Ce yielded a straight line, allowing for the determination of qm and KL.

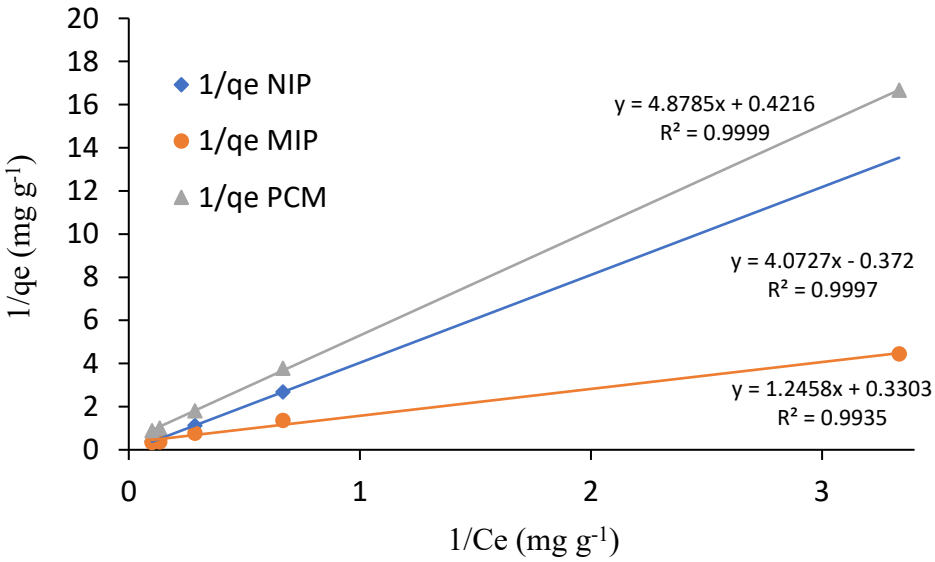


Figure 34: Langmuir linear plot of t-MCA MIP, NIP and PCM MIP

Table 10 displays the Langmuir and Freundlich isotherm parameters for the adsorption of t-4MCA onto MIPs, NIPs, and PCM. The Langmuir model deposits monolayer adsorption on a uniform surface with a limited number of identical adsorption sites. The experimental q values (qexp) 2.94 mg g^{-1} for the MIP, 2.53 mg g^{-1} for the NIP, and 1.12 mg g^{-1} for the PCM align well with the calculated maximum adsorption capacity (qm) derived from the Langmuir model which are 3.00 mg g^{-1} for the MIP, 2.60 mg g^{-1} for the NIP, and 2.40 mg g^{-1} for the PCM, demonstrating a strong correlation between the Langmuir model and the experimental data for all three polymers. The Langmuir constant (KL), in Table 10 is indicative of the affinity between the adsorbate and the adsorbent, is 0.240 mL μg^{-1} for the MIP, 0.150 mL μg^{-1} for the NIP, and 0.137 mL μg^{-1} for the PCM. The elevated KL value for the MIP signifies a greater binding affinity of t-4MCA to the imprinted cavities than the NIP and PCM MIP. The elevated R^2 values (0.9935 - 0.9999) for the Langmuir model signify an excellent fit to the experimental data for all three polymers, indicating that the adsorption of t-4MCA on these materials is primarily monolayer adsorption.

© University of Venda

The Freundlich isotherm model, which describes multilayer adsorption on a heterogeneous surface, is represented in its linearized form as equation (7).

$$\log(qe) = \log(KF) + \left(\frac{1}{n}\right) * \log(Ce) \quad \ldots\ldots\ldots\ldots\ldots\ldots (7)$$

where KF is the Freundlich constant related to adsorption capacity, and 1/n is the Freundlich exponent indicating adsorption intensity (Salahudeen & Alhassan, 2022). A plot of log(qe) versus log(Ce) yielded a straight line, from which KF and 1/n were determined.

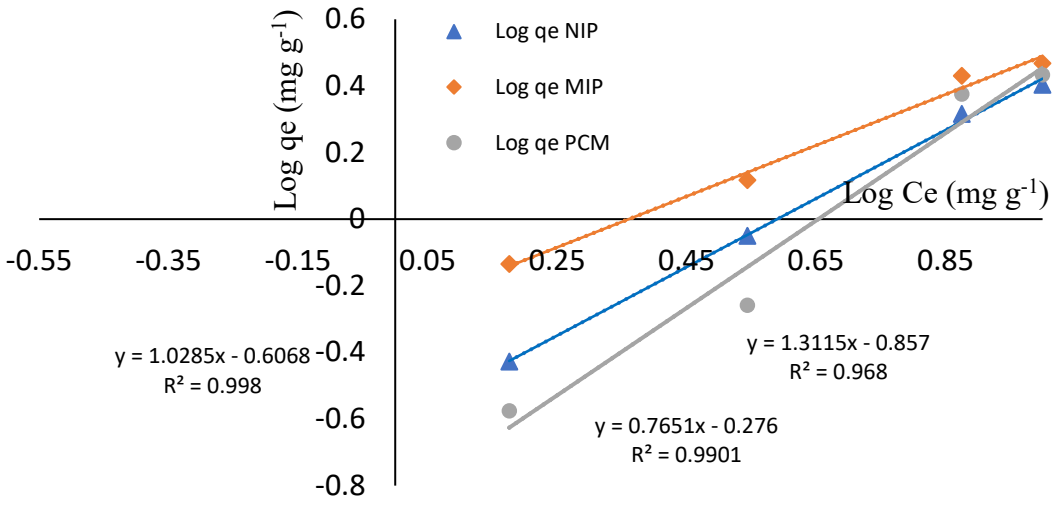


Figure 35: Freundlich linear plot of t-MCA MIP, NIP and PCM MIP

The Freundlich model characterizes multilayer adsorption on a heterogeneous surface exhibiting diverse adsorption energies. The R^2 values for the Freundlich model (0.9680 - 0.9980) suggest a satisfactory fit to the experimental data, albeit marginally inferior to those of the Langmuir model in certain instances. The result indicates that although monolayer adsorption predominates, there may be a certain extent of multilayer adsorption, particularly in the MIP, possibly attributable to the existence of the imprinted cavities

© University of Venda

Table 10: Langmuir and Freundlich isotherm parameters for t-4MCA adsorption

Polymer	Isotherm Model	Parameter	Value	R^2	q - Exp
MIP	Langmuir	q_m (mg g^{-1})	3.000	0.9935	2.94
		KL (mL μg^{-1})	0.240		
	Freundlich	KF	0.530	0.9901	
		n	1.307		
NIP	Langmuir	q_m (mg g^{-1})	2.600	0.9997	2.53
		KL (mL μg^{-1})	0.150		
	Freundlich	KF	0.248	0.9980	
		n	0.970		
PCM	Langmuir	q_m (mg g^{-1})	2.400	0.9999	1.12
		KL (mL μg^{-1})	0.137		
	Freundlich	KF	0.139	0.9680	
		n	0.762		

4.9 Selective adsorption and competitive evaluation of t-4MCA

Investigations to determine the selectivity of the synthesized t-4MCA MIPs and NIPs on the analogues, ferulic acid, t-4HCA, Et-MOPA individually and in competition with the t-4MCA analyte as binary solutions were conducted. The method's performance was evaluated using linearity, limits of detection (LOD), limits of quantification (LOQ), dynamic linear range and adsorption capacity of optimized parameters. The optimized conditions were 10 mg L^{-1} of analyte and 10 mg polymers as the mass of sorbent at pH 7 for a time of 60 min in a 5:5 v/v solution of methanol and water. The linearity was determined from calibration curves prepared by varying analyte concentrations as in Figure 36. Quantification of the analytes, ferulic acid, t-4MCA, t-4HCA, and Et-MOPA was calculated using the internal standard method from the ratio of the standard peak area of the analyte to that of the internal standard. A Summary of the parameters found are presented in Table 11.

© University of Venda

Excellent linearity in the range 0.01 – 50 mg L^{-1} was obtained from calibration curves as in Figure 36 with a correlation coefficient ranging from 0.9983 - 0.9992 as indicated in Table 11. The results indicated a strong linear relationship between analyte concentration and detector response within the tested range, validating the method's suitability for quantitative analysis. The LOD range was from 0.04834 - 0.06033 mg L^{-1}, demonstrating the method's sensitivity for detecting low analyte concentrations, and the LOQ range was from 0.14649 - 0.18283 mg L^{-1}, confirming the method's ability to quantify the analytes at low concentrations accurately. The values are sufficiently low for the intended application and indicated the method's reliability for trace analysis. The adsorption capacities of the t-4MCA MIP and the corresponding NIP were evaluated individually and in binary mixtures for t-4MCA, ferulic acid, t-4HCA, and Et-MOPA. The results, expressed as the percentage of analyte adsorbed from a 10 mg L^{-1} solution, are presented in Table 12 and Figure 37. The kd, k and k` values are presented in Table 13.

Table 11: Parameters for the method validation of five phenolic acids

Analyte	Matrix fitted modelling	R^2	LOD (mg L^{-1})	LOQ (mg L^{-1})	Linear range
t-4MCA	y = 1.8324 x - 5E-05	0.9992	0.06023	0.18251	0.01 - 50
Ferulic acid	y = 0.6537 x + 0.0052	0.9983	0.04834	0.14649	0.01 - 50
t-4HCA	y = 1.5414 x + 0.0141	0.9989	0.06033	0.18283	0.01 - 50
Et-MOPA	y = 1.5391 x + 0.0027	0.9990	0.05777	0.17506	0.01 - 50

© University of Venda

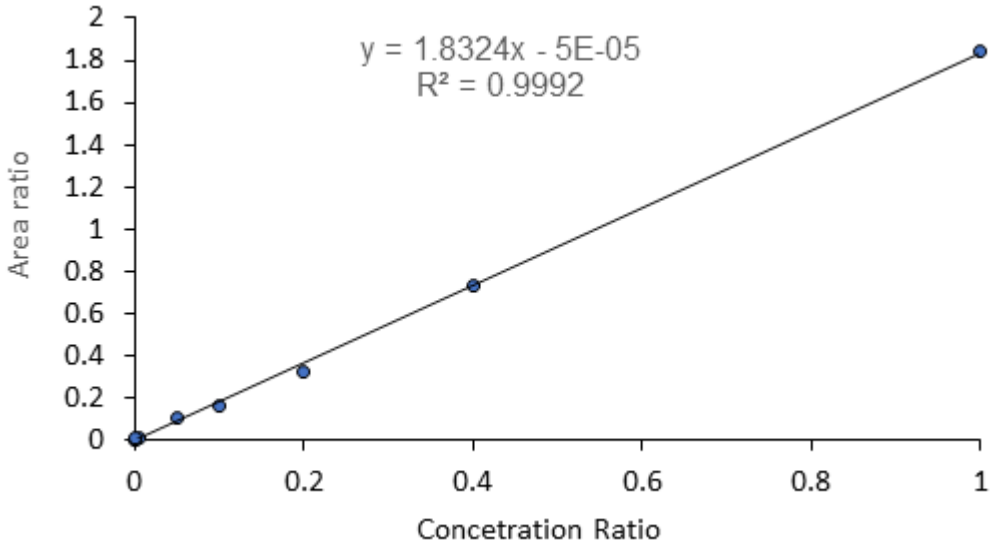


Figure 36: Calibration curve of trans-4-methoxy cinnamic acid

4.9.1 Selectivity studies, binding of t-4MCA and structural analogs

To evaluate the selectivity of the synthesized t-4MCA MIP, batch binding experiments were performed using t-4MCA and three structural analogs, ferulic acid, t-4HCA and Et-MOPA. The experiments were conducted to assess the MIP's ability to discriminate between the template molecule and compounds with varying degrees of structural similarity. A NIP was used as a control to determine the extent of non-specific binding. The results, expressed as % analyte adsorbed, are presented in Figure 37 and Table 12.

As expected, the MIP exhibited significantly higher adsorption of the template molecule, t-4MCA (65.50 ± 1.2%), compared to the NIP (36.29 ± 0.5%). The results confirmed the successful creation of specific binding sites within the MIP. The high kd value for the MIP (759.53) compared to the NIP (227.83) further supports this. The MIP also showed appreciable adsorption of ferulic acid (44.13 ± 0.65%), significantly greater than the NIP (12.51 ± 0.13%). The obtained results suggest that the MIP, while imprinted for t-4MCA, also exhibits some affinity for the structurally similar ferulic acid. The kd values (315.98 for MIP, 33.74 for NIP) reflect this difference in affinity. Ferulic acid differs from t-4MCA by possessing an additional methoxy group at the 3-position of the benzene ring, hence the difference in adsorption. Adsorption of t-4HCA was also higher on the MIP (52.89 ± 0.2%) than on the NIP (44.08 ± 0.12%), although the difference was less pronounced than for t-4MCA or ferulic acid. Finally, the MIP showed slightly higher adsorption of Et-MOPA (9.35 ± 0.11%) compared to the NIP (4.82 ± 0.10%) but the lowest percentage of

© University of Venda

all analogues. The results suggested that Et-MOPA has the weakest interaction with the t-4MCA MIP among the tested analogues, likely due to greater structural differences from the template. The lower kd values (41.28 for MIP, 20.24 for NIP) confirm this. The t-4MCA MIP exhibited an affinity for the structural analogues, with the order of affinity being t-4MCA > t-4HCA > ferulic Acid > Et-MOPA in single-analyte solutions.

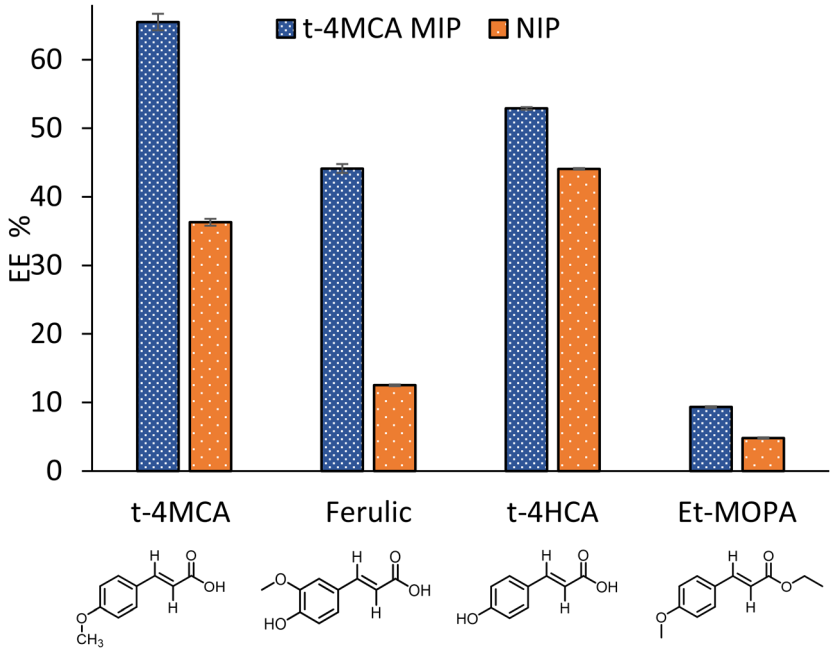


Figure 37: Selectivity of t-4MCA MIP and NIP for t-4MCA and its structural analogs

4.9.2 Competitive binding of t-4MCA and structural analogs

The presence of competing analytes significantly altered the adsorption profiles. In the t-4MCA/ferulic acid binary mixture. The MIP's adsorption of t-4MCA decreases significantly in the presence of ferulic acid (from 65.50% to 47.48%). The NIP's adsorption of t-4MCA is almost the same as the MIP (46.35%), this means the selectivity for t-4MCA is almost completely lost in the presence of ferulic acid. Ferulic acid is effectively competing with t-4MCA for binding sites, this could possibly be a result of steric hindrance. The extra -OH group on ferulic acid might cause steric hindrance within the imprinted cavity, preventing optimal binding when t-4MCA is also present. While both have carboxylic acid groups, ferulic acid, due to the OH group, is more hydrophilic and has different hydrophobic interaction.

© University of Venda

The MIP's adsorption of ferulic acid is quite low (13.00%) compared to the single-analyte experiment (44.13%). The NIP adsorption is slightly higher (14.82%) than the MIP. The above crucial finding suggested that in the mixture, the NIP binds ferulic acid slightly better than the MIP. The findings suggest that the MIP's binding sites, when presented with both t-4MCA and ferulic acid, are preferentially occupied by t-4MCA, leaving ferulic acid to bind non-specifically and even slightly better in the NIP. The selectivity factor (k = 2.40) as seen in Table 13 indicated that the MIP still showed some preference for t-4MCA over ferulic acid. The k' (0.356) value however, reveals that the NIP demonstrates better selectivity in this scenario. The results suggest that this is likely because the NIP has fewer, less specific binding sites overall.

In the t-4MCA/t-4HCA mixture t-4MCA MIP adsorption of t-4MCA is significantly reduced (27.78%) compared to single and ferulic solution. The NIP adsorption is very low (0.93%). The relative selectivity (k' = 2.34) shows that the MIP retains a preference for t-4MCA over t-4HCA, even with the reduced overall adsorption, this is the highest selectivity shown in the competition, where t-4HCA MIP is (17.85%).

For the t-4MCA/ Et-MOPA mixture, t-4MCA MIP adsorption is significantly reduced (17.15%) compared to the other solutions. Et-MOPA MIP adsorption (47.24%) is almost identical to NIP (46.34%). While t-4MCA adsorption decreases due to competition, Et-MOPA adsorption is much higher than when it was the sole analyte. The high selectivity factor (k = 18.40) indicated a strong preference of the MIP for t-4MCA over Et-MOPA, despite the high Et-MOPA adsorption percentage. The fact that both MIP and NIP showed high Et-MOPA adsorption in the mixture suggests a possible interaction between t-4MCA and Et-MOPA that enhances Et-MOPA's binding to both polymers.

While the t-4MCA MIP shows a degree of cross-reactivity with structural analogues, it retains a significant preference for the target molecule, t-4MCA, as evidenced by its consistently higher adsorption than the NIP in all competitive scenarios.

© University of Venda

University of Venda
Creating Future Leaders

Table 12: Concentration (%) of analytes adsorbed by polymers from individual analytes of 10 mg L^{-1} and binary solution (n = 3)

	% t-4MCA adsorbed		% Ferulic acid adsorbed		% t-4HCA adsorbed		% Et-MOPA adsorbed	
	MIP	NIP	MIP	NIP	MIP	NIP	MIP	NIP
t-4MCA	65.50 (1.20)	36.29 (0.5)	–	–	–	–	–	–
Ferulic acid	–	–	44.13 (0.65)	12.51 (0.13)	–	–	–	–
t-4HCA	–	–	–	–	52.89 (0.20)	44.08 (0.12)	–	–
Et-MOPA	–	–	–	–	–	–	9.35 (0.11)	4.82 (0.10)
t-4MCA / Ferulic acid	47.48 (0.25)	46.35 (0.09)	13.00 (0.40)	14.82 (0.15)	–	–	–	–
t-4MCA / t-4HCA	27.78 (1.54)	0.93 (2.0)	–	–	17.85 (1.57)	5.79 (0.57)	–	–
t-4MCA / Et-MOPA	17.15 (0.14)	12.82 (0.19)	–	–	–	–	47.24 (0.13)	46.34 (0.15)

Table 13: kd, k and k' for individual analytes and the mixtures of 10 mg L^{-1} each solution couples

	kd		k		k'	
Analytes	MIP	NIP	MIP	NIP	MIP	NIP
t-4MCA	759.53	227.83	–	–	–	–
Ferulic acid	315.98	33.74	–	–	–	–
t-4HCA	449.13	315.28	–	–	–	–
Et-MOPA	41.28	20.24	–	–	–	–
Mixture of t-4MCA / Ferulic acid	–	–	2.40	6.75	0.356	–
Mixture of t-4MCA / t-4HCA	–	–	1.69	0.72	2.340	–
Mixture of t-4MCA / Et-MOPA	–	–	18.40	11.25	1.635	–

© University of Venda

Part B

4.10 Photoisomerization of t-4MCA to generate c-4MCA and t-4MCA mixture

To investigate the photoisomerization behavior of t-4MCA and determine the optimal conditions for generating a mixture of *cis* and *trans* isomers, a series of irradiation experiments were conducted using a 254 nm UV lamp. The *cis/trans* mixture is necessary for subsequent MIP studies, comparing binding affinities. The goal was to maximize the formation of c-4MCA while minimizing potential degradation. Solutions of t-4MCA in methanol 10 mg L^{-1} were irradiated in quartz tubes using a 254 nm UV lamp for a total of 12 h, with samples taken at preset times (0, 1,3, 6 and 12 h). Results are presented in Table 14 and Figure 38

Table 14: Photoisomerization of t-4MCA to *cis/trans* ratios at different irradiation time

Irradiation time (h)	% t-4MCA	% c-4MCA	*trans*/*cis* ratio
0	100	0	-
1	94.06	5.94	15.8
3	70.87	29.13	2.4
6	51.79	48.21	1.1
12	39.47	60.53	0.7

At time zero, the sample consisted of essentially pure t-4MCA (100%). Upon irradiation, the percentage of c-4MCA increased progressively, reaching 60.53% after 12 h. Correspondingly, the *trans*/*cis* ratio decreased from 15.8 to 0.7 at 12 h, indicating a predominance of the *cis* isomer at this point. The data reveal a rapid initial conversion to c-4MCA within the first 3 h, followed by a slower rate of isomerization at longer irradiation times. The behavior is typical of photochemical *trans-cis* isomerizations, where a photostationary state is approached as the irradiation time increases (Homma et al., 2023; Jeon et al., 2023). Based on these results, an irradiation time of 6 h provides a near 1:1 mixture of *trans* and *cis* isomers (51.79% t-4MCA and 48.21% c-4MCA, *trans*/*cis* ratio = 1.1). The mixture is suitable for subsequent MIP studies where a comparison of binding affinities for both isomers is desired. While 12 h of irradiation produces a higher proportion of c-4MCA, the increased risk of photodegradation makes the 6-h time point a more optimal choice.

© University of Venda

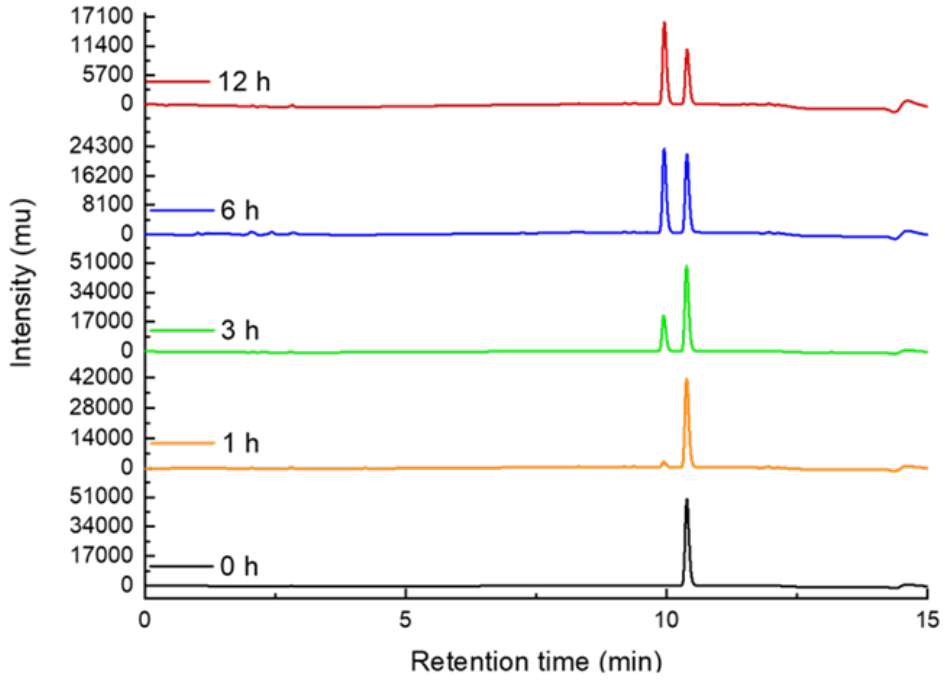


Figure 38: HPLC chromatograms showing the photoisomerization of t-4MCA to c-4MCA over time.

Close examination of the HPLC chromatograms Figure 38 and the total integrated peak areas for the 4-MCA isomers reveal evidence of photodegradation, particularly at longer irradiation times. Although pre*cis*e quantification of degradation products was not performed, a noticeable decrease in the combined peak area of t-4MCA and c-4MCA was observed at 12 h compared to earlier time points. Furthermore, several minor, unidentified peaks appeared in the chromatograms at 12 h, which were not present in the initial t-4MCA solution.

These observations suggested that, in addition to the desired *trans-cis* isomerization, competing photodegradation pathways become significant at extended irradiation times (Yağcı et al., 2021). Cinnamic acid derivatives are known to be susceptible to various photochemical reactions, including dimerization, decarboxylation, and oxidation (Chandra et al., 2019; Lubbers et al., 2019; Rahman et al., 2024).

© University of Venda

4.11 Selective extraction of *trans*-4-MCA from *cis/trans* mixtures using MIPs

To evaluate the t-4MCA MIPs capacity for selective extraction of *trans*-4MCA from complex mixtures, batch binding experiments were conducted utilizing pre-irradiated 4-MCA solutions with specified *cis/trans* ratios. Three distinct mixtures were utilized, each reflecting varying initial compositions: Mixture A (39.12% *trans*, 60.88% *cis*), Mixture B (49.64% *trans*, 50.36% *cis*), and Mixture C (59.80% *trans*, 40.20% *cis*). The evaluation of MIP performance in conditions pertinent to real-world scenarios involving isomeric mixtures was enabled by the method design. The findings, encompassing calculated distribution coefficients (kd), selectivity coefficients (k and k'), and statistical significance, are detailed in Table 15 and illustrated in Figure 39.

Table 15: Concentration (%) of analyte adsorbed, kd, k and k` of polymers from an adsorbed 10 mg L^{-1} solution irradiated to varying percentages of initial c-4MCA and t-4MCA couples.

		Mixture A		Mixture B		Mixture C	
		39.12% *trans*	60.88% *cis*	49.64% *trans*	50.36% *cis*	59.80% *trans*	40.20% *cis*
MIP		30.09	42.05	35.49	32.87	25.96	19.41
NIP		27.77	41.81	31.33	28.49	21.64	15.36
kd	MIP	172.18	290.25	220.04	195.84	140.22	96.36
	NIP	153.79	287.38	182.49	159.39	110.50	72.59
k	MIP	0.59		1.12		1.46	
	NIP	0.54		1.15		1.52	
k'		1.12		1.21		1.27	

In Mixture A, which was initially *cis*-rich, the MIP removed a higher percentage of the *cis* isomer (42.05%) than the *trans* isomer (30.09%). The distribution coefficients, kd (*cis*) = 290.25 and kd (*trans*) = 172.18, also indicated a greater affinity for the *cis* isomer under these conditions. The results suggested the presence of binding sites that, while perhaps originally intended for *trans*, can also accommodate *cis*, or that the high *cis* concentration outcompetes *trans* for binding sites. However, in Mixture B, with a nearly 1:1 *trans*: *cis* ratio, the MIP removed a slightly higher percentage of the *trans* isomer (35.49%) than the *cis* isomer (32.87%), suggesting a shift in selectivity. The kd values reflect this shift, (*trans*) = 220.04 and kd (*cis*) = 195.84, indicating a slight preference for the *trans* isomer. The results suggested that when the isomers are present in roughly equal amounts, the imprinted cavities designed for *trans* do exert a detectable selective effect. In Mixture C, initially *trans*-rich, the MIP again removed a greater percentage of the *trans* isomer

© University of Venda

(25.96%) compared to the *cis* isomer (19.41%). The kd values support this, kd (*trans*) = 140.22 and kd (*cis*) = 96.36. The MIP again shows a preference for binding and removing the *trans* isomer, further supporting the presence of *trans*-selective binding sites. The NIP also adsorbed both isomers, but with consistently lower kd values compared to the MIP, with Mixture B, kd (*trans*) = 182.49, kd(*cis*) = 159.39; Mixture C, kd (*trans*) = 110.50, kd (*cis*) = 72.59. The relative selectivity coefficient (k'), comparing MIP to NIP selectivity, was greater than 1 for all mixtures, confirming that the imprinting process enhanced selectivity, although the direction of that selectivity varied with the initial isomer ratio.

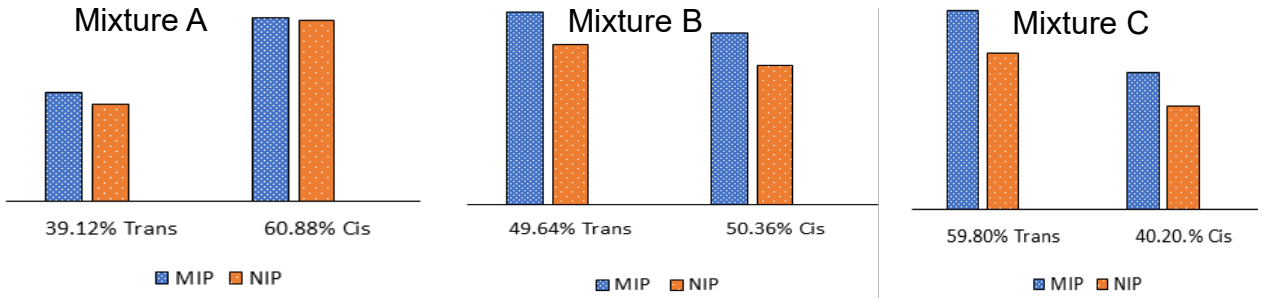


Figure 39: Graphical representation of the adsorbed percentage of t-4MCA in three *cis/trans* isomeric ratio mixtures

The *trans*-4MCA imprinted MIP exhibited a complex and concentration-dependent selectivity profile for *cis* and *trans* isomers of 4-MCA. While the MIP was designed to preferentially bind the *trans* isomer, its actual behavior is influenced by the initial *cis*/*trans* ratio of the mixture. The results were a crucial finding, as they suggested that the MIP's performance in a real-world application (e.g., purifying a reaction mixture) will depend on the isomeric composition of that mixture.

© University of Venda

4.12 Photoisomerization of t-4MCA in the presence of t-4MCA MIP, NIP with a control sample

Batch binding experiments were conducted to investigate the influence of t-4MCA MIPs on the photoisomerization equilibrium of t-4MCA analyte. Aliquots of t-4MCA solution were irradiated in the presence of t-4MCA-imprinted MIP, a corresponding NIP and a control sample without any polymer. The reactions were carried out in sealed quartz tubes under UV irradiation (254 nm) for 3 h, with additional samples analyzed after 12 h. The isomeric composition of the supernatant was determined by HPLC analysis. Results are illustrated in Table 16 and Figures 40 and 41.

Table 16: Isomer concentrations (mg L^{-1}) and degradation of 4-MCA from 0-12 h of irradiation in the presence of t-4MCA MIP and NIP.

Polymer	c-4MCA	t-4MCA	Total 4-MCA	Degradation	% c-4MCA	% t-4MCA
NIP 3 h	4.88	2.75	7.62	0.59	63.98	36.02
MIP 3 h	5.24	2.43	7.66	0.55	68.33	31.67
Ctrl 3 h	2.35	5.40	7.76	0.45	30.34	69.66
NIP 12 h	3.13	3.43	6.56	1.65	47.72	52.30
MIP 12 h	4.38	2.31	6.69	1.52	65.47	34.53
Ctrl 12h	3.31	2.58	5.89	2.32	56.20	43.80
Initial			8.21	0.00		

After 3 h, a control sample (no polymer) reached a *cis/trans* ratio of approximately 30.34% *cis* and 69.66 % *trans*. As seen in Table 16 and Figure 40, the introduction of the MIP shifted this equilibrium markedly, resulting in a solution containing 68.33% *cis* and 31.67% *trans* isomer, representing a 37.99 percentage point increase in the *cis* isomer proportion compared to the control. The NIP also promoted the *cis* form, reaching 63.98% *cis* and 36.02% *trans*, but this increase (33.64 percentage points compared to the control) was less pronounced than that observed with the MIP.

© University of Venda

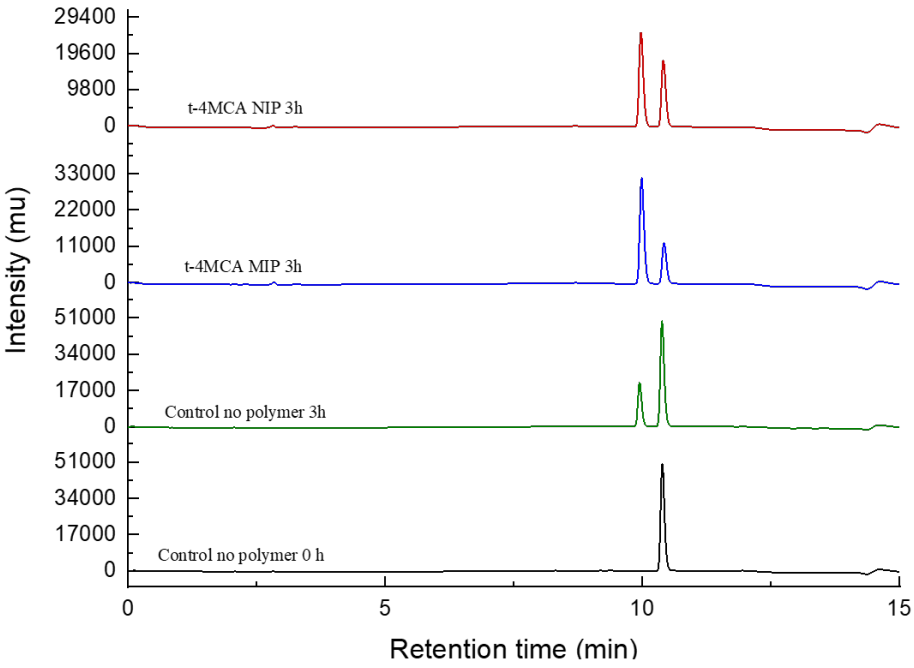


Figure 40: 3 h HPLC chromatogram of t-4MCA with MIP, NIP, and the control

On extending the photoirradiation to 12 h as depicted in Figure 41, the control sample's *cis/trans* ratio reached 56.18% *cis* and 43.82% *trans* composition. The MIP-treated sample at 12 h contained 65.43% *cis* and 34.57% *trans* isomer, a 9.25 percentage point increase compared to control. The NIP sample in the 12 h sample exhibited 47.72% and 52.30% in *cis* and *trans*, respectively, and a 8.46 decrease of percentage points in *cis*, compared to the 12 h control and a 8.48% increase in the *trans*. The results demonstrated that while the MIP and NIP influence the photoisomerization equilibrium, the MIP exerts a considerably stronger and more persistent effect, favoring the formation of the *cis* isomer of 4-MCA, even over longer irradiation periods whilst the NIP exhibited a disfavoring of the *cis* and favoring the *trans* formation.

© University of Venda

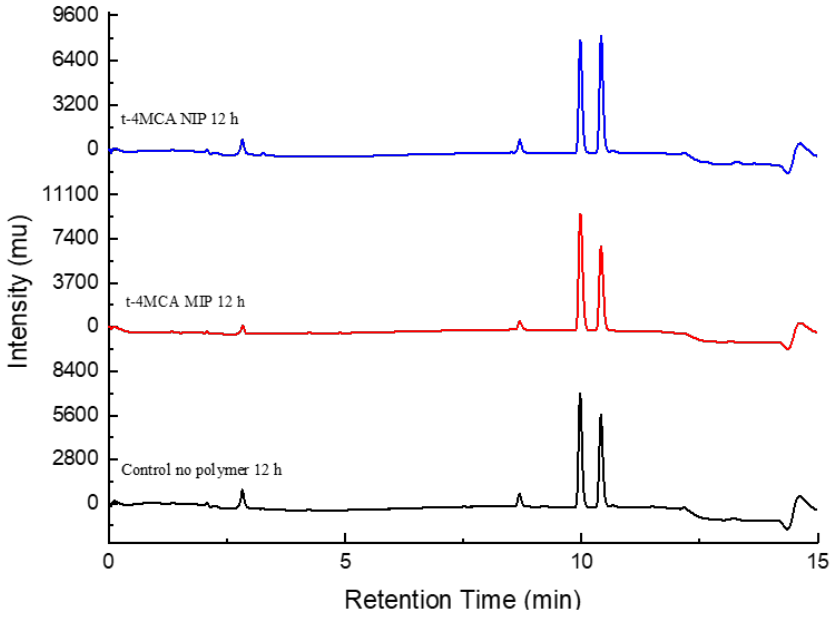


Figure 41: 12 h HPLC chromatogram of t-4MCA with MIP, NIP, and the control

4.12.1 Kinetic analysis of photoisomerization

Figure 42 and Figure 43 present the time-dependent evolution of the *cis* and *trans* isomer percentages in the presence of the t-4MCA MIP and NIP. It is noteworthy that the initial rate of *trans*-to-*cis* conversion is faster in the presence of the MIP and NIP than in the control. The observation is likely due to initial weak and non-specific interactions for t-4MCA analyte to both isomers at times below its optimum absorption time between 1h to 2 h. The non-specific interaction likely increased the local concentration of t-4MCA onto the polymer surface, potentially enhancing the absorption of UV light and accelerating the reaction. The phenomenon, although not a true catalytic effect, is sometimes observed with polymeric materials in photochemical reactions.

© University of Venda

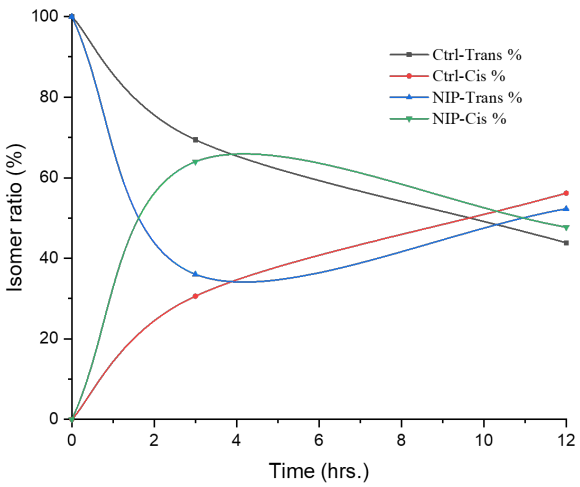


Figure 42: Effect of NIP on t-4MCA photoisomerization kinetics

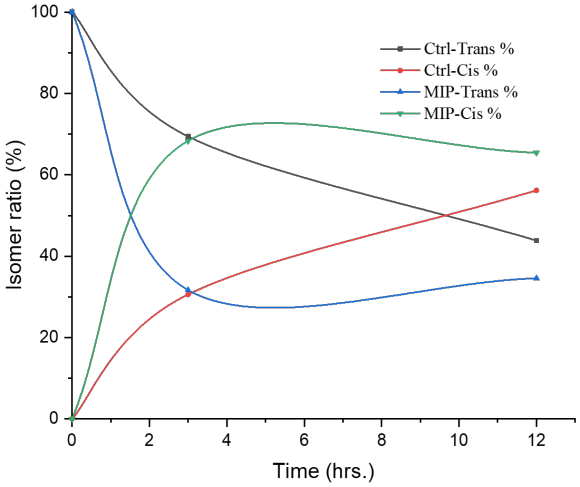


Figure 43: Effect of MIP on t-4MCA photoisomerization kinetics

4.12.2 Equilibrium shift and isomer selectivity

The MIP ultimately leads to a significantly higher proportion of the *cis* isomer at both 3 and 12 h compared to both the control and the NIP (Table 16, Figures 40 and 43). After 3 h, the MIP sample contained 68.41% *cis*-4MCA, while the control and NIP samples contained 30.28% and 64.04% *cis*-4-MCA, respectively.

The key finding demonstrates that the MIP is not simply influencing the reaction rate; it is shifting the thermodynamic equilibrium of the photoisomerization. The equilibrium shift is attributed to the selective binding and subsequent isomerization within the MIP cavities. While the *trans* isomer was preferentially bound, the confined environment and specific interactions within the imprinted sites likely lowered the activation energy for the *trans*-to-*cis* conversion of the bound molecule. Once formed, the *cis* isomer, having a lower affinity for the binding site due to its altered geometry, is more readily released into solution.

The 12 h data further corroborates the equilibrium shift. Importantly, careful examination of Figures 41, 43 and Table 16 reveal a critical detail, at 12 h, the MIP sample maintains a higher *cis* percentage (65.47%) than both the control (56.20%) and, crucially, the NIP (54.57%) conclusively demonstrated that the MIP effect is not merely a kinetic acceleration, it is a true thermodynamic shift in favour of the *cis* isomer. The *trans* percentage in the MIP sample (34.53%) is lower than both the Control (43.80%) and the NIP (45.43%). This persistent difference at extended reaction times where all samples have had ample

© University of Venda

opportunity to reach equilibrium, is strong evidence for the MIP's selective stabilization of the *cis* isomer. Figure 43 visually confirms this in the chromatograms, the *cis* peak is noticeably larger than the *trans* for the MIP. It can be noticed as well that both are significantly larger than the NIP and the control, supporting the conclusion of reduced degradation.

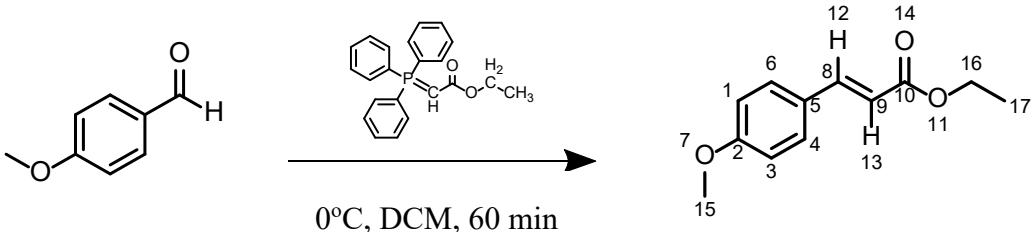
The t-4MCA MIP demonstrated a significant and selective effect on the photoisomerization of t-4MCA, shifting the equilibrium towards the *cis* isomer by lowering the activation energy resulting from the cavity interaction with the template. This is in contrast to the NIP, which initially accelerates the reaction but ultimately leads to a slightly lower *cis* isomer than the control at longer reaction times. This is due to NIPs weak non-specific binding only acting as sequestrating agent for the *trans* isomer hence shifting the equilibrium towards the formation of the *trans* isomer.

Table 1 also provides data on the degradation of 4-MCA. All samples show a decrease in total 4MCA concentration over time, indicating that UV irradiation leads to some decomposition. Notably, the degradation is less pronounced in the MIP and NIP samples at 3 h compared to the control, suggesting a possible protective effect of the polymers against photodegradation. This observation can be visually confirmed in Figure 42. At 12 h, all samples show significant degradation, but even then the relative percentages of the isomers and the chromatograms (Figure 43) support the MIP's selectivity.

Similarly, in supramolecular chemistry, host-guest complexation has been used to control reaction pathways (Long et al., 2024; Xin-Kun Ma & Liu, 2021; Wu et al., 2021). Our findings demonstrated a similar effect, but using a synthetic polymer (the MIP) to achieve stereo-control. The observed *cis* enrichment, while counterintuitive to the initial expectation of *trans* enrichment based solely on the template, highlights a potentially valuable application of MIPs, indirectly isolating a less-favored isomer by selectively removing its more stable counterpart.

© University of Venda

4.13 Synthesis of ethyl (E)-3-(4-methoxyphenyl) acrylate using the Wittig reaction (8)



Scheme 1: Synthesis of ethyl (E)-3-(4-methoxyphenyl) acrylate

Ethyl (E)-3-(4-methoxyphenyl) acrylate was synthesized as in scheme 1 using commercially available 4-methoxy benzaldehyde and a synthesized ylied ethyl 2-(triphenylphosphoranylidene) acetate at 0 ºC in dichloromethane as a solvent for 60 min. The reaction was monitored using a TLC plate as seen Figure 44 which indicated that the reaction takes longer than 10 min, at 24 min the reaction was still continuing as can be observed, the Rf value of ethyl (E)-3-(4-methoxyphenyl) acrylate was 0.88 with 50/50% ethyl acetate and petroleum ether. After the workup, 580 mg of pale-yellow oil was obtained and was of adequate purity for analysis by ^{1}H NMR, ^{13}C NMR, and IR.

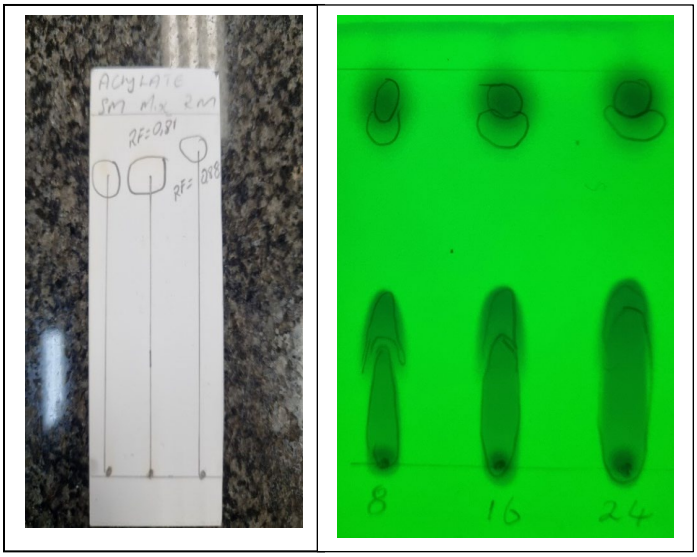


Figure 44: TLC visualization of Wittig reaction progress of the synthesis of ethyl (E)-3-(4-methoxyphenyl) acrylate from 4-methoxy benzaldehyde

© University of Venda

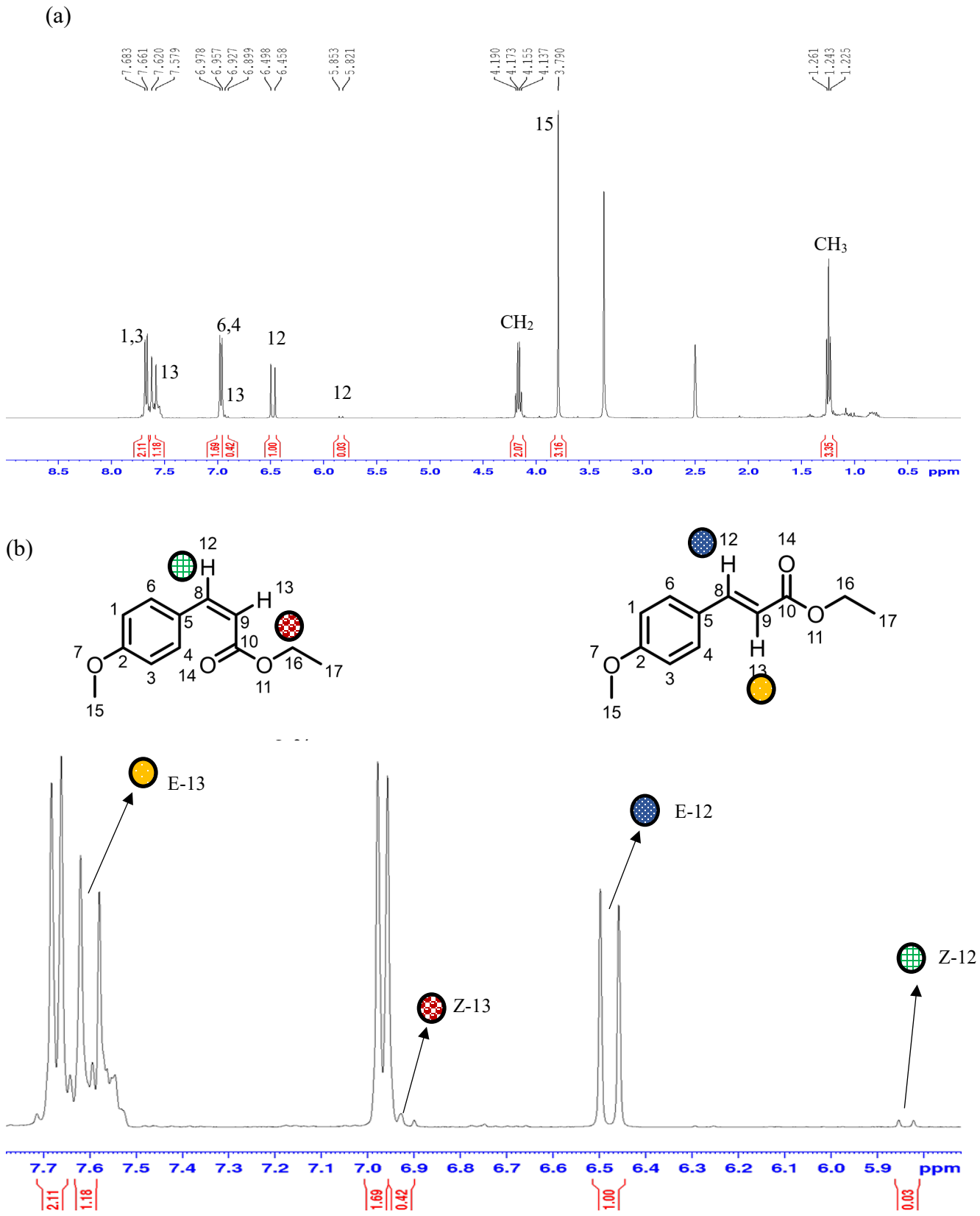
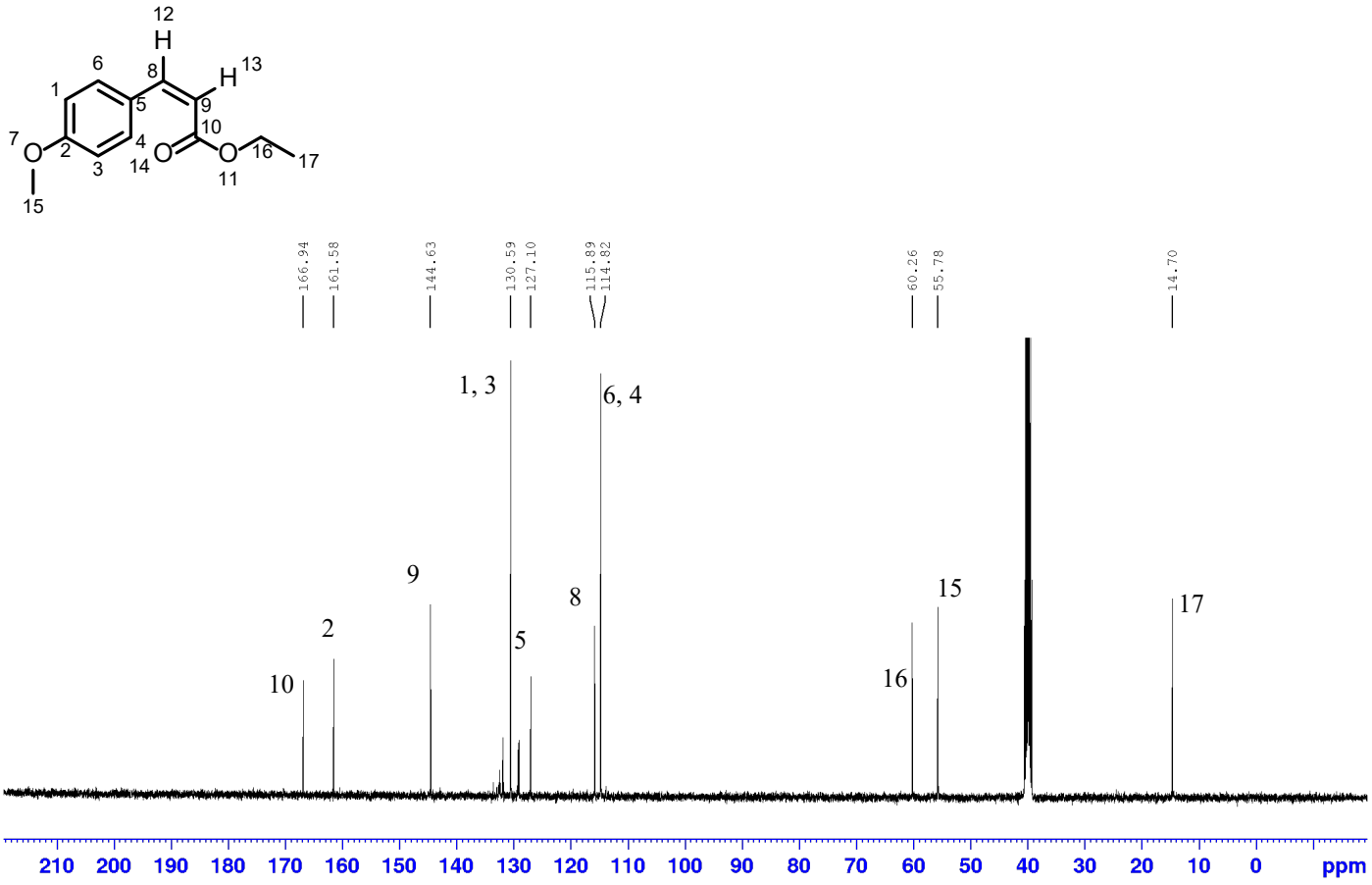


Figure 45: ^{1}H NMR spectrum (a) aromatic expansion (b) of ethyl (E)-3-(4-methoxyphenyl) acrylate as synthesized according to scheme 1

© University of Venda

Figure 45 presents the ^{1}H NMR spectrum of ethyl (E)-3-(4-methoxyphenyl) acrylate , obtained in DMSO. The spectrum exhibit a characteristic pattern of signals confirming the successful formation of the conjugated ester and providing detailed information about its stereochemistry and purity. The aromatic region (δ 6.9-7.7 ppm) displayed characteristic signals for a para-substituted benzene ring, with integrated areas consistent with the assigned structure, although with slight deviations due to signal overlap. The alkene region featured two doublets, one at δ 6.48 ppm (J = 16 Hz, 1.00H) and one obscured within the aromatic signals around δ 7.6 ppm (J =16Hz), these definitively establish the *trans* (E) configuration. A minor *cis* (Z) isomer is identified by a small doublet at δ 5.8 ppm (J = 12.8 Hz, 0.03H). The methoxy singlet (δ 3.79 ppm, 3.16H) and ethyl ester signals (δ 4.17 ppm, q, ~7 Hz, 2.02H; δ 1.24 ppm, t, ~7 Hz, 3.38H) are also present and consistent with the structure. The integration ratio of the major and minor alkene signals confirms a 97:3 *trans/cis* ratio (approximately). The spectrum, therefore, demonstrated the successful and highly E-stereoselective synthesis of the target compound in high purity.

(a)



© University of Venda

(b)

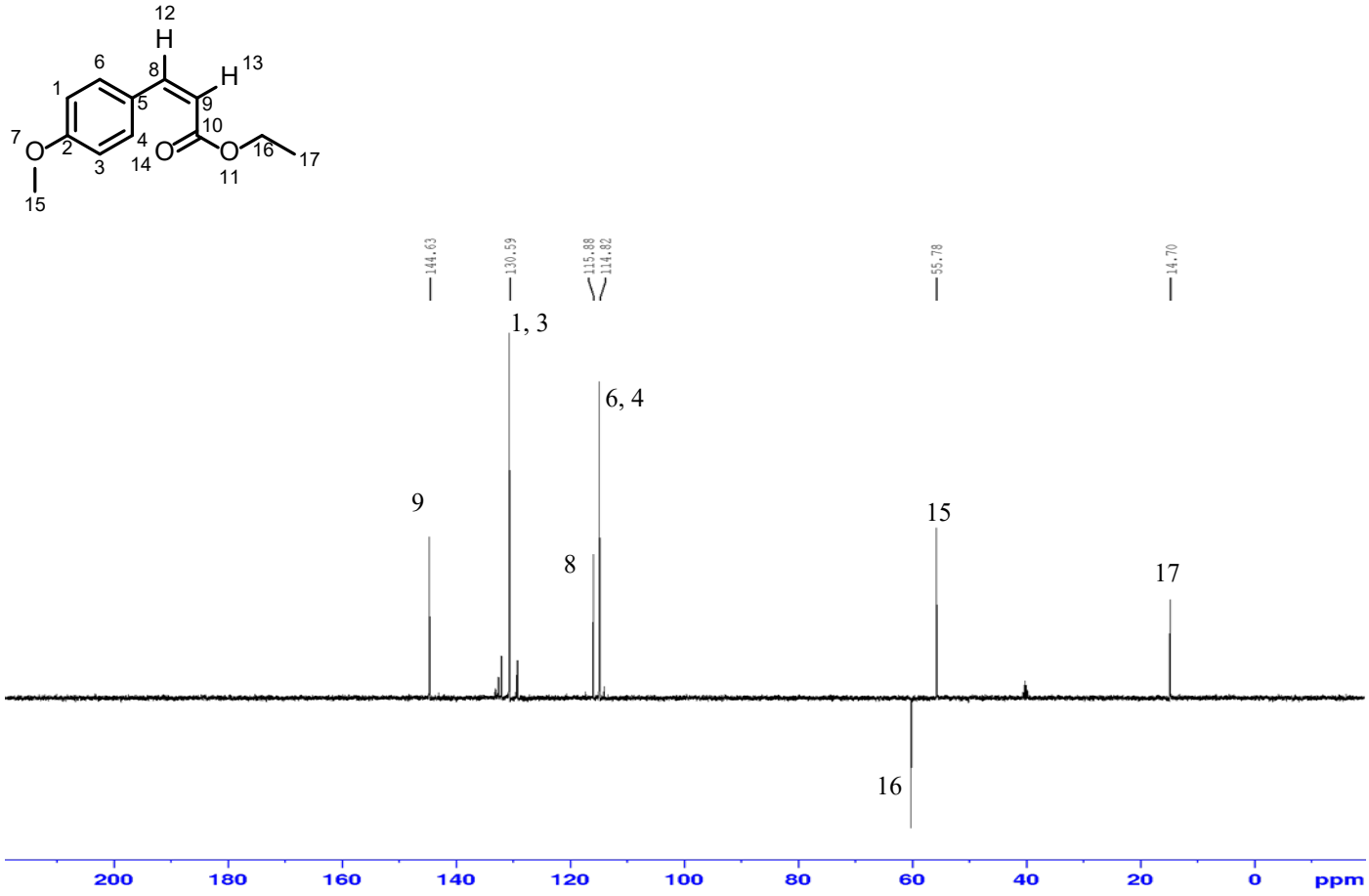


Figure 46: ^{13}C NMR spectrum (a) DEPT-135 NMR spectrum (b) of ethyl (E)-3-(4-methoxyphenyl) acrylate as synthesized according to scheme 1

Figure 46 presents the DEPT-135 and ^{13}CNMR spectrum of ethyl (E)-3-(4-methoxyphenyl) acrylate, confirming the carbon types and supporting the assigned structure. Positive signals CH and CH_3 were observed at δ 144.63 (alkene CH), 130.59 (aromatic CH), 115.88 (alkene CH), note its proximity to another signal, 114.82 (aromatic CH), 55.78 (methoxy CH_3) and 14.70 (ethyl CH_3) ppm. A negative signal (CH_2 at δ 60.26 ppm) identifies the ethyl ester CH_2. The DEPT-135 data, combined with the ^{1}H and standard ^{13}C NMR, confirmed the successful synthesis of ethyl (E)-3-(4-methoxyphenyl) acrylate.

© University of Venda

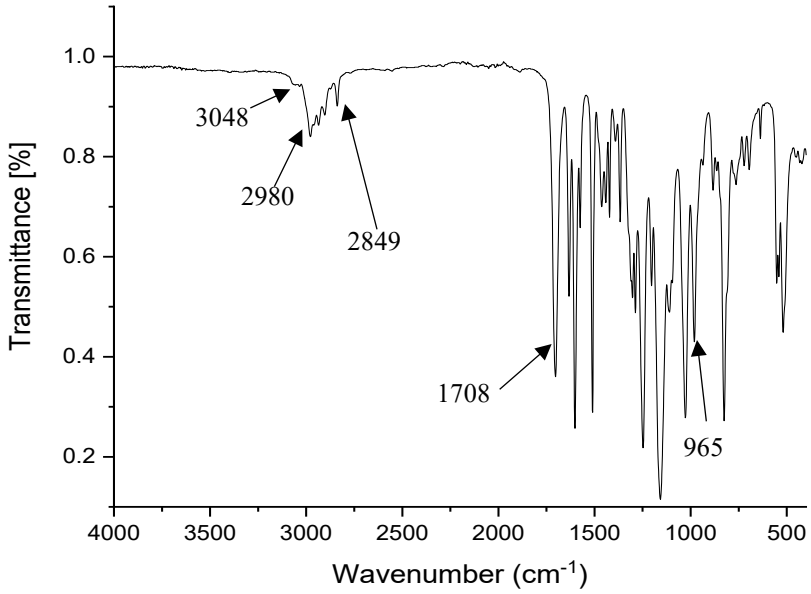


Figure 47: FTIR spectrum of ethyl (E)-3-(4-methoxyphenyl) acrylate

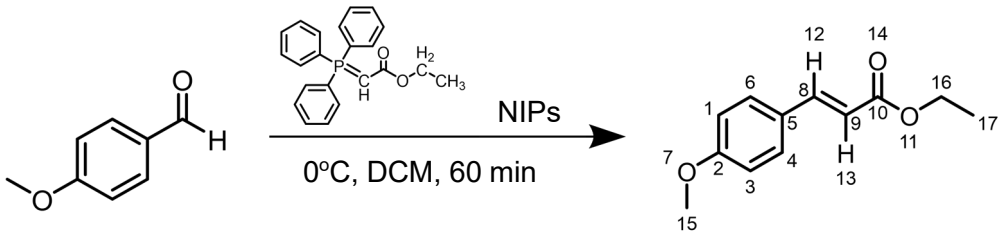
The FTIR spectrum (Figure 47) of ethyl (E)-3-(4-methoxyphenyl) acrylate confirmed the presence of expected functional groups, supporting successful synthesis. A strong carbonyl stretch at 1708 cm^{-1} indicated the conjugated ester. Aromatic C-H stretches appeared around 3049 cm^{-1}, while aliphatic C-H stretches from the ethyl and methoxy groups are observed between 2849 and 2980 cm^{-1}. Characteristic aromatic ring vibrations (C=C) are present at 1605, 1574, and a very strong peak at 1511 cm^{-1}, indicative of para-substitution. Strong C-O stretches from the ester and methoxy groups are found between 1028 and 1311 cm^{-1}. Crucially, a sharp peak at 965 cm^{-1} confirms the *trans* alkene configuration via the =C-H out-of-plane bend, and a vinylic =C-H is observed at 3048 cm^{-1}. Finally, a para-disubstituted bending was observed at 830 cm^{-1}. The FTIR data, therefore, provided further evidence for the structure of ethyl (E)-3-(4-methoxyphenyl) acrylate .

If the *cis* isomer were present in a larger amount, an additional peak would be expected in the 675-730 cm^{-1} region. The intensity of that peak would be proportional to the concentration of the *cis* isomer.

© University of Venda

4.14 Synthesis of ethyl (E)-3-(4-methoxyphenyl) acrylate using the Wittig reaction (8) in the presence of MIPs and NIPs

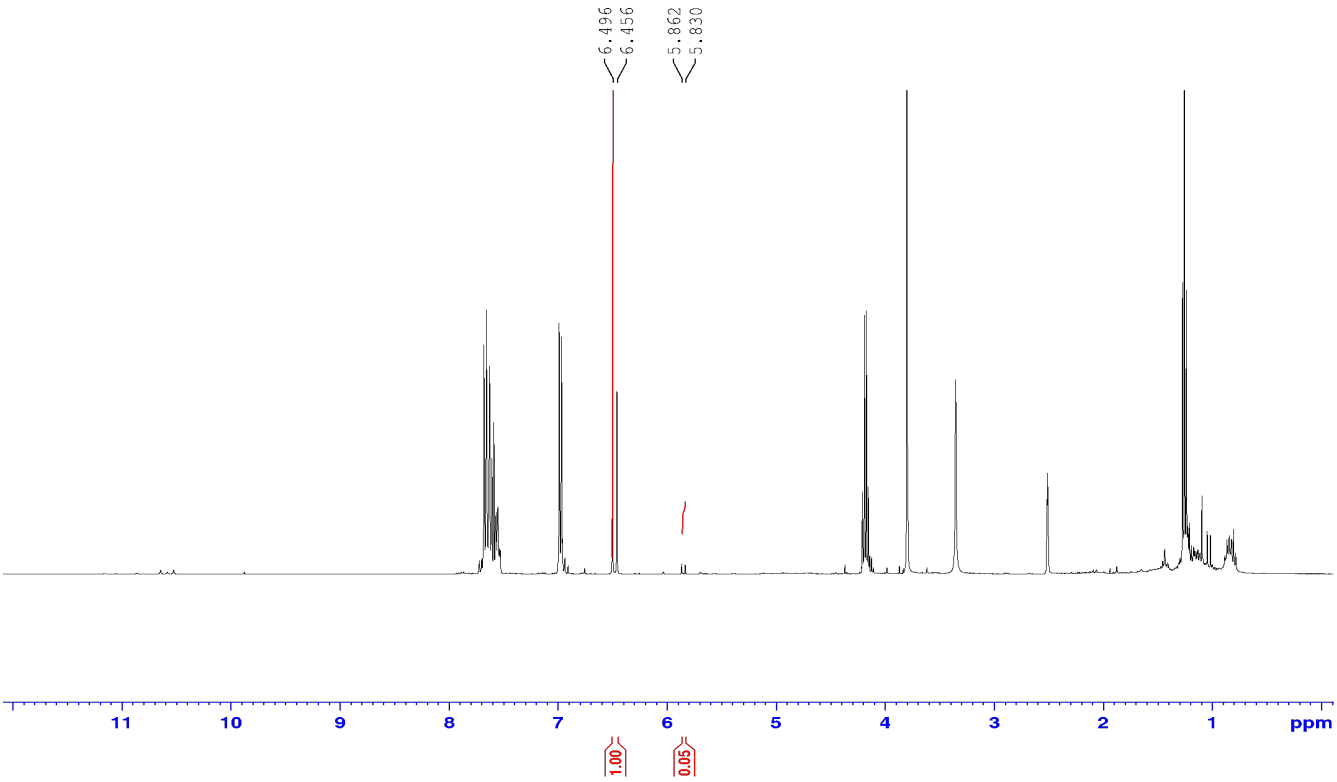
4.14.1 Synthesis in the in the presence of the NIPs



Scheme 2: Synthesis of ethyl (E)-3-(4-methoxyphenyl) acrylate using NIPs as a catalyst

In separate experiments, ethyl (E)-3-(4-methoxyphenyl) acrylate was synthesized following the identical procedure as in Scheme 1, but with the addition of 300 mg of synthesized NIPs as depicted in Scheme 2. The reaction was monitored using a TLC plate. After the workup, a pale-yellow oil was obtained and was of adequate purity for analysis by ^{1}H NMR, ^{13}C NMR, and IR.

(a)



© University of Venda

(b)

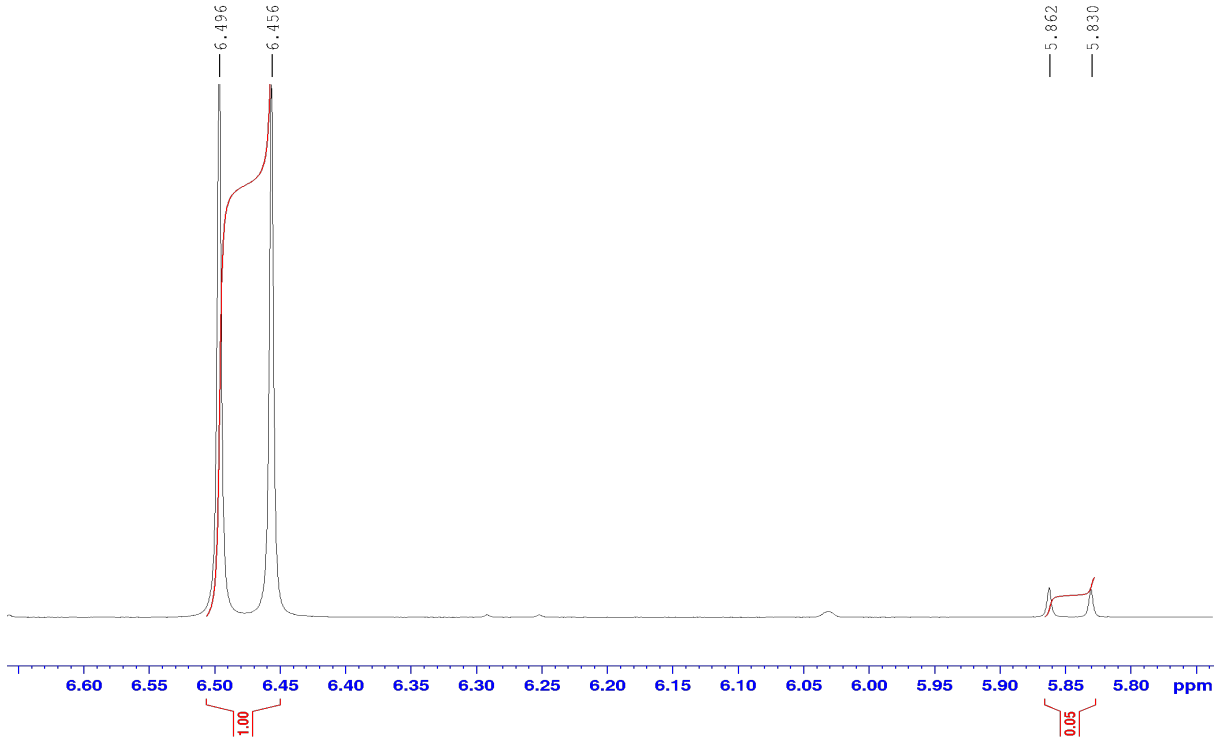


Figure 48: ^{1}H NMR spectrum (a) aromatic expansion (b) of ethyl (E)-3-(4-methoxyphenyl) acrylate as synthesized according to scheme 2

The analysis of the product derived from the NIP-mediated reaction, as depicted in the ^{1}H NMR spectrum in Figure 48, demonstrated a significant similarity to the control. The characteristic peaks for the *trans* alkene proton (δ 6.47 ppm) and the *cis* alkene proton (δ 5.84 ppm) were observed, confirming the formation of the intended product. A subtle but significant difference was noted in the integration values of the alkene signals, indicating a *cis/trans* ratio of 1:20 (5% *cis*) in the NIP reaction. HPLC analysis was conducted to support these findings, with the pertinent data displayed in Table 16.

Table 17: HPLC analysis of *trans* and *cis* isomers in control, NIP, and MIP reactions

Condition	Area *trans*	Area *cis*	*Trans* ratio (%)	*Cis* ratio (%)
Control	121445	3627	97.1001	2.8999
NIP	120265	6437	94.9199	5.0801
MIP	113592	5294	95.5472	4.4528

© University of Venda

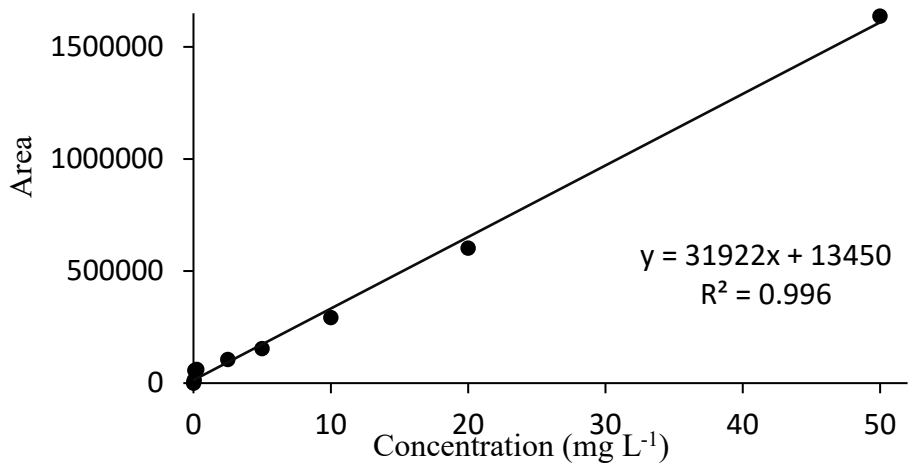
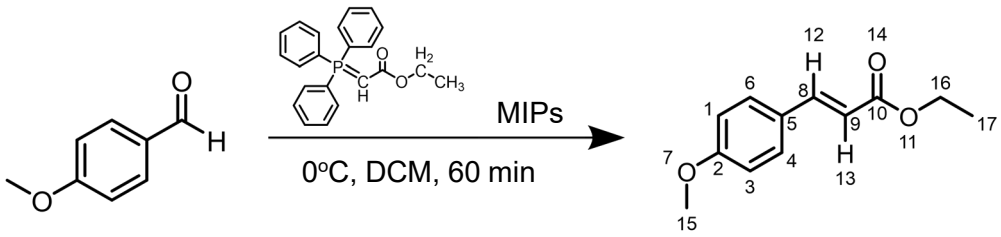


Figure 49: Calibration curve Et-MOPA using HPLC

The NIP condition entry indicates a *trans* isomer percentage of 94.92% and a *cis* isomer percentage of 5.08%. The HPLC data aligns well with the *cis/trans* ratio established from the ^{1}H NMR spectrum of the NIP reaction product. The results from the two analytical techniques exhibit a strong correlation. In conclusion, both the control and NIP-mediated reactions predominantly yield the *trans* isomer, however, a slight increase in the proportion of the *cis* isomer is noted with NIPs, indicating a minor but quantifiable effect of the polymer on the reaction's stereoselectivity.

4.14.2 Synthesis in the in the presence of the MIPs



Scheme 3: Synthesis of ethyl (E)-3-(4-methoxyphenyl) acrylate using MIPs as the catalyst

In other separate experiments, performed at the same time, ethyl (E)-3-(4-methoxyphenyl) acrylate was synthesized following the identical procedure as in Scheme 1, with the addition of 300 mg of synthesized MIPs as depicted in Scheme 3. The reaction was monitored using a TLC. After the workup, a pale-yellow oil was obtained and was of adequate purity for analysis by ^{1}H NMR, ^{13}C NMR, and IR.

© University of Venda

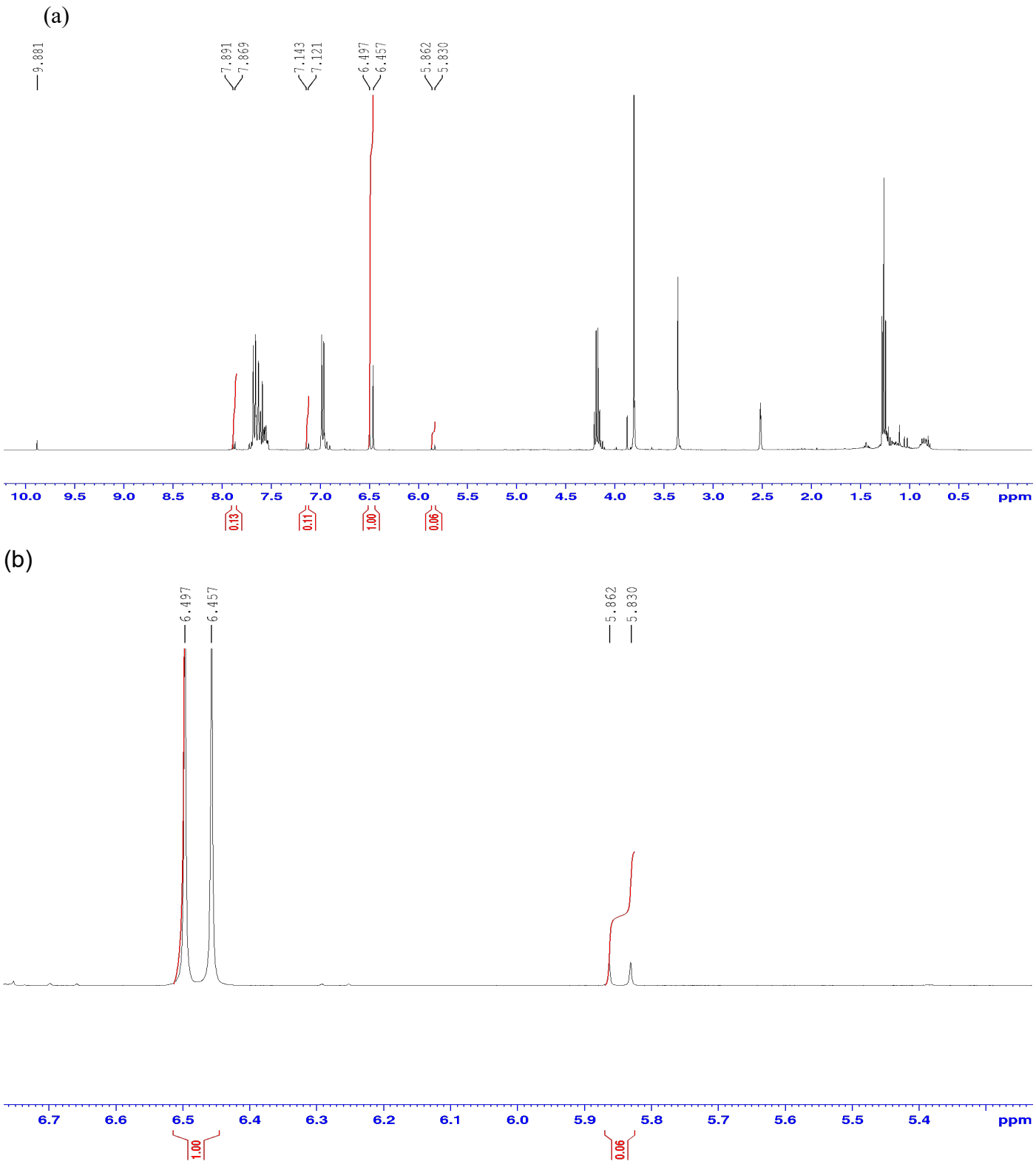


Figure 50: [1]H NMR spectrum (a) aromatic expansion (b) ethyl (E)-3-(4-methoxyphenyl) acrylate as synthesized according to scheme 3

© University of Venda

The analysis of the reaction mixture from the synthesis of ethyl (E)-3-(4-methoxyphenyl) acrylate , as illustrated in Scheme 3, indicated substantial indications of incomplete conversion of the starting components. The ^{1}H NMR spectrum (Figure 50) displayed a distinct singlet at roughly 9.88 ppm, clearly suggesting the presence of an aldehyde proton, which is ascribed to unreacted para-anisaldehyde starting material. The spectrum indicated the synthesis of the expected ethyl (E)-3-(4-methoxyphenyl) acrylate , nevertheless, the presence of the aldehyde peak differentiates this MIP-mediated reaction from the control and NIP reactions (Scheme 1).

The HPLC study in Table 16 offered more clarity regarding product distribution. The MIP reaction yielded a *trans*/*cis* ratio of 95.55 %: 4.45 %. While the *trans* isomer predominates in all cases, it is noteworthy that the *cis* ratio in the MIP reaction (4.45%) is higher than that of the control reaction (2.90%), although slightly lower than the NIP reaction (5.08%). Even with incomplete conversion, the MIP still influenced the stereoselectivity, producing a higher proportion of *cis* product than the unmodified control reaction. This observation, coupled with the presence of unreacted starting material, suggest that the MIP was not simply acting as an inert support. Instead, the MIP likely exhibits preferential binding affinity acting as a "sink" for the starting material (p-anisaldehyde) or perhaps even more so for the *trans* product, thereby slowing down the reaction rate, and, in relative terms, favors to a small degree, the formation of *cis* product compared to a reaction with no polymer additive.

The study showed that while MIPs and NIPs somewhat promote *trans*-selectivity in the Wittig reaction, MIPs can also hinder the complete conversion of starting materials to products, possibly through substrate or product binding. Optimizing MIP synthesis and reaction conditions is crucial to enhance conversion and stereoselectivity. Further investigations should focus on quantifying binding affinities and exploring alternative MIP formulations.

© University of Venda

Chapter 5

Conclusion

This concluding chapter summarizes the overall aim, key results, and significant findings from the present work. Additionally, it examines the unexpected obstacles faced during the project's implementation. Ultimately, recommendations for practical applications and proposals for future research avenues, based on the existing work, are provided.

© University of Venda

5.1 Conclusion

This study aimed to synthesize t-4MCA-based MIPs and investigate their capacity to selectively enhance and purify the (*trans*)-isomer from mixtures, utilizing both photoisomerization and Wittig reactions. The synthesis of t-4MCA MIPs was accomplished effectively, along with the successful creation of "dummy" paracetamol (PCM) MIPs and their corresponding non-imprinted polymers (NIPs) through precipitation polymerization. EGDMA served as the cross-linking agent, MAA functioned as the functional monomer, 1,1'-azobis (cyclohexanecarbonitrile) acted as the initiator, and a combination of 8% ethanol and chloroform was utilized as the porogen.

Characterization using FTIR, TGA, SEM-EDX, XRD, and BET analysis confirmed the formation of amorphous, mesoporous polymers with high thermal stability of up to 389^{o}C. The MIPs exhibited significantly higher surface areas and pore volumes and size than the NIPs, confirming the successful creation of imprinted cavities. Complete template removal was verified by UV-Vis spectroscopy and optimization of adsorption parameters was successfully achieved. Batch binding studies optimized key parameters for t-4MCA adsorption, including solvent (1:1 v/v methanol/water), polymer mass (10 mg), pH (7), and contact time (60 min) and initial concentration of 10 mg L^{-1}. These optimized conditions were used for subsequent selectivity and application studies. The swelling studies revealed distinct solvent preferences for each polymer, with the NIP showing highest swelling in ethanol, the t-4MCA MIP in acetonitrile (82.07%), and the PCM MIP in methanol (83.50%). These differences in swelling behavior, despite the common MAA-co-EGDMA backbone, highlighted the influence of the imprinted cavities on the overall polymer-solvent interactions.

The t-4MCA MIP exhibited notable selectivity for t-4MCA compared to structural analogs (ferulic acid, t-4HCA, and Et-MOPA) in single-analyte solutions, with the order of adsorption being t-4MCA > t-4HCA > ferulic acid > Et-MOPA, ranked from highest to lowest. Competitive binding experiments indicated that this selectivity faced challenges and diminished when competing structurally similar compounds, especially ferulic acid, were present, which highlights the significance of matrix effects. The order of cross reactivity was determined to be t-4MCA > ferulic acid > t-4HCA and Et-MOPA.

The photoirradiation of t-4MCA effectively produced mixtures of *cis* and *trans* isomers. Importantly, the t-4-MCA MIP, in contrast to the original hypothesis, exhibited a distinct capacity to alter the photoisomerization

© University of Venda

equilibrium in favor of the *cis* isomer. The initial reaction rate was observed to be faster for both MIP and NIP in comparison to the control. However, the MIP-treated samples demonstrated a consistently higher percentage of the *cis* isomer at extended irradiation times of 12 h, relative to both the control and the NIP. The NIP initially accelerated the reaction but ultimately led to a slightly lower *cis* percentage compared to the control. This suggests that non-specific interactions may slightly favor *trans* formation or hinder *cis* formation or potentially increase the degradation of the *cis* isomer.

The Wittig reaction was successfully used to synthesise Et-MOPA, establishing a foundation for subsequent comparisons. The utilization of MIPs in the Wittig reaction still resulted in the slight increase in the *cis* isomer giving potential that on optimizing reaction conditions suitable for the MIPs in the Wittig reaction and using polymers that generate a considerably large adsorption capacity and imprinting factor will somewhat improve the difference.

Answering research questions

The synthesis and characterization of the t-4MCA MIPs were accomplished effectively. The presence of the double bond in t-4MCA did not hinder the successful synthesis of MIP. The stability of the polymers was confirmed, and the presence of the imprinting effect was clearly observable. The MIPs exhibited a selectivity that varied with concentration. Although intended for *trans*, the preferential extraction in mixtures was influenced by the *cis/trans* ratio. In the photoisomerization experiments, the MIP significantly influenced the equilibrium, favoring the formation of the *cis* isomer. MIPs exhibited a degree of cross-reactivity with structural analogs, notably ferulic acid, while maintaining a preference for t-4MCA in competitive binding studies. The photoirradiation resulted in what were expected *cis* and *trans* isomers. The proportions were strongly affected by the presence of the MIP and NIP. The baseline Wittig reaction generated the anticipated result. Can the synthesized MIPs substantially increase the ratio of the *trans*-isomer in the end product? Yes, but unexpectedly in the photoisomerization reaction, rather than through simple extraction. The MIP altered the equilibrium in favor of the *cis* configuration, exhibiting a stereo-directing effect rather than merely a selective binding effect. This represents the most important and original discovery.

© University of Venda

Future studies need to focus on:

- Synthesize molecularly imprinted polymers (MIPs) with either ferulic acid or 4-hydroxycinnamic acid as templates, then employ them in the Wittig reaction to generate their isomers. Compare the findings with the present research.
- Extensive kinetic modeling, establishing a kinetic model that includes both rate acceleration and equilibrium shift to quantitatively characterize the behavior of the MIP.
- Computational analyses use molecular docking and molecular dynamics simulations to explore the specific interactions between the MIP and the *cis* and *trans* isomers at the molecular scale.
- Alternative MIP designs, synthesizing *cis*-imprinted MIPs to investigate their capacity to preferentially promote *cis* production.
- Evaluating the Wittig reaction and the capacity of the MIP, along with a *cis*-imprinted MIP, to affect the stereochemistry of the reaction.
- Degradation studies examining the individual isomers could provide useful insight.
- Investigating the application of various ratios of monomer to crosslinker. This may provide evidence regarding the stability of the synthesized polymers.

This research conclusively demonstrates the stereo-directing capability of MIPs in photochemical reactions, presenting a novel strategy for regulating isomer ratios and paving the way for the advancement of more efficient and selective synthetic methodologies. The unforeseen result, favoring the *cis* isomer, underscores the significance of comprehending the intricate interactions among MIP binding affinity, reaction kinetics, and thermodynamic equilibrium. This comprehension is essential for the systematic design of MIPs for specific applications in chemical synthesis and separation.

© University of Venda

References

Adeleke, V. T., Ebenezer, O., Lasich, M., Tuszyński, J. A., Robertson, S., & Mugo, S. M. 2024. Design and Optimization of Molecularly Imprinted Polymer Targeting Epinephrine Molecule: A Theoretical Approach. *Polymers*.*16*(16), p 2341

Akhiani, A. R., Mehrali, M., Tahan Latibari, S., Mehrali, M., Mahlia, T. M. I., Sadeghinezhad, E., & Metselaar, H. S. C. 2015. One-step preparation of form-stable phase change material through self-assembly of fatty acid and graphene. *The Journal of Physical Chemistry C*.*119*(40), pp 22787–22796

Alsudir, S. A., Iqbal, Z., & Lai, E. P. C. 2012. Competitive CE-UV Binding Tests for Selective Recognition of Bisphenol A by Molecularly Imprinted Polymer Particles. *Electrophoresis*.*33*(8), pp 1255–1262

Amarh, F. A., Kangmennaa, A., Agorku, E. S., & Voegborlo, R. B. 2024. A state-of-the-art review of trends in molecularly imprinted polymers in the clean-up of pesticides in environmental samples. *Sustainable Environment*.*10*(1), p 2298067

Aminnezhad, S., Aljelehawy, Q. H. A., Rezaei, M., Mohammadi, M. R., Zonobian, M. A., Nazari, M., Fathi, F., Dadpour, S., Habibi, P., Kashanian, S., Ashengroph, M., Mohammadzade, H., Azarakhsh, Y., Kahrizi, S., Alavi, M., & Xu, Z. 2024. Revolutionizing Medicine: Molecularly Imprinted Polymers as Pre*cis*ion Tools In Cancer Diagnosis and Antibiotic Detection. *Cellular and Molecular Biology*.*70*(5), pp 100–110

An, K., Kang, H., & Tian, D. 2019. Fabrication and Evaluation of Controllable Core/Shell Magnetic Molecular Imprinted Polymers Based on Konjac Glucomannan for Trichlorfon. *Journal of Applied Polymer Science*.*137*(30)

Anantharaju, P. G., Reddy, D. B., Anand, M. P., Chitturi, Ch. M. K., Vimalambike, M. G., & Madhunapantula, S. V. 2017. Induction of Colon and Cervical Cancer Cell Death by Cinnamic Acid Derivatives Is Mediated Through the Inhibition of Histone Deacetylases (HDAC). *Plos One*.*12*(11), p e0186208

© University of Venda

Anene, A., Chevalier, Y., & Hbaïeb, S. 2024. Molecularly Imprinted Polyaniline as Solid-Phase Material for the Extraction of UV Filters From Waters. *Separation Science Plus*.*7*(11)

Ao, Q., Zhao, H., Tong, T., Peng, Y., & Zhao-yang, H. 2022. Enantioseparation of Basic Drugs by Reverse Phase High-performance Liquid Chromatography System Using Carboxymethyl-β-cyclodextrin as Chiral Mobile Phase Additive. *Chirality*.*34*(8), pp 1128–1139

Ariani, M. D., Zuhrotun, A., Manesiotis, P., & Hasanah, A. N. 2024. Synthesis of molecularly imprinted polymer with a methacrylate derivative monomer for the isolation of ethyl p-methoxycinnamate as an active compound from Kaempferia galanga L. extracts. *RSC advances*.*14*(19), pp 13521–13534

Auffrant, A., Jaun, B., Jarowski, P. D., Houk, K. N., & Diederich, F. 2004. Peralkynylated Buta-1,2,3-Trienes: Exceptionally Low Rotational Barriers of Cumulenic C=C Bonds in the Range of Those of Peptide C=N Bonds. *Chemistry—A European Journal*.*10*(12), pp 2906–2911

Avigo, L., Furman, C., Ghinet, A., Sandu, T., Wynendaele, E., Wielgomas, B., Spiegeleer, B. D., & Lipka, E. 2023. Evaluation of Greenness and Analytical Performances of Separative Methods for Chiral Separation of Novel Lactam-based P2RX7-antagonists. *Electrophoresis*.*45*(3–4), pp 218–233

Ayudhya, C. C. N., Graidist, P., & Tipmanee, V. 2022. Potential Stereoselective Binding of *Trans*-(±)-Kusunokinin and *Cis*-(±)-Kusunokinin Isomers to CSF1R. *Molecules*.*27*(13), p 4194

Baeza, G., Sarriá, B., Bravo, L., & Mateos, R. 2016. Exhaustive Qualitative LC-DAD-MSn Analysis of Arabica Green Coffee Beans: Cinnamoyl-Glycosides and Cinnamoylshikimic Acids as New Polyphenols in Green Coffee. *Journal of Agricultural and Food Chemistry*.*64*(51), pp 9663–9674

Baggiani, C., Giovannoli, C., Anfossi, L., Passini, C., Baravalle, P., & Giraudi, G. 2012. A connection between the binding properties of imprinted and nonimprinted polymers: A change of perspective in molecular imprinting. *Journal of the American Chemical Society*.*134*(3), pp 1513–8

© University of Venda

Bagheri, A. R., Arabi, M., Ghaedi, M., Ostovan, A., Wang, X., Li, J., & Chen, L. 2019. Dummy Molecularly Imprinted Polymers Based on a Green Synthesis Strategy for Magnetic Solid-Phase Extraction of Acrylamide in Food Samples. *Talanta*.*195*, pp 390–400

Barajas-Ramírez, J. A., Cabrera-Ramírez, A. H., & Aguilar-Raymundo, V. G. 2022. Antioxidant Activity, Total Phenolic, Tannin, and Flavonoid Content of Five Plants Used in Traditional Medicine in Penjamo, Guanajuato. *Chemistry & Biodiversity*.*20*(1)

Barsbay, M., & Mehrnia, M. 2020. Development of Molecularly-Imprinted Fluorescent Fabric Based Sensor System for the Recognition of a Model Azo-Dye Molecule, in Proceedings of the 2nd International Online Conference on Nanomaterials, 15–30 November 2020, MDPI: Basel, Switzerland.

Baumann, P., Kirchherr, H., Berney, P., & Hiemke, C. 2012. Flupentixol: Relevance of Stereoselective Therapeutic Drug Monitoring. *Psychopharmacology*.*221*(4), pp 719–720

Becskereki, G., Horvai, G., & Tóth, B. 2021. The Selectivity of Molecularly Imprinted Polymers. *Polymers (Basel)*.*13*(11)

Berger, T. A., & Berger, B. K. 2013. Two minute separation of the *cis*-and *trans*-isomers of vitamin K1 without heptane, chlorinated solvents, or acetonitrile. *Chromatographia*.*76*(3), pp 109–115

Bernhardt, M., Cruz-Garcia, Y., Rech, A., Meierjohann, S., Erhard, F., Schilling, B., & Schlösser, A. 2022. Extending the Mass Spectrometry-Detectable Landscape of MHC Peptides by Use of Restricted Access Material. *Analytical Chemistry*.*94*(41), pp 14214–14222

Betzenbichler, G., Huber, L., Kräh, S., Morkos, M. K., Siegle, A. F., & Trapp, O. 2022. Chiral Stationary Phases and Applications in Gas Chromatography. *Chirality*.*34*(5), pp 732–759

Butkevičiūtė, A., Liaudanskas, M., Kviklys, D., Gelvonauskienė, D., & Janulis, V. 2020. The Qualitative and Quantitative Compositions of Phenolic Compounds in Fruits of Lithuanian Heirloom Apple Cultivars. *Molecules*.*25*(22), p 5263

© University of Venda

Butt, M. S., & Sultan, M. T. 2011. Coffee and its consumption: Benefits and risks. *Critical Reviews in Food Science and Nutrition*.*51*(4), pp 363–373

Bylka, W. 2004. E-and Zp-methoxycinnamic acid from Aquilegia vulgaris. *Acta poloniae pharmaceutica*.*61*(4), pp 307–308

Cabaleiro-Lago, C., Hasterok, S., Wingren, A. G., & Tassidis, H. 2023. Recent Advances in Molecularly Imprinted Polymers and Their Disease-Related Applications. *Polymers*.*15*(21), p 4199

Camunas-Alberca, S. M., Morán-Garrido, M., Sáiz, J., Gil-de-la-Fuente, A., Barbas, C., & Gradillas, A. 2023. Integrating the Potential of Ion Mobility Spectrometry-Mass Spectrometry in the Separation and Structural Characterisation of Lipid Isomers. *Frontiers in Molecular Biosciences*.*10*

Castillo-Aguirre, A., Rivera-Monroy, Z. J., & Maldonado, M. 2019. Analysis by RP-HPLC and Purification by RP-SPE of the C-Tetra(p-Hydroxyphenyl)resorcinolarene Crown and Chair Stereoisomers. *Journal of Analytical Methods in Chemistry*.*2019*, pp 1–6

Ceramella, J., Iacopetta, D., Franchini, A., Luca, M. D., Saturnino, C., Andreu, I., Sinicropi, M. S., & Catalano, A. 2022. A Look at the Importance of Chirality in Drug Activity: Some Significative Examples. *Applied Sciences*.*12*(21), p 10909

Cervantes-Díaz, A., Mateo-Miranda, M., Torrado-Cubero, N., Alonso-Prados, J. L., & Sandín-España, P. 2024. Stereoisomeric separation of the chiral herbicide profoxydim and residue method development in rice by QuEChERS and LC–MS/MS. *Food Chemistry*.*443*, p 138536 Elsevier

Chandra, S., Roy, A., Jana, M., & Pahan, K. 2019. Cinnamic Acid Activates PPARα to Stimulate Lysosomal Biogenesis and Lower Amyloid Plaque Pathology in an Alzheimer's Disease Mouse Model. *Neurobiology of Disease*.*124*, pp 379–395

Chen, L., Capone, D. L., & Jeffery, D. W. 2019. Analysis of Potent Odour-Active Volatile Thiols in Foods and Beverages With a Focus on Wine. *Molecules*.*24*(13), p 2472

© University of Venda

Chen, Y., Sun, J., Han, Y., & Yan, C. 2021. Water Modulated Diastereoselective Synthesis Of*cis*/*trans*-Spiro[indoline-3,6′-Naphtho[2,3-c]carbazoles]. *The Journal of Organic Chemistry*.*86*(14), pp 9263–9279

Cheng, S., & Qi, G. 2020. Microwave Synthesis of McM-41 and Its Application in CO2 Absorption by Nanofluids. *Journal of Nanomaterials*.*2020 (1)*, pp 1–13

Chieffi, C., Camuto, C., De-Giorgio, F., Torre, X. de la, Diamanti, F., Mazzarino, M., Trapella, C., Marti, M., & Botrè, F. 2020a. Metabolic Profile of the Synthetic Drug 4,4′-Dimethylaminorex in Urine by LC–MS-based Techniques: Selection of the Most Suitable Markers of Its Intake. *Forensic Toxicology*.*39*(1), pp 89–100

Chieffi, C., Camuto, C., De-Giorgio, F., Torre, X. de la, Diamanti, F., Mazzarino, M., Trapella, C., Marti, M., & Botrè, F. 2020b. Metabolic Profile of the Synthetic Drug 4,4′-Dimethylaminorex in Urine by LC–MS-based Techniques: Selection of the Most Suitable Markers of Its Intake. *Forensic Toxicology*.*39*(1), pp 89–100

Clifford, M. N. 2019. Chlorogenic acids and other cinnamates—Nature, occurrence, dietary burden, absorption and metabolism. *Journal of the Science of Food and Agriculture*.*99*(12), pp 5137–5146

Coelho, M. M., Fernandes, C., Remião, F., & Tiritan, M. E. 2021. Enantioselectivity in Drug Pharmacokinetics and Toxicity: Pharmacological Relevance and Analytical Methods. *Molecules*.*26*(11), p 3113

Danylec, B., Schwarz, L. J., Harris, S. J., Boysen, R. I., & Hearn, M. T. 2015. The Application of Template Selectophores for the Preparation of Molecularly Imprinted Polymers. *Molecules*.*20*(9), pp 17601–13

Decompte, E., Lobaz, V., Monperrus, M., Deniau, E., & Save, M. 2020. Molecularly Imprinted Polymer Colloids Synthesized by Miniemulsion Polymerization for Recognition and Separation of Nonylphenol. *Acs Applied Polymer Materials*.*2*(8), pp 3543–3556

Dong, Z., Fan, P., Chen, Q., & Chen, C. 2020. Facile Conversion of *Cis* Into *Trans* Oxane as Liquid Crystals. *Scientific Reports*.*10*(1)

© University of Venda

Drakontaeidi, A., & Pontiki, E. 2024. Multi-Target-Directed Cinnamic Acid Hybrids Targeting Alzheimer's Disease. *International Journal of Molecular Sciences*.*25*(1), p 582

Durndell, L. J., Cucuzzella, C., Parlett, C. M. A., Isaacs, M. A., Wilson, K., & Lee, A. F. 2019. Platinum Catalysed Aerobic Selective Oxidation of Cinnamaldehyde to Cinnamic Acid. *Catalysis Today*.*333*, pp 161–168

Edgar, M., Percival, B., Gibson, M., Masania, J., Beresford, K., Wilson, P. B., & Grootveld, M. 2019. Benchtop NMR Spectroscopy and Spectral Analysis of the *cis*- And *trans*-Stilbene Products of the Wittig Reaction. *Journal of Chemical Education*.*96*(9), pp 1938–1947

Eisler, R. 2003. Chrysotherapy: A Synoptic Review. *Inflammation Research*.*52*(12), pp 487–501

Espinoza-Torres, S., López, R., Sotomayor, M. D. P. T., Tuesta, J. C., Picasso, G., & Khan, S. 2023. Synthesis, Characterization, and Evaluation of a Novel Molecularly Imprinted Polymer (MIP) for Selective Quantification of Curcumin in Real Food Sample by UV-Vis Spectrophotometry. *Polymers*.*15*(16), p 3332

Fahri, H., Zulfikar, M. A., & Azis, M. Y. 2024. Synthesis of Molecularly Imprinted Polymers With Magnetite Cores for Ibuprofen Adsorption. *Jurnal Kimia Sains Dan Aplikasi*.*27*(1), pp 28–34

Fathi Til, R., Mohammadi, R., Alizadeh-Khaledabad, M., Wilson, L. D., & Pirsa, S. 2020. Synthesis, characterization and adsorption behavior of sinapic acid imprinted polymer via precipitation polymerization. *Journal of Polymer Research*.*27*, pp 1–12

Feng, G., Gao, M., Wang, L., Chen, J., Hou, M., Wan, Q., Lin, Y., Xu, G., Qi, X., & Chen, S. 2022. Dual-resolving of positional and geometric isomers of C=C bonds via bifunctional photocycloaddition-photoisomerization reaction system. *Nature Communications*.*13*(1), p 2652

Fjæstad, K. Y., Rømer, A. M. A., Goitea, V., Johansen, A. Z., Thorseth, M., Carretta, M., Engelholm, L. H., Grøntved, L., Junker, N., & Madsen, D. H. 2022. Blockade of Beta-Adrenergic Receptors Reduces

© University of Venda

Cancer Growth and Enhances the Response to Anti-Ctla4 Therapy by Modulating the Tumor Microenvironment. *Oncogene*.*41*(9), pp 1364–1375

Fumagalli, C., Maurizi, N., Marchionni, N., & Fornasari, D. 2020. B-Blockers: Their New Life From Hypertension to Cancer and Migraine. *Pharmacological Research*.*151*, p 104587

Gai, T., Nie, J., Ding, Z., Wu, W., & Liu, X. 2023. Progress of Rapid Detection of Pesticides in Fruits and Vegetables. *Frontiers in Food Science and Technology*.*3*

Gaspari, R., Prota, A. E., Bargsten, K., Cavalli, A., & Steinmetz, M. O. 2017. Structural Basis of *cis*- and *trans*-Combretastatin Binding to Tubulin. *Chem*.*2*(1), pp 102–113

Ghanem, B., Seoane-Vazquez, E., Brown, L. M., & Rodríguez-Monguió, R. 2023. Analysis of the Gene Therapies Authorized by the United States Food and Drug Administration and the European Medicines Agency. *Medical Care*.*61*(7), pp 438–447

Gkika, D. A., Tolkou, A. K., Lambropoulou, D. A., Bikiaris, D. N., Kokkinos, P., Kalavrouziotis, I. K., & Kyzas, G. Z. 2024. Application of molecularly imprinted polymers (MIPs) as environmental separation tools. *RSC Applied Polymers*.*2*(2), pp 127–148

Goff, N. L., Fomba, I., Prost, É., Merlier, F., Haupt, K., Duma, L., Fayeulle, A., & Falcimaigne-Cordin, A. 2020. Renewable Plant Oil-Based Molecularly Imprinted Polymers as Biopesticide Delivery Systems. *Acs Sustainable Chemistry & Engineering*.*8*(42), pp 15927–15935

Grenet, E., Géant, P., & Salom-Roig, X. J. 2021. Crystallization-Induced Diastereomer *Trans*formation of A-Bromo A′-Sulfinyl Ketones. Diastereodivergent Synthesis of (+)-A-Conhydrine and (−)-B-Conhydrine. *Organic Letters*.*23*(21), pp 8539–8542

Grünherz, L., Fertsch, S., Andree, C., Munder, B., Schulz, T., Wolter, A., & Abdallah, A. 2022. Autologous Breast Reconstruction in a Patient With Thalidomide Embryopathy: Case Report. *AME Surgical Journal*.*2*, pp 39–39

© University of Venda

Gryko, K., Kalinowska, M., Ofman, P., Choińska, R., Świderski, G., Świsłocka, R., & Lewandowski, W. 2021. Natural Cinnamic Acid Derivatives: A Comprehensive Study on Structural, Anti/Pro-Oxidant, and Environmental Impacts. *Materials (Basel)*.*14*(20)

Guarducci, M. A., Manetto, S., Pierini, M., Mazzoccanti, G., & Villani, C. 2024. Design, Synthesis, and Applications of Bis-Amido HPLC Pirkle-Type Chiral Stationary Phases. *Chirality*.*36*(9)

Gunatilleke, S. S., & Barrios, A. 2008. Tuning the Au(I)-Mediated Inhibition of Cathepsin B Through Ligand Substitutions. *Journal of Inorganic Biochemistry*.*102*(3), pp 555–563

Gupta, M., & Khanna, J. 2018. Clomiphene Citrate: The Changing Landscape. *International Journal of Basic & Clinical Pharmacology*.*7*(8), p 1437

Hadjipavlou-Litina, D., & Pontiki, E. 2014. Aryl-Acetic and Cinnamic Acids as Lipoxygenase Inhibitors With Antioxidant, Anti-Inflammatory, and Anticancer Activity.pp 361–377

Han, Y., Zhang, J., Hu, C. -qin, Zhang, X., Ma, B., & Zhang, P. 2019. In Silico ADME and Toxicity Prediction of Ceftazidime and Its Impurities. *Frontiers in Pharmacology*.*10*

Hancu, G., Papp, L. A., Székely-Szentmiklósi, B., & Kelemen, H. 2022. The Use of Antibiotics as Chiral Selectors in Capillary Electrophoresis: A Review. *Molecules*.*27*(11), p 3601

Hasanah, A. N., Rahayu, D., Pratiwi, R., Rostinawati, T., Megantara, S., Saputri, F. A., & Puspanegara, K. H. 2019. Extraction of atenolol from spiked blood serum using a molecularly imprinted polymer sorbent obtained by precipitation polymerization. *Heliyon*.*5*(4) Elsevier

Hasanah, A. N., Safitri, N., Zulfa, A., Neli, N., & Rahayu, D. 2021. Factors Affecting Preparation of Molecularly Imprinted Polymer and Methods on Finding Template-Monomer Interaction as the Key of Selective Properties of the Materials. *Molecules*.*26*(18), p 5612

Havnen, H., Hansen, M., Spigset, O., & Hegstad, S. 2020. Enantiomeric separation and quantification of R/S-amphetamine in serum using semi-automated liquid-liquid extraction and ultra-high performance

© University of Venda

supercritical fluid chromatography-tandem mass spectrometry. *Drug Testing and Analysis*.*12*(9), pp 1344–1353

Homma, K., Chang, A. C., Yamamoto, S., Ueki, T., & Nakanishi, J. 2023. Polarity Does Not Matter: Molecular Weight Reverses the Photoisomerization-Induced Phase Separation of an Azobenzene-Bearing Polymer. *Macromolecular Rapid Communications*.*44*(14)

Hroboňová, K., & Špačková, A. 2020. Application of Selective Polymeric Sorbents for Simple Coumarins Extraction From Deodorant Samples. *Acta Chimica Slovaca*.*13*(1), pp 56–62

Hu, T., Zhao, Q., Wang, M., Zhou, K., Xia, Z., & Huang, Y. 2023. Improved Selectivity of Molecularly Imprinted Polymers Based on the Synergistic Action of Hydrogen Bond and Electrostatic Interaction. *Journal of Molecular Recognition*.*36*(7)

Huang, P., Jiang, X., Dai, Z., Zhang, Q., Chen, X., Ma, L., Gao, W., & Xiong, X. 2024. Oxygen-Rich Porous Organic Polymer for Thermal Energy Storage. *Physica Status Solidi (A)*.*221*(20)

Huang, S., Liu, W., Li, Y., Zhang, K., Zheng, X., Wu, H., & Tang, G. 2021. Design, Synthesis, and Activity Study of Cinnamic Acid Derivatives as Potent Antineuroinflammatory Agents. *Acs Chemical Neuroscience*.*12*(3), pp 419–429

Hubner, E. M., Schützinger, S., Molnárová, K., & Schmid, M. G. 2024. Screening of Astec® CHIRALDEX™ G-PN and LIPODEX™ D gas chromatography columns for enantioseparation of amphetamine derivatives. *Chirality*.*36*(5), p e23676

Ikeda, C., Manabe, Y., Tomonaga, N., Wada, T., Maoka, T., & Sugawara, T. 2020. Evaluation of Intestinal Absorption of Dietary Halocynthiaxanthin, a Carotenoid From the Sea Squirt Halocynthia Roretzi. *Marine Drugs*.*18*(12), p 588

Janicki, P. K., Singh, A., Sharma, A., & Ruiz-Velasco, V. 2023. Dissimilar Effects of Stereoisomers and Racemic Hydroxychloroquine on Ca2+ Oscillations in Human Induced Pluripotent Stem Cell-derived Cardiomyocytes. *Physiological Reports*.*11*(14)

© University of Venda

Jayasinghe, G. D. T. M., & Moreda-Piñeiro, A. 2021. Molecularly Imprinted Polymers for Dispersive (Micro)Solid Phase Extraction: A Review. *Separations*.*8*(7), p 99

Jeon, H. I., Jo, S., Jeon, S., Jun, T., Moon, J., Cho, J. H., Ahn, H., Lee, S., Ryu, D. Y., & Russell, T. P. 2023. Repairable Macroscopic Monodomain Arrays From Block Copolymers Enabled by Photoplastic and Photodielectric Effects. *ACS Nano*.*17*(9), pp 8367–8375

Jiang, X., Liu, Z., & Sun, N. 2022. Specific Recognition of in Situ Self-Assembly Prepared and Molecularly Imprinted Metal–Organic Frameworks in Selective Removal of Norfloxacin. *Industrial & Engineering Chemistry Research*.*61*(34), pp 12609–12618

Joke Chow, A. L., & Bhawani, S. A. 2016. Synthesis and Characterization of Molecular Imprinting Polymer Microspheres of Cinnamic Acid: Extraction of Cinnamic Acid from Spiked Blood Plasma. *International Journal of Polymer Science*.*2016*, p 2418915

Jurin, M., Kontrec, D., & Roje, M. 2024. HPLC and SFC Enantioseparation of (±)-*Trans*-B-Lactam Ureas on Immobilized Polysaccharide-Based Chiral Stationary Phases—The Introduction of Dimethyl Carbonate as an Organic Modifier in SFC. *Separations*.*11*(2), p 38

Jurkovičová, T., Vaňkátová ,Petra, Cigl ,Martin, Novotná ,Vladimíra, Hamplová ,Věra, Pociecha ,Damian, & and Podoliak, N. 2024. Synthesis, chiral separation and physical properties of the cinnamic acid derivatives exhibiting short-pitch cholesteric and TGB phases. *Liquid Crystals*.*51*(13–14), pp 2370–2380 Taylor & Fran*cis*

Khan, A., Sarwar, M. G., & Ali, S. 2024. Reactivity and Stability of (Hetero)Benzylic Alkenes via the Wittig Olefination Reaction. *Molecules*.*29*(2), p 501

Khanal, S., Pachya, U., Thapaliya, S., Magar, S. R., Panthi, B., & Khatri, A. 2022. Congenital Limb Deficiency: A Case Report. *Journal of Nepal Medical Association*.*60*(249), pp 485–487

Kim, S. R., & Kim, Y. C. 2000. Neuroprotective phenylpropanoid esters of rhamnose isolated from roots of Scrophularia buergeriana. *Phytochemistry*.*54*(5), pp 503–509

© University of Venda

Koesdjojo, M. T., Tennico, Y. H., & Remcho, V. T. 2007. 18 Molecularly imprinted polymers as sorbents for separations and extractions. In *Separation Science and Technology*. S. Ahuja, & H. Rasmussen (Eds) *Separation Science and Technology*.pp 479–503, vol 8 Academic Press

Konzock, O., Mohedano, M. T., Cibin, I., Chen, Y., & Norbeck, J. 2023. Cinnamic Acid and P-Coumaric Acid Are Metabolized to 4-Hydroxybenzoic Acid By Yarrowia Lipolytica. AMB Express, 13(1), 84

Kotowska, U., Struk-Sokołowska, J., & Piekutin, J. 2021. Simultaneous Determination of Low Molecule Benzotriazoles and Benzotriazole UV Stabilizers in Wastewater by Ultrasound-Assisted Emulsification Microextraction Followed by GC–MS Detection. *Scientific Reports*.*11*(1)

Kumar, N., & Goel, N. 2019. Phenolic acids: Natural versatile molecules with promising therapeutic applications. *Biotechnology reports (Amsterdam, Netherlands),* 24, e00370

Kumar, R., Vashisth, D., Misra, A., Akhtar, Md. Q., Jalil, S. U., Shanker, K., Gupta, M. M., Rout, P. K., Gupta, A. K., & Shasany, A. K. 2016. RNAi Down-Regulation of Cinnamate-4-Hydroxylase Increases Artemisinin Biosynthesis in Artemisia Annua. *Scientific Reports*.*6*(1)

Lanfredi, S., Nobre, M. A. L., Poon, P. S., & Matos, J. 2020. Hybrid Material Based on an Amorphous-Carbon Matrix and ZnO/Zn for the Solar Photocatalytic Degradation of Basic Blue 41. *Molecules*.*25*(1)

Le, P. H., Ho, L., Le, D. H. T., & Nguyen, V. 2023. Purification of Coffee Polyphenols Extracted From Coffee Pulps (Coffee Arabica L.) Using Aqueous Two-Phase System. *Molecules*.*28*(15), p 5922

Leicach, S. R., & Chludil, H. D. 2014. Chapter 9—Plant Secondary Metabolites: Structure–Activity Relationships in Human Health Prevention and Treatment of Common Diseases. In *Studies in Natural Products Chemistry*. Atta-ur-Rahman (Ed) *Studies in Natural Products Chemistry*.pp 267–304, vol 42 Elsevier

Leischner, C., Burkard, M., Michel, A., Berchtold, S., Niessner, H., Marongiu, L., Busch, C., Frank, J., Lauer, U. M., & Venturelli, S. 2021. Comparative Analysis of the Antitumor Activity of *Cis*- and *Trans*-Resveratrol in Human Cancer Cells with Different p53 Status. *Molecules*.*26*(18)

© University of Venda

Li, J., Zhou, X., Yan, Y., Shen, D., Lu, D., Guo, Y., Xie, L., & Deng, B. 2022. Selective Recognition of Gallic Acid Using Hollow Magnetic Molecularly Imprinted Polymers With Double Imprinting Surfaces. *Polymers*.*14*(1), p 175

Li, N., Ng, T. B., Wong, J. H., Qiao, J. X., Zhang, Y. N., Zhou, R., Chen, R. R., & Liu, F. 2013. Separation and purification of the antioxidant compounds, caffeic acid phenethyl ester and caffeic acid from mushrooms by molecularly imprinted polymer. *Food chemistry*.*139*(1–4), pp 1161–1167

Li, Y., Zhang, Y., Lu, X., Sun, S., Xiao, Y., Wang, Y., Jin, X., & Ma, X. 2023. Surface-up Click Access to Allylimidazolium Bridged Cyclodextrin Dimer Phase for Efficient Enantioseparation. *Journal of Separation Science*.*46*(11)

Lima, V. N., Oliveira-Tintino, C. D. M., Santos, E. S., Morais, L. P., Tintino, S. R., Freitas, T. S., Geraldo, Y. S., Pereira, R. L. S., Cruz, R. P., Menezes, I. R. A., & Coutinho, H. D. M. 2016. Antimicrobial and enhancement of the antibiotic activity by phenolic compounds: Gallic acid, caffeic acid and pyrogallol. *Microbial Pathogenesis*.*99*, pp 56–61

Lin, Z., Zhang, B., Yu, Z., & Li, H. 2020. The Effectiveness and Safety of Topical B-receptor Blocker in Treating Superficial Infantile Haemangiomas: A Meta-analysis Including 20 Studies. *British Journal of Clinical Pharmacology*.*86*(2), pp 199–209

Lipka, E. 2023. Chiral Separation by Supercritical Fluid Chromatography. *Chiral Separations and Stereochemical Elucidation: Fundamentals, Methods, and Applications*.pp 85–102 Wiley Online Library

Liu, Jin, Cai, X., Liu, J., Liang, D., Chen, K., Tang, S., & Bao, X. 2022. Study on the Preparation of Estrone Molecularly Imprinted Polymers and Their Application in a Quartz Crystal Microbalance Sensor via a Computer-Assisted Design. *International Journal of Molecular Sciences*.*23*(10), p 5758

© University of Venda

Liu, Jinfeng, He, X., Zheng, S., Zhu, A., & Wang, J. 2022. The Mitochondrial Unfolded Protein Response: A Novel Protective Pathway Targeting Cardiomyocytes. *Oxidative Medicine and Cellular Longevity*.*2022*, pp 1–19

Liu, Jing, Lefevere, H., Coussement, L., Delaere, I., De Meyer, T., Demeestere, K., Höfte, M., Gershenzon, J., Ullah, C., & Gheysen, G. 2024. The Phenylalanine Ammonia-lyase Inhibitor AIP Induces Rice Defence Against the Root-knot Nematode Meloidogyne Graminicola. *Molecular Plant Pathology*.*25*(1)

Liu, M., Hong, L., Zhu, Y., Epsztein, R., Shi, T., Sun, Y., Xu, Z., Sun, S., & Xing, W. 2023. Constructing Biocatalytic Nanochannel Membranes for Unidirectional Isomer Conversion and Separation. *Aiche Journal*.*69*(11)

Liu, Z., Xu, Z., Wang, D., Yang, Y., Duan, Y., Ma, L., Lin, T., & Liu, H. 2021. A Review on Molecularly Imprinted Polymers Preparation by Computational Simulation-Aided Methods. *Polymers*.*13*(16), p 2657

Long, X., Chen, H., Wang, C., Wu, H., Li, L., Xing, Y., & Zhang, C. 2024. Host-Guest-Induced Electronic State Triggers Two-Electron Oxygen Reduction Electrocatalysis. Nature communications, 15(1), 9222

Lorigo, M., Quintaneiro, C., Breitenfeld, L., & Cairrao, E. 2024. Exposure to UV-B filter octylmethoxycinnamate and human health effects: Focus on endocrine disruptor actions. *Chemosphere*.*358*, p 142218

Lu, R., Xu, J., Wang, Z., Zhang, S., Wang, H., Xu, H., & Lv, M. 2022. Semisynthesis and Pesticidal Activities of Novel Cholesterol Ester Derivatives Containing Cinnamic Acid-like Fragments. *Molecules*.*27*(23)

Lubbers, R. J. M., Dilokpimol, A., Navarro-Muñoz, J. C., Peng, M., Wang, M., Lipzen, A., Ng, V., Grigoriev, I. V., Visser, J., Hildén, K. S., & Vries, R. P. de. 2019. Cinnamic Acid and Sorbic Acid Conversion Are Mediated by the Same *Trans*criptional Regulator in Aspergillus Niger. *Frontiers in Bioengineering and Biotechnology*.*7*

© University of Venda

Lythgoe, M. P., Desai, A., Gyawali, B., Savage, P., Krell, J., Warner, J. L., & Khaki, A. R. 2022. Cancer Therapy Approval Timings, Review Speed, and Publication of Pivotal Registration Trials in the US and Europe, 2010-2019. *Jama Network Open*.*5*(6), p e2216183

Ma, Xingbin, Lin, H., Yong, Y., Ju, X., Li, Y., Liu, X., Yu, Z., Wujin, C., She, Y., Zhang, J., & El-Aty, A. M. A. 2022. Molecularly Imprinted Polymer-Specific Solid-Phase Extraction for the Determination of 4-Hydroxy-2(3H)benzoxazolone Isolated From Acanthus Ilicifolius Linnaeus Using High-Performance Liquid Chromatography-Tandem Mass Spectrometry. *Frontiers in Nutrition*.*9*

Ma, Xin-Kun, & Liu, Y. 2021. Supramolecular Purely Organic Room-Temperature Phosphorescence. *Accounts of Chemical Research*.*54*(17), pp 3403–3414

Maciel, E. V. S., Mejía-Carmona, K., & Lanças, F. M. 2020. Evaluation of Two Fully Automated Setups for Mycotoxin Analysis Based on Online Extraction-Liquid Chromatography–Tandem Mass Spectrometry. *Molecules*.*25*(12), p 2756

Madaraboina, M., Reddy, B. S., Boddupalli, V. S. K., Reddy, P. S., Anireddy, J. S., Budhdev, R. R., Bandichhor, R., & Achanta, S. 2023. Development of a Practical and Scalable Process for Lifitegrast. *Organic Process Research & Development*.*27*(11), pp 2035–2044

Madhu, J., Vengaipandian, S., Santhanam, A., Natarajan, M., & Velauthapillai, D. 2023. Adsorption of CO2 Using “Sugar Cube”-Shaped Zeolite a Type Derived From Thermally Treated Kaolin and NaOH. *Energy & Fuels*.*37*(15), pp 11152–11176

Madsen, D. H., Fjæstad, K. Y., Johansen, A. Z., Linder, H., Baker, K. J., Schattefor, M., Thorseth, M., Siersbæk, M., Perez-Penco, M., Rahbech, A., Saló, S. F., Engelholm, L. H., Svane, I. M., Andersen, M. H., Junker, N., Grøntved, L., & Straten, P. thor. 2024. B-Adrenergic Signaling Blockade Attenuates Metastasis Through Activation of Cytotoxic CD4 T Cells.Daniel Madsen, Klaire Fjaestad, Astrid Zedlitz Johansen et al. β-adrenergic signaling blockade attenuates metastasis through activation of cytotoxic CD4 T cells, 30 December, PREPRINT (Version 1) available at Research Square

© University of Venda

Madsen, M., Roussis, S. G., Schniepp, E., Rentel, C., & Capaldi, D. C. 2019. Assay Determination by Mass Spectrometry for Oligonucleotide Therapeutics. *Rapid Communications in Mass Spectrometry*.*33*(22), pp 1774–1780

Maestro, A., Malviya, B. K., Auer, G., Ötvös, S. B., & Kappe, C. O. 2024. A Robust Heterogeneous Chiral Phosphoric Acid Enables Multi Decagram Scale Production of Optically Active N,S-Ketals. *Green Chemistry*.*26*(8), pp 4593–4599

Malekipour, M. H., Shirani, F., Moradi, S., & Taherkhani, A. 2023. Cinnamic Acid Derivatives as Potential Matrix Metalloproteinase-9 Inhibitors: Molecular Docking and Dynamics Simulations. *Genomics & Informatics*.*21*(1), p e9

Mancera-Arteu, M., Benavente, F., Sanz-Nebot, V., & Giménez, E. 2023. Sensitive Analysis of Recombinant Human Erythropoietin Glycopeptides by on-Line Phenylboronic Acid Solid-Phase Extraction Capillary Electrophoresis Mass Spectrometry. *Journal of Proteome Research*.*22*(3), pp 826–836

Maria, L. D., Arcadio, F., Gabetta, G., Merli, D., Alberti, G., Zeni, L., Cennamo, N., & Pesavento, M. 2024. An Optical Device Based on a Chemical Chip and Surface Plasmon Platform for 2-Furaldehyde Detection in Insulating Oil. *Sensors*.*24*(16), p 5261

Martinenghi, L. D., Jønsson, R., Lund, T., & Jenssen, H. 2020. Isolation, Purification, and Antimicrobial Characterization of Cannabidiolic Acid and Cannabidiol From Cannabis Sativa L. *Biomolecules*.*10*(6), p 900

Masuda, Y., Ikeshita, D., Higashida, K., Yoshida, M., Ishida, N., Murakami, M., & Sawamura, M. 2023. Photocatalytic 1,2-Phosphorus-Migrative [3 + 2] Cycloaddition of Tri(t-Butyl)phosphine With Terminal Alkynes. *Journal of the American Chemical Society*.*145*(34), pp 19060–19066

Meléndez-Marmolejo, J., Díaz de León-Martínez, L., Galván-Romero, V., Villarreal-Lucio, S., Ocampo-Pérez, R., Medellín-Castillo, N. A., Padilla-Ortega, E., Rodríguez-Torres, I., & Flores-Ramírez, R. 2022. Design and application of molecularly imprinted polymers for adsorption and environmental

© University of Venda

assessment of anti-inflammatory drugs in wastewater samples. *Environmental Science and Pollution Research*.*29*(30), pp 45885–45902

Meléndez-Marmolejo, J., León-Martínez, L. D. de, Galván-Romero, V., Villarreal-Lucio, D. S., Ocampo-Pérez, R., Medellín-Castillo, N. A., Padilla-Ortega, É., Rodríguez, I., & Flores-Ramírez, R. 2022. Design and Application of Molecularly Imprinted Polymers for Adsorption and Environmental Assessment of Anti-Inflammatory Drugs in Wastewater Samples. *Environmental Science and Pollution Research*.*29*(30), pp 45885–45902

Miliovsky, M., Svinyarov, I., Prokopova, E., Batovska, D., Stoyanov, S., & Bogdanov, M. G. 2015. Synthesis and Antioxidant Activity of Polyhydroxylated *Trans*-Restricted 2-Arylcinnamic Acids. *Molecules*.*20*(2), pp 2555–2575

Monisha, T. R., Ismailsab, M., Masarbo, R., Nayak, A. S., & Karegoudar, T. B. 2018. Degradation of cinnamic acid by a newly isolated bacterium Stenotrophomonas sp. TRMK2. *3 Biotech*.*8*(8), p 368

Mpanza, N. M., Godman, B., Keele, G., & Matlala, M. 2022. Trends in the Utilization of Medicines Sold in the Private Sector Post- Registration in South Africa and the Implications for Similar Countries. *BMC Public Health* 23, 192

Mpupa, A., Dinc, M., Mizaikoff, B., & Nomngongo, P. N. 2021. Exploration of a Molecularly Imprinted Polymer (MIPs) as an Adsorbent for the Enrichment of Trenbolone in Water. *Processes*.*9*(2), p 186

Mrówka, J., Gackowski, M., Lityńska-Dobrzyńska, L., Bernasik, A., Kosydar, R., Drelinkiewicz, A., & Hasik, M. 2020. Poly(methylvinylsiloxane)-Based High Internal Phase Emulsion-Templated Materials (polyHIPEs)—Preparation, Incorporation of Palladium, and Catalytic Properties. *Industrial & Engineering Chemistry Research*.*59*(44), pp 19485–19499

Mukasa, D., Wang, M., Min, J., Yang, Y., Solomon, S., Han, H., Ye, C., & Gao, W. 2023. A Computationally Assisted Approach for Designing Wearable Biosensors Toward Non-Invasive Personalized Molecular Analysis. *Advanced Materials*.*35*(35)

© University of Venda

Munjal, N. S., Shukla, R., & Singh, T. R. 2019. Chemometric Approach to Estimate Kinetic Properties of Paclitaxel Prodrugs and Their Substructures for Solubility Prediction Through Molecular Modelling and Simulation Studies. *Journal of Chemometrics*.*33*(11)

Muralikrishna, K., Satyanarayana, V., Kumar, G. C., & Yadav, J. S. 2019. Studies Towards the Synthesis of Aldgamycin – M. *Chemistryselect*.*4*(11), pp 3002–3005

Murcia-Morales, M., Cutillas, V., & Fernández-Alba, A. R. 2019. Supercritical Fluid Chromatography and Gas Chromatography Coupled to Tandem Mass Spectrometry for the Analysis of Pyrethroids in Vegetable Matrices: A Comparative Study. *Journal of Agricultural and Food Chemistry*.*67*(46), pp 12626–12632

Mutz, M., Kösters, D., Wynands, B., Wierckx, N., & Marienhagen, J. 2023. Microbial Synthesis of the Plant Natural Product Precursor P-Coumaric Acid With Corynebacterium Glutamicum. *Microbial Cell Factories*.*22*(1)

Mwanza, C., Zhang, W.-Z., Kalulu, M., & Ding, S.-N. 2024. Advancing green chemistry in environmental monitoring: The role of electropolymerized molecularly imprinted polymer-based electrochemical sensors. *Green Chemistry*. 26, pp 11490-11517

Nadim, A. H., El-Aal, M. A. A., Al-Ghobashy, M. A., & El-Saharty, Y. S. 2021. Facile Imprinted Polymer for Label-Free Highly Selective Potentiometric Sensing of Proteins: Case of Recombinant Human Erythropoietin. *Analytical and Bioanalytical Chemistry*.*413*(14), pp 3611–3623

Natić, M., Zagorac, D. D., Jakanovski, M., Smailagić, A., Čolić, S., Meland, M., & Akšić, M. F. 2024. Fruit Quality Attributes of Organically Grown Norwegian Apples Are Affected by Cultivar and Location. *Plants*.*13*(1), p 147

Nehela, Y., Mazrou, Y. S. A., Taha, N., Elzaawely, A. A., Xuan, T. D., Makhlouf, A. H., & El-Nagar, A. 2023. Hydroxylated Cinnamates Enhance Tomato Resilience to Alternaria Alternata, the Causal Agent of Early Blight Disease, and Stimulate Growth and Yield Traits. *Plants*.*12*(9), p 1775

© University of Venda

Nessiem, M. A., Riad, S. M., Salah, A., & arafa, reham M. 2024. Chiral Separation of Racemic Atracurium Through B-Cyclodextrin Sulphated Sodium Modified Gold Nanoparticles/Pencil Graphite Electrode: An Eco-Friendly Voltammetric Behavior of *Cis*atracurium Isomer in Real Samples. *Journal of the Electrochemical Society*.*171*(10), p 107508

Newbronner, E., & Wadman, R. 2021. Depression and Anxiety Symptoms in UK Thalidomide Survivors: A Brief Survey. *Disabilities*.*1*(1), pp 23–29

Niaei, N., Hassanpour, S., & Petr, J. 2024. Chiral Resolution of Cationic Piperazine Derivatives by Capillary Electrophoresis Using Sulfated B-cyclodextrin. *Electrophoresis*.*45*(17–18), pp 1479–1486

Niu, J., Du, M., Wu, W., Yang, J., & Chen, Q. 2024. Advances in the Selection of Functional Monomers for Molecularly Imprinted Polymers: A Review. *Journal of Separation Science*.*47*(16)

Nuro, A., Murtaj, B., & Marku, E. 2022. Some of the Characteristic Substances in the Devola River, Albania. *Zastita Materijala*.*63*(1), pp 37–49

Olbrycht, M., Bajek-Bil, A., Balawejder, M., Poplewska, I., Piątkowski, W., & Antos, D. 2021. Development of a Route to the Most Active Nafronyl Stereoisomer by Coupling Asymmetric Synthesis and Chiral Chromatography Separation. *Chemical Engineering & Technology*.*44*(9), pp 1686–1692

Pali-Schöll, I., Lucia, M. D., Jackson, H. A., Janda, J., Mueller, R. S., & Jensen-Jarolim, E. 2017. Comparing Immediate-type Food Allergy in Humans and Companion Animals—Revealing Unmet Needs. *Allergy*.*72*(11), pp 1643–1656

Pan, Q., & Kong, W. 2024. Ligand Controlled Stereodivergent Construction of 1,3-Nonadjacent Stereocenters via Nickel-Catalyzed Reductive Cyclization/Cross-Couplings. *Wuhan University Journal of Natural Sciences*.*29*(3), pp 195–197

Pandya, P. A., Shah, P. A., & Shrivastav, P. S. 2020. Analytical separation of four stereoisomers of luliconazole using supercritical fluid chromatography: Thermodynamic aspects and simulation study with chiral stationary phase. *Journal of Chromatography A*.*1625*, p 461299

© University of Venda

Papp, L. A., Foroughbakhshfasaei, M., Fiser, B., Horváth, P., Kiss, E., Sekkoum, K., Gyéresi, Á., Hancu, G., Noszál, B., Szabó, Z., & Tóth, G. 2019. Reversed-phase HPLC Enantioseparation of Pantoprazole Using a Teicoplanin Aglycone Stationary Phase—Determination of the Enantiomer Elution Order Using HPLC-CD Analyses. *Chirality*.*32*(2), pp 158–167

Perry, L. T., Bhasale, A. L., Fabbri, A., Lexchin, J., Puil, L., Joarder, M., & Mintzes, B. 2019. Comparative Analysis of Medicines Safety Advisories Released by Australia, Canada, the United States, and the United Kingdom. *Jama Internal Medicine*.*179*(7), p 982

Petrusová, Z., Slouka, Z., Vobecká, L., Polezhaev, P., Hasal, P., Přibyl, M., & Izák, P. 2021. Microreaction and Membrane Technologies for Continuous Single-Enantiomer Production: A Review. *Catalysis Reviews*.*65*(3), pp 773–821

Pham, C., Le, K., Draves, M., & Seoane-Vazquez, E. 2023. Assessment of FDA-Approved Drugs Not Recommended for Use or Reimbursement in Other Countries, 2017-2020. *Jama Internal Medicine*.*183*(4), p 290

Phillips, A. M. F., & Pombeiro, A. J. L. 2023. Atropselective Organocatalytic Synthesis of Chiral Compounds Containing Nitrogen Along the Axis of Chirality. *Symmetry*.*15*(6), p 1261

Poonsri, W., Pengsook, A., Pluempanupat, W., Yooboon, T., & Bullangpoti, V. 2019. Evaluation of Alpinia Galanga (Zingiberaceae) Extracts and Isolated *Trans*-Cinnamic Acid on Some Mosquitoes Larvae. *Chemical and Biological Technologies in Agriculture*.*6*(1)

Promkatkaew, M., Boonsri, P., Suramitr, S., Karpkird, T., Wolschann, P., & Hannongbua, S. 2023. Stability improvement of UV-filter between methoxy cinnamic acid derivatives and cyclodextrins inclusion complexes based on DFT and TD-DFT investigations. *Journal of Molecular Graphics and Modelling*.*125*, p 108619

© University of Venda

Quaglia, M., Chenon, K., Hall, A. J., De Lorenzi, E., & Sellergren, B. 2001. Target Analogue Imprinted Polymers with Affinity for Folic Acid and Related Compounds. *Journal of the American Chemical Society*.*123*(10), pp 2146–2154

Rahman, P., Chakraborty, N., Patel, B. K., & Rajbongshi, K. K. 2024. Iodine-Promoted Sulfoximidation of Cinnamic Acids via Oxidative C═C Bond Cleavage. *The Journal of Organic Chemistry*.*89*(15), pp 10472–10484

Reddy, B. S., & Dubey, P. K. 2023. Chirality and Drug Activity. *Resonance*.*28*(3), pp 447–464

Riedel, F., Puertas-Bartolomé, M., Enrico, L. L. T., Fink-Straube, C., Duong, C. N., Gherlone, F., Huang, Y., Valiante, V., Campo, A. del, & Sankaran, S. 2023. Engineered Living Materials for the Conversion of a Low-Cost Food-Grade Precursor to a High-Value Flavonoid. *Frontiers in Bioengineering and Biotechnology*.*11*

Robertson, D. W., Katzenellenbogen, J. A., Long, D. J., Rorke, E. A., & Katzenellenbogen, B. S. 1982. Tamoxifen antiestrogens. A comparison of the activity, pharmacokinetics, and metabolic activation of the *cis* and *trans* isomers of tamoxifen. *Journal of Steroid Biochemistry*.*16*(1), pp 1–13

Rulence, A., Perreault, V., Thibodeau, J., Firdaous, L., Fliss, I., & Bazinet, L. 2023. Nisin Purification From a Cell-Free Supernatant by Electrodialysis in a Circular Economy Framework. *Membranes*.*14*(1), p 2

Ruwizhi, N., & Aderibigbe, B. A. 2020. Cinnamic Acid Derivatives and Their Biological Efficacy. *International Journal of Molecular Sciences*.*21*(16), p 5712

Ryang, J., Yan, Y., Song, Y., Liu, F., & Ng, T. B. 2019. Anti-Hiv, Antitumor and Immunomodulatory Activities of Paclitaxel From Fermentation Broth Using Molecular Imprinting Technique. *AMB Express*.*9*(1) 194

Saad, S. E. A., Aburawi, S. M., Rahoumh, A. A., Rahoumh, A. A., & Abdraheem, A. 2022. Influence of B-Blockers on the Activity of Some Anti-Epileptic Drugs on Convulsions Induced by Picrotoxin in Mice. *Libyan Journal of Medical Research*.*16*(2), pp 127–134

© University of Venda

Saffati, G., Kassab, J., Rendon, D. O., Hinojosa-González, D. E., Kronstedt, S., Lipshultz, L. I., & Khera, M. 2024. Safety and Efficacy of Enclomiphene and Clomiphene for Hypogonadal Men. *Translational Andrology and Urology*.*13*(9), pp 1984–1990

Salahudeen, N., & Alhassan, A. J. 2022. Adsorption of Crystal Violet on Rice Husk Activated Carbon. *Journal of Engineering Sciences*.*9*(1), pp F11–F15

Salem, M. A., Yoshida, T., Souza, L. P. de, Alseekh, S., Bajdzienko, K., Fernie, A. R., & Giavalisco, P. 2020. An Improved Extraction Method Enables the Comprehensive Analysis of Lipids, Proteins, Metabolites and Phytohormones From a Single Sample of Leaf Tissue Under Water-deficit Stress. *The Plant Journal*.*103*(4), pp 1614–1632

Sant'Ana, T. da S., Latorres, J. M., & Martins, V. G. 2024. Upcycling of Beer Industry Wastewater: Biosurfactant Production and Application in Brewery Effluent Treatment. *Environmental Quality Management*.*34*(2)

Schieber, A. 2018. Chemistry and bioactivity of naturally occurring cinnamic acid derivatives. (),. *Natural Product Reports*.*35*(3), pp 250–280

Segawa, H., Iwata, Y. T., Yamamuro, T., Kuwayama, K., Tsujikawa, K., Kanamori, T., & Inoue, H. 2018. Simultaneous chiral impurity analysis of methamphetamine and its precursors by supercritical fluid chromatography–tandem mass spectrometry. *Forensic Toxicology*.*37*, pp 145–153

Seibert, E., Hubner, E.-M., & Schmid, M. G. 2025. Chiral Separation and Determination of Enantiomer Elution Order of Novel Ketamine Derivatives Using CE-UV and HPLC-UV-ORD. *Separations*.*12*(2)

Sellergren, B. 2000. *Molecularly imprinted polymers: Man-made mimics of antibodies and their application in analytical chemistry*.

Seog, D. J. H., Kien, N. V., & Ryoo, J. J. 2023. Amino Alcohol-derived Chiral Stationary Phases. *Chirality*.*35*(10), pp 739–752

© University of Venda

Shafqat, S. S., Bhawani, S. A., Bakhtiar, S., & Ibrahim, M. N. M. 2023. Template-Assisted Synthesis of Molecularly Imprinted Polymers for the Removal of Methyl Red From Aqueous Media. *BMC Chemistry*.*17*(1)

Shagufta, Ahmad, I., Mathew, S., & Rahman, S. 2020. Recent progress in selective estrogen receptor downregulators (SERDs) for the treatment of breast cancer. *RSC Medicinal Chemistry*.*11*(4), pp 438–454

Shi, J., Lin, Z., Kou, S., Wang, B., & Jiang, S. 2021. Enantioseparation of Mandelic Acid and Substituted Derivatives by High-performance Liquid Chromatography With Hydroxypropyl-β-cyclodextrin as Chiral Mobile Additive and Evaluation of Inclusion Complexes by Molecular Dynamics. *Chirality*.*33*(10), pp 675–684

Shi, X., Liu, F., & Mao, J. 2016. The CGC enantiomer separation of 2-arylcarboxylic acid esters by using β-cyclodextrin derivatives as chiral stationary phases. *Anal Chim Acta*.*912*, pp 156–62

Shipman, M., Sproules, S., Wilson, C., & Symes, M. D. 2019. Towards a Better Understanding of the Electrosynthesis of 2,5-Dicarboxy-2,5-Dihydrofurans: Structure, Mechanism and Influence Over Stereochemistry. *Royal Society Open Science*.*6*(7), p 190336

Silva, A. T., Bento, C. M., Pena, A. C., Figueiredo, L. M., Prudêncio, C., Aguiar, L., Silva, T., Ferraz, R., Gomes, M. S., Teixeira, C., & Gomes, P. 2019. Cinnamic Acid Conjugates in the Rescuing and Repurposing of Classical Antimalarial Drugs. *Molecules*.*25*(1), p 66

Singh, R., & Singh, M. 2022. Design of Imprinting Matrix for Dual Template Sensing via Electropolymerized Polythiophene Films. *Journal of Molecular Recognition*.*35*(8)

Sokka, I. K., Imlimthan, S., Sarparanta, M., Maaheimo, H., Johansson, M. P., & Ekholm, F. S. 2021. Halogenation at the Phenylalanine Residue of Monomethyl Auristatin F Leads to a Favorable *cis*/*trans* Equilibrium and Retained Cytotoxicity. *Molecular Pharmaceutics*.*18*(8), pp 3125–3131

© University of Venda

Song, Q., Wang, Y., Tang, S., Meng, X., Wang, F., Hu, D., & Zhang, Y. 2021. Enantioselective Analysis and Degradation Studies of Four Stereoisomers of Difenoconazole in Citrus by Chiral Liquid Chromatography–Tandem Mass Spectrometry. *Journal of Agricultural and Food Chemistry*.*69*(1), pp 501–510

Speed, T. J., McIntyre, J. P., & Thamattoor, D. M. 2004. Wittig Reaction Using a Stabilized Phosphorus Ylid: An Efficient and Stereoselective Synthesis of Ethyl *trans*-Cinnamate. *Journal of Chemical Education*.*81*(9), p 1355

Speranza, B., Cibelli, F., Baiano, A., Carlucci, A., Raimondo, M. L., Campaniello, D., Viggiani, I., Bevilacqua, A., & Rosaria Corbo, M. 2020. Removal Ability and Resistance to Cinnamic and Vanillic Acids by Fungi. *Microorganisms*.*8*(6), p 930

Stamatelatou, K., Blika, P. S., Ntaikou, I., & Lyberatos, G. 2012. Integrated Management Methods for the Treatment and/or Valorization of Olive Mill Wastes. In *Novel Technologies in Food Science: Their Impact on Products, Consumer Trends and the Environment*. A. McElhatton, & P. J. do Amaral Sobral (Eds) *Novel Technologies in Food Science: Their Impact on Products, Consumer Trends and the Environment*.pp 65–118 New York, NY: Springer New York

Suryana, S., Mutakin, Rosandi, Y., & Hasanah, A. N. 2021. An Update on Molecularly Imprinted Polymer Design through a Computational Approach to Produce Molecular Recognition Material with Enhanced Analytical Performance. *Molecules*.*26*(7)

Suwanwong, Y., Kulkeratiyut, S., Prachayasittikul, V., & Boonpangrak, S. 2014. Effects of Polymerization Methods and Functional Monomers on Curcumin Imprinted Polymer Properties. *Separation Science and Technology*.*49*(7), pp 1086–1095

Tang, S., Meng, X., Wang, F., Lin, Q., Feng, T., Hu, D., & Zhang, Y. 2022. Four Propiconazole Stereoisomers: Stereoselective Bioactivity, Separation via Liquid Chromatography–Tandem Mass Spectrometry, and Dissipation in Banana Leaves. *Journal of Agricultural and Food Chemistry*.*70*(3), pp 877–886

© University of Venda

Tani, H., Hikami, S., Takahashi, S., Kimura, Y., Matsuura, N., Nakamura, T., Yamaga, M., & Koshino, H. 2019. Isolation, Identification, and Synthesis of a New Prenylated Cinnamic Acid Derivative From Brazilian Green Propolis and Simultaneous Quantification of Bioactive Components by LC-MS/MS. *Journal of Agricultural and Food Chemistry*.*67*(44), pp 12303–12312

Tchekalarova, J., Pechlivanova, D., Rangelov, M., Todorova, N., Stoyanova, T., Assenov, B., & Todorov, P. 2024. A Novel Cinnamic and Caffeic Acid-conjugated Peptide Analogs With Anticonvulsant and Analgesic Potency: Comparative Analyses of *trans*/*Cis* Isomers. *Drug Development Research*.*85*(5)

Thach, U. D., Thị, H. H. N., Pham, T. D., Đào, H. H., & Nhu-Trang, T. 2021. Synergetic Effect of Dual Functional Monomers in Molecularly Imprinted Polymer Preparation for Selective Solid Phase Extraction of Ciprofloxacin. *Polymers*.*13*(16), p 2788

Til, R. F., Alizadeh-Khaledabad, M., Mohammadi, R., Pirsa, S., & Wilson, L. D. 2020. Molecular imprinted polymers for the controlled uptake of sinapic acid from aqueous media. *Food & function*.*11*(1), pp 895–906

Tiwari, M., & Pattanayek, S. K. 2024. Melamine-imprinted quartz Crystal Microbalance Sensor for Its Detection in Milk. *Journal of Applied Polymer Science*.*141*(24)

Tsao, R. 2020. Chemistry and biological activities of cinnamic acid and its derivatives. *Critical Reviews in Food Science and Nutrition*.*60*(13), pp 2164–2191

Tukker, A. M., & Westerink, R. H. S. 2021. Novel Test Strategies for in Vitro Seizure Liability Assessment. *Expert Opinion on Drug Metabolism & Toxicology*.*17*(8), pp 923–936

Urbańska, M. 2024. Application of Polysaccharide-Based Columns for the Separation of Racemic Mixtures Obtained Based on (R,S)-2-Octanol by Reversed-Phase Chiral Liquid Chromatography. https://doi.org/10.20944/preprints202403.0796.v1

Vadagam, N., Haridasyam, S. B., Venkatanarayana, M., Lakka, N. S., & Chinnakadoori, S. R. 2023. Separation and Simultaneous Estimation of Enantiomers and Diastereomers of Muscarinic Receptor

© University of Venda

Antagonist Solifenacin Using Stability-indicating Normal-phase HPLC Technique With Chiral Stationary Phase Amylose Tris-(3,5-dimethylphenylcarbamate). *Chirality*.*36*(2)

Vaisnav, G., Chakraborty, A. K., & Karole, S. 2023. Design, Synthesis and Evaluation of Some Novel Derivatives of Cinnamic Acid as Anti-Inflammatory Agents. *World Journal of Biology Pharmacy and Health Sciences*.*14*(1), pp 088–096

Vrobel, O., & Tarkowski, P. 2023. Can Plant Hormonomics Be Built on Simple Analysis? A Review. *Plant Methods*.*19*(1)

Wang, C., Wang, X., Wang, J., Di, S., Wang, Z., Hao, X. Q., Zhao, H., Changshan, Z., & Qi, P. 2021. Removal of Matrix Interferences by Nano-MgO and Co-Adsorbents for Accurate Multi-Pesticide Residue Analysis in the Chinese Medicinal Herb, Paeoniae Radix Alba. *Journal of Analytical Methods in Chemistry*.*2021*, pp 1–10

Wang, F., Wang, Y., Min, Y., Li, J., Zhang, L., Zheng, T., Shen, J., & Okamoto, Y. 2022. Preparation of Cellulose Derivative Bearing Bulky 4-(2-benzothienyl)phenylcarbamate Substituents as Chiral Stationary Phase for Enantioseparation. *Chirality*.*34*(5), pp 701–710

Wang, S., Kang, O., & Kwon, D. 2021. *Trans*-Cinnamaldehyde Exhibits Synergy With Conventional Antibiotic Against Methicillin-Resistant Staphylococcus Aureus. *International Journal of Molecular Sciences*.*22*(5), p 2752

Wang, Yaqian, Liu, H., Yang, X., & Wang, L. 2022. Aquatic toxicity and aquatic ecological risk assessment of wastewater-derived halogenated phenolic disinfection byproducts. *Science of The Total Environment*.*809*, p 151089

Wang, Yuying, Zhuo, S., Hou, J., Li, W., & Ji, Y. 2019. Construction of B-Cyclodextrin Covalent Organic Framework-Modified Chiral Stationary Phase for Chiral Separation. *Acs Applied Materials & Interfaces*.*11*(51), pp 48363–48369

© University of Venda

Wang, Z., Shuhua, X., Liu, J., Haiqin, M., Wang, Y., Tian, Y., & Hou, W. 2020. Effects of Light Irradiation on Essential Oil Biosynthesis in the Medicinal Plant Asarum Heterotropoides Fr. Schmidt Var. Mandshuricum (Maxim) Kitag. *Plos One*.*15*(9), p e0237952

Wei, Y., Kang, H., Ren, Y., Qin, G., Shuang, S., & Dong, C. 2013. A Simple Method for the Determination of Enantiomeric Composition of Propranolol Enantiomers. *The Analyst*.*138*(1), pp 107–110

Willey, C., & Calip, G. S. 2019. How Did Research on Medication Safety in Pregnancy Define, Develop and Advance the Field of Pharmacoepidemiology? *Clinical Therapeutics*.*41*(12), pp 2464–2466

Wu, H., Wang, H., Qi, F., Xia, T., Xia, Y., Xu, J., & Zhang, X. 2021. An Activatable Host–Guest Conjugate as a Nanocarrier for Effective Drug Release Through Self-Inclusion. *Acs Applied Materials & Interfaces*.*13*(29), pp 33962–33968

Xia, C. N., Li, H. B., Liu, F., & Hu, W. X. 2008. Synthesis of *trans*-caffeate analogues and their bioactivities against HIV-1 integrase and cancer cell lines. *Bioorg Med Chem Lett*.*18*(24), pp 6553–7

Xie, C., Yu, K., Zhong, D., Yuan, T., Ye, F., Jarrell, J. A., Millar, A., & Chen, X. 2011. Investigation of Isomeric *Trans*formations of Chlorogenic Acid in Buffers and Biological Matrixes by Ultraperformance Liquid Chromatography Coupled With Hybrid Quadrupole/Ion Mobility/Orthogonal Acceleration Time-of-Flight Mass Spectrometry. *Journal of Agricultural and Food Chemistry*.*59*(20), pp 11078–11087

Xie, L., Xiao, N., Li, L., Xie, X., & Li, Y. 2020. Theoretical Insight into the Interaction between Chloramphenicol and Functional Monomer (Methacrylic Acid) in Molecularly Imprinted Polymers. *International Journal of Molecular Sciences*.*21*(11)

Xie, X., Huang, D., & Li, Z. 2024. Bioproduction of Rare d-Allulose From d-Glucose via Borate-Assisted Isomerization. *Journal of Agricultural and Food Chemistry*.*72*(6), pp 3036–3044

Xu, H.-H., Yang, L., Tang, M., Ye, A.-P., Tu, B., Jiang, Z., & Yi, J. 2022. From *Cis*-Lobeline to *Trans*-Lobeline: Study on the Pharmacodynamics and Isomerization Factors. *Molecules*.*27*(19), p 6253

© University of Venda

Yağcı, B. B., Zorlu, Y., & Türkmen, Y. E. 2021. Template-Directed Photochemical Homodimerization and Heterodimerization Reactions of Cinnamic Acids. *The Journal of Organic Chemistry*.*86*(18), pp 13118–13128

Yan, Y., Cai, X., Cheng, S., Xie, X.-X., Lan, Y., Wu, S., Fan, J., Zheng, S., Cai, S., & Zhang, W. 2022. Beta-cyclodextrin Covalent Organic Framework Coated Silica Composite as Chiral Stationary Phase for High-performance Liquid Chromatographic Separation. *Separation Science Plus*.*5*(12), pp 671–681

Yoshimi, Y., Katsumata, Y., Osawa, N., Ogishita, N., & Kadoya, R. 2023. Synthesis of fluorescent Molecularly Imprinted Polymer Nanoparticles Sensing Small Neuro*trans*mitters with High Selectivity Using Immobilized Templates with Regulated Surface Density. *Nanomaterials*.*13*(1), p 212

Yu, B. 2023. Revitalizing Thalidomide: Advancements in Drug Design and Therapeutic Strategies. *Theoretical and Natural Science*.*15*(1), pp 7–12

Zahedi, P., Fallah-Darrehchi, M., Nadoushan, S. A., Aeinehvand, R., Bagheri, L., & Najafi, M. 2017. Morphological, thermal and drug release studies of poly (methacrylic acid)-based molecularly imprinted polymer nanoparticles immobilized in electrospun poly (ε-caprolactone) nanofibers as dexamethasone delivery system. *Korean Journal of Chemical Engineering*.*34*, pp 2110–2118

Zeng, Q., Huang, Z., Li, D., & Li, L. 2024. Preparation of a bis-triazolyl Bridged B-cyclodextrin Stationary Phase and Its Application for Enantioseparation of Chiral Compounds by HPLC. *Chirality*.*36*(2)

Zhan, W., Yun, J., Li, Q., & Wang, S. Y. 2019. Study on Unbalanced Competitive Adsorption of Two Ginsenosides by Molecularly Imprinted Polymers. *Key Engineering Materials*.*821*, pp 144–152

Zhang, C., Xu, Q., Hou, H., Wu, J., Zheng, Z., & Ouyang, J. 2020. Efficient Biosynthesis of Cinnamyl Alcohol by Engineered Escherichia Coli Overexpressing Carboxylic Acid Reductase in a Biphasic System. *Microbial Cell Factories*.*19*(1)

Zhang, T., Liu, F., Wang, J., Li, N., & Li, K. 2002. Molecular recognition properties of salicylic acid-imprinted polymers. *Chromatographia*.*55*, pp 447–451

© University of Venda

Zhang, X. 2023. Chemical Synthesis of Chiral Drugs. *Theoretical and Natural Science*.*3*(1), pp 134–140

Zhang, Y., Deng, J., Tian, H., Qi, H., Xiong, T., Lin, S., Dong, Y., Luo, L., Wu, D., Zhang, K., Ji, M., Du, T., Sheng, L., Chen, X., & Xu, H. 2024. Design, Synthesis, and Bioevaluation of Novel Reversibly Photoswitchable PI3K Inhibitors Based on Phenylazopyridine Derivatives Toward Light-Controlled Cancer Treatment. *Journal of Medicinal Chemistry*.*67*(5), pp 3504–3519

Zhang, Z., Ma, L., Yuan, H., Chen, Z., & Lv, Y. 2023. Solid-Phase Screening and Synthesis of Molecularly Imprinted Nanoparticles for Selective Recognition and Detection of Brain Natriuretic Peptide. *Advanced Healthcare Materials*.*12*(13)

Zhao, L., Chen, F., Guo, F., Liu, W., & Liu, K. 2019. Enantioseparation of Chiral Perfluorooctane Sulfonate (PFOS) by Supercritical Fluid Chromatography (SFC): Effects of the Chromatographic Conditions and Separation Mechanism. *Chirality*.*31*(10), pp 870–878

Zhao, Z. 2024. Enzyme-Catalyzed Synthesis in Pharmaceutical Manufacturing. *Highlights in Science Engineering and Technology*.*91*, pp 277–282

Zheng, B., He, X., Zhang, Q., & Duan, M. 2022. A Novel Molecularly Imprinted Membrane for Highly Sensitive Electrochemical Detection of Paracetamol. *International Journal of Electrochemical Science*.*17*(7), p 220736

Zheng, X., Renslow, R., Makola, M. M., Webb, I., Deng, L., Thomas, D., Govind, N., Ibrahim, Y., Kabanda, M. M., Dubery, I. A., Heyman, H. M., Smith, R., Madala, N. E., & Baker, E. 2017. Structural Elucidation of *cis*/*trans* Dicaffeoylquinic Acid Photoisomerization Using Ion Mobility Spectrometry-Mass Spectrometry. *The Journal of Physical Chemistry Letters*.*8*(7), pp 1381–1388

Zhi, K., Li, Z., Luo, H., Ding, Y., Chen, F., Tan, Y., & Liu, H. 2023. Selective Adsorption of Quercetin by the Sol-Gel Surface Molecularly Imprinted Polymer. *Polymers*.*15*(4), p 905

© University of Venda

Zolfaghari, B., Yazdiniapour, Z., Sadeghi, M., Akbari, M., Troiano, R., & Lanzotti, V. 2020. Cinnamic Acid Derivatives From Welsh Onion (Allium Fistulosum) and Their Antibacterial and Cytotoxic Activities. *Phytochemical Analysis*.*32*(1), pp 84–90

Zuo, J., Ma, P., Li, Z., Zhang, Y., Xiao, D., Wu, H., & Dong, A. 2022. Application of Molecularly Imprinted Polymers in Plant Natural Products: Current Progress and Future Perspectives. *Macromolecular Materials and Engineering*.*308*(3)

© University of Venda

Appendix

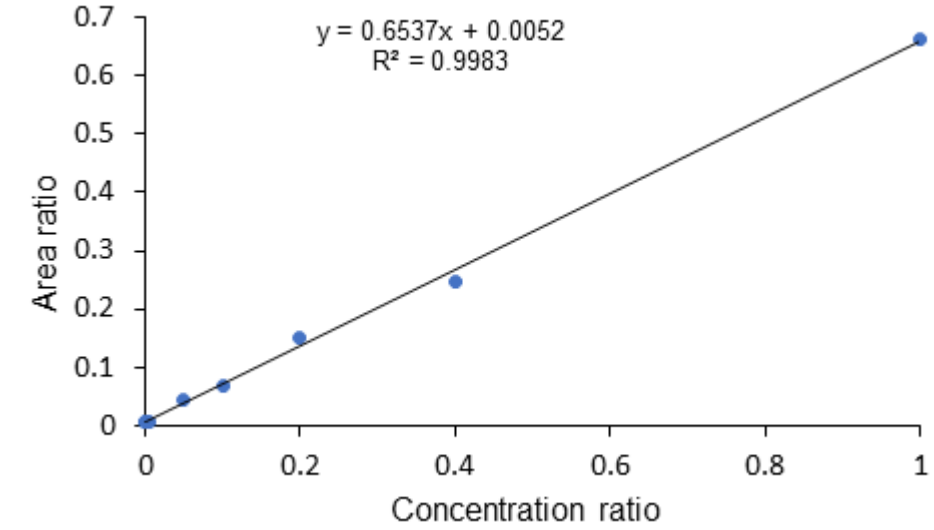


Figure: A1 Calibration curve of ferulic acid

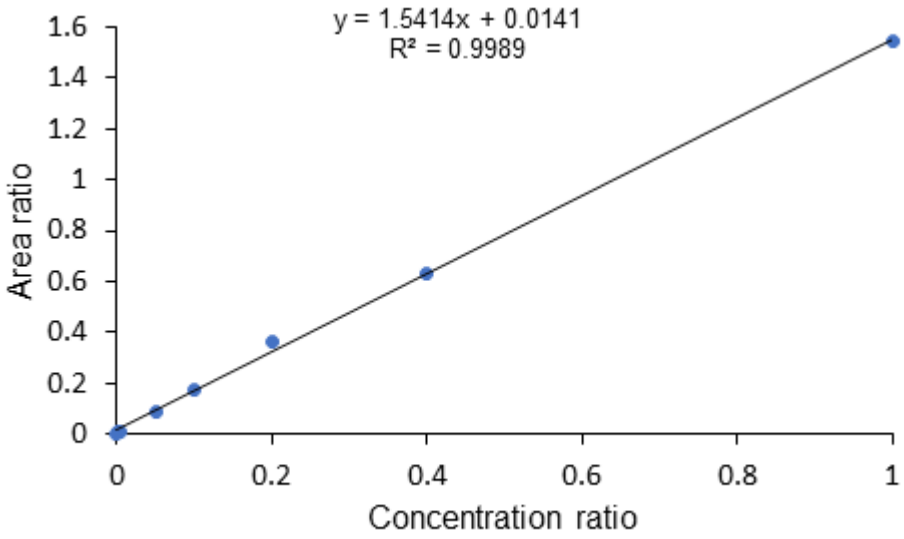


Figure: A2 Calibration curve of 4-Hydroxy cinnamic acid

© University of Venda

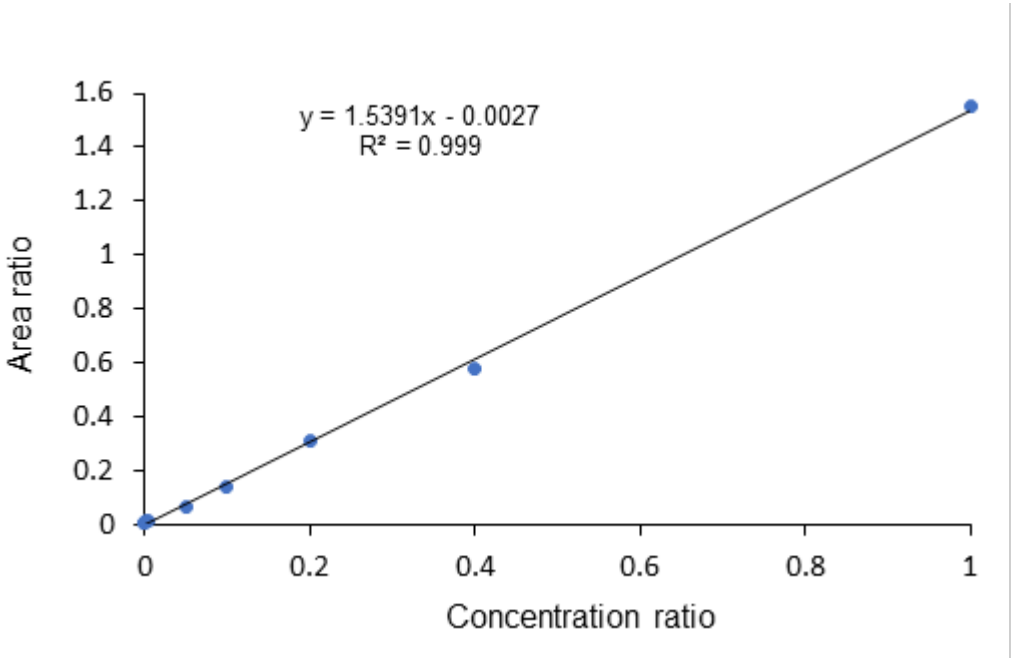
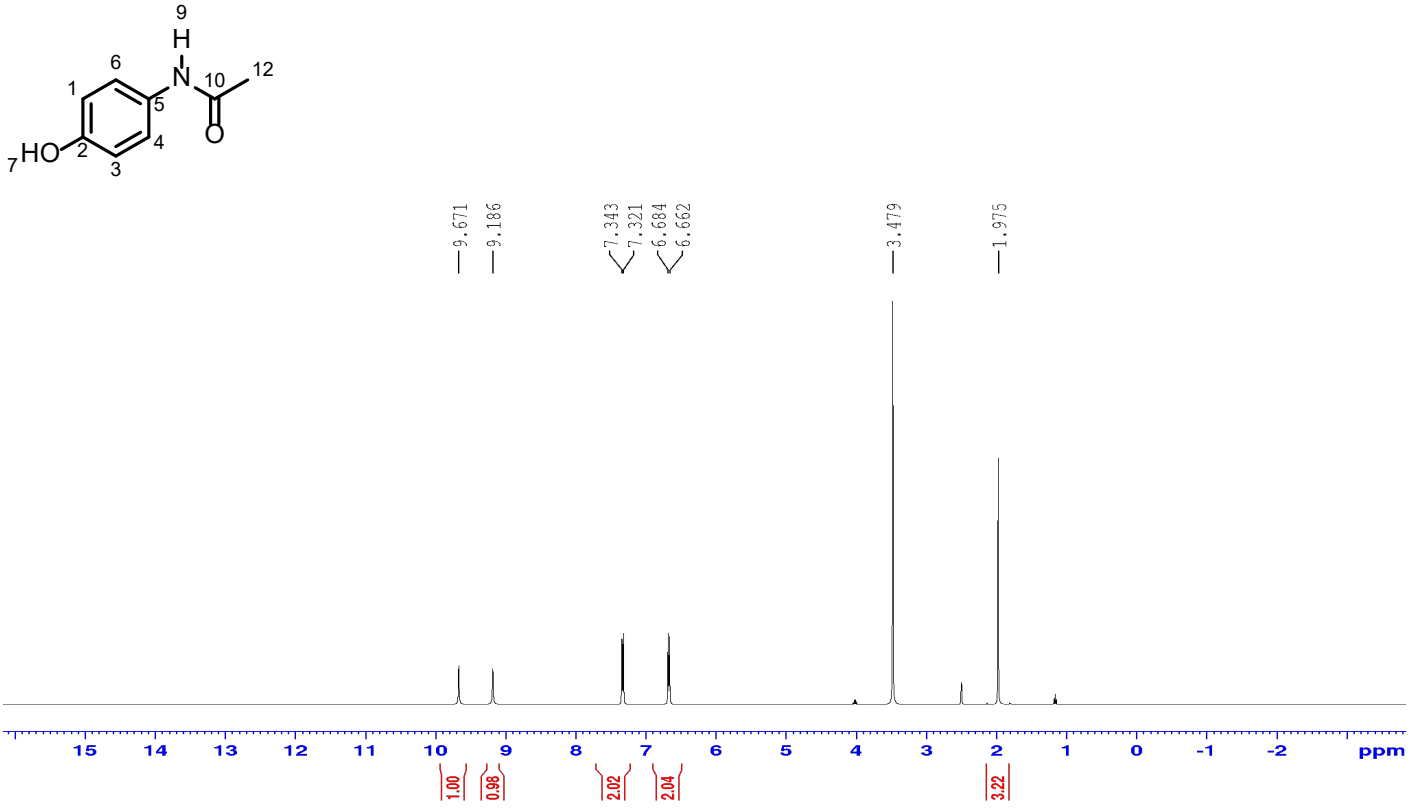


Figure: A3 Calibration curve of ethyl (E)-3-4(-methoxyphenyl) acrylate



© University of Venda

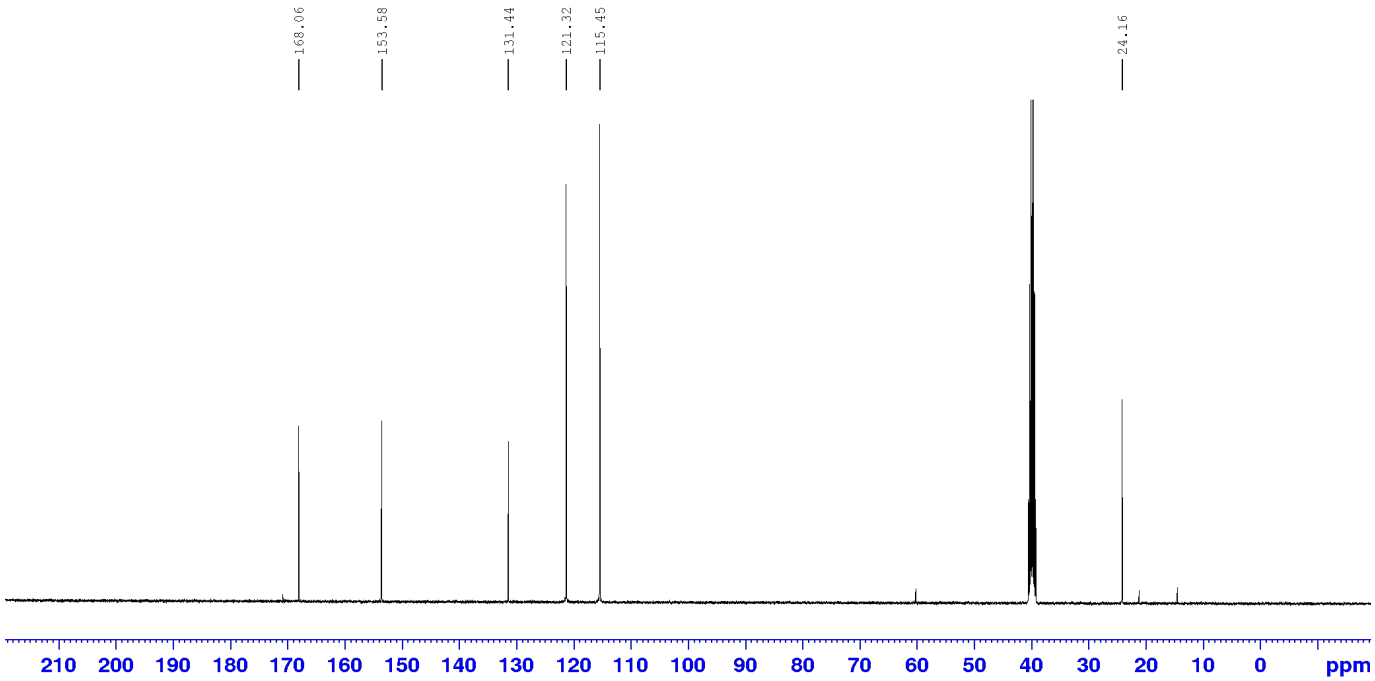


Figure A4: ^{1}H-NMR/^{13}C-NMR spectra of paracetamol

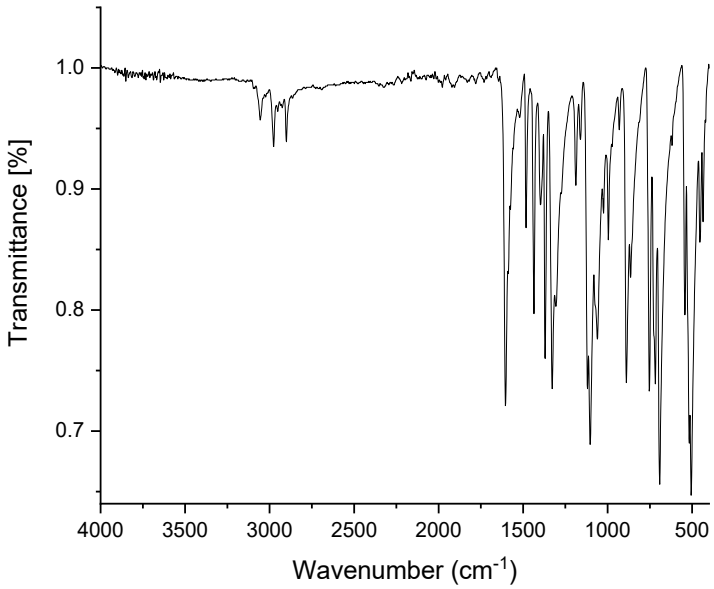


Figure A5: FTIR of paracetamol

.

© University of Venda

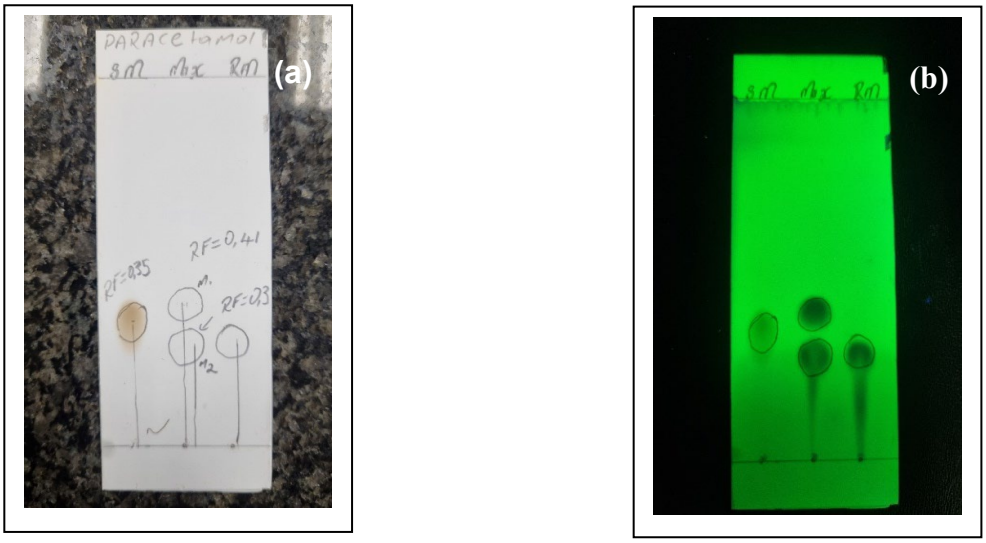


Figure A6: The reported Rf value of Hydroxycinnamic acid was 0.3 with 50/50 % ethyl acetate and petroleum ether (a) without UV-light (b) Under UV-light

© University of Venda

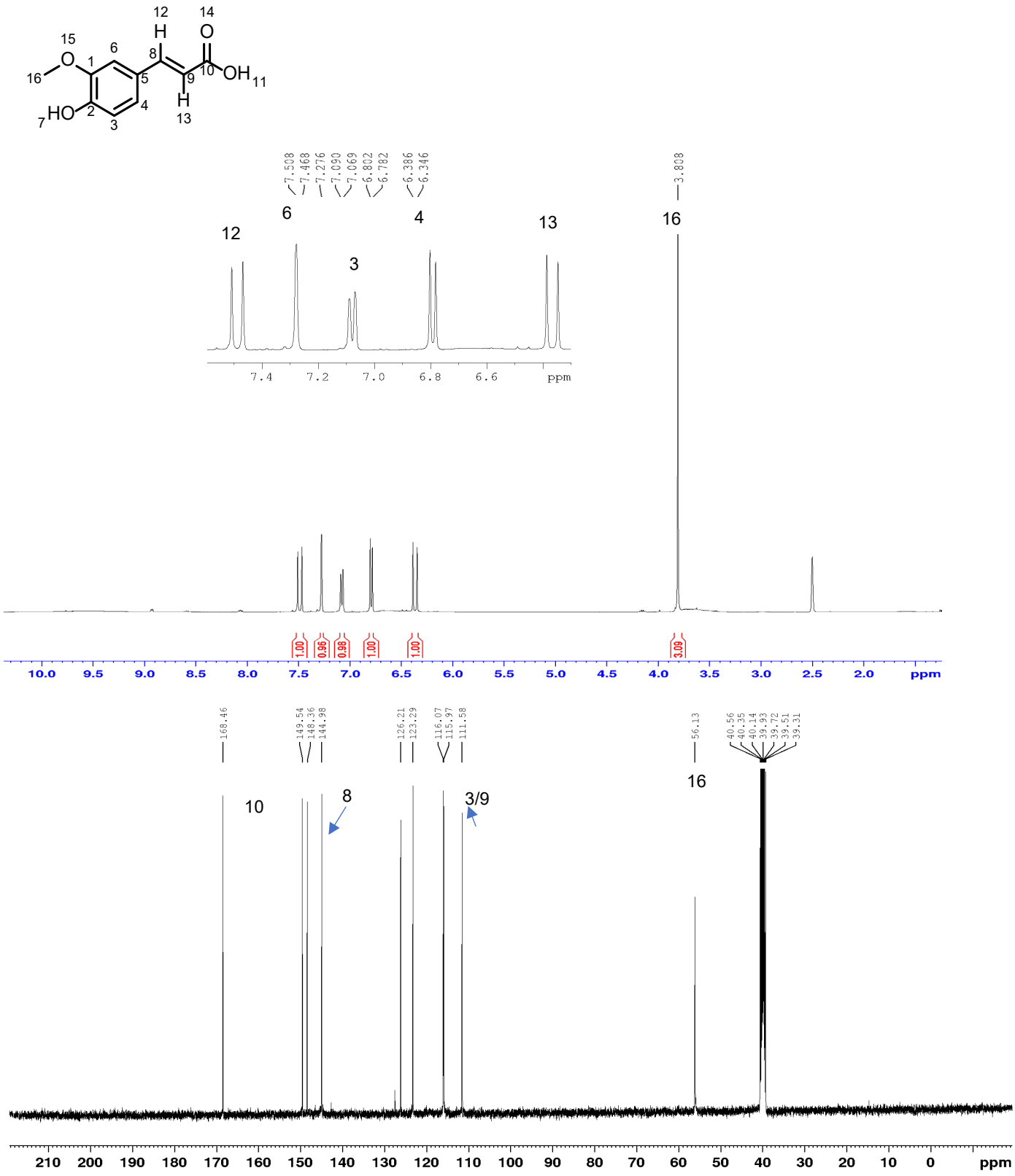


Figure A7: ^{1}H-NMR/^{13}C-NMR spectra of ferulic acid synthesized by procedure B

© University of Venda

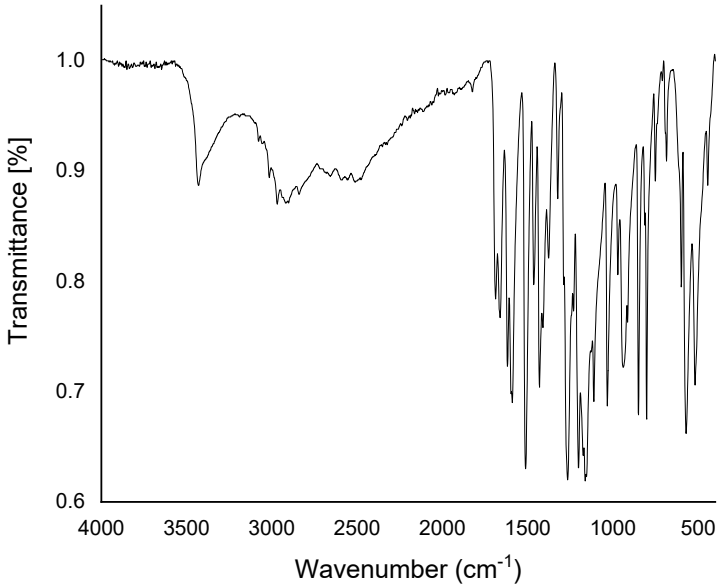


Figure A8: FTIR spectra and TLC visualization of ferulic acid

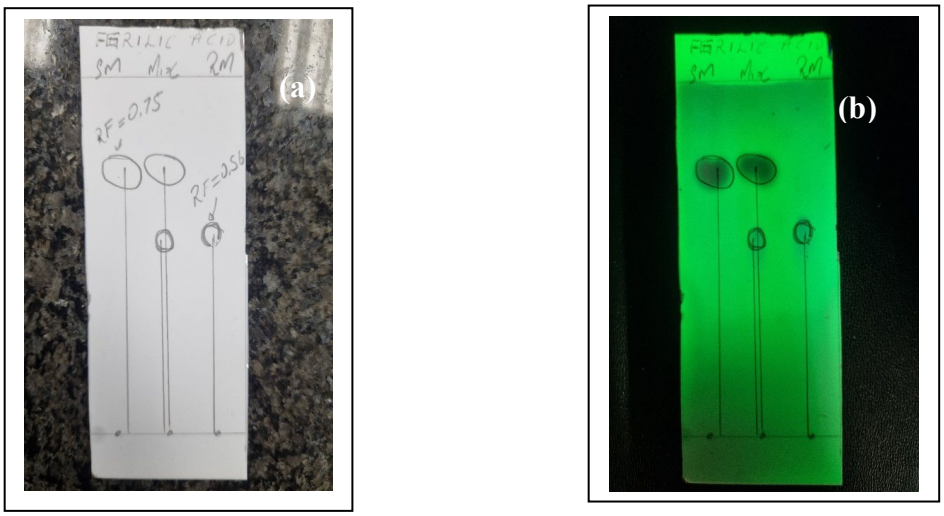
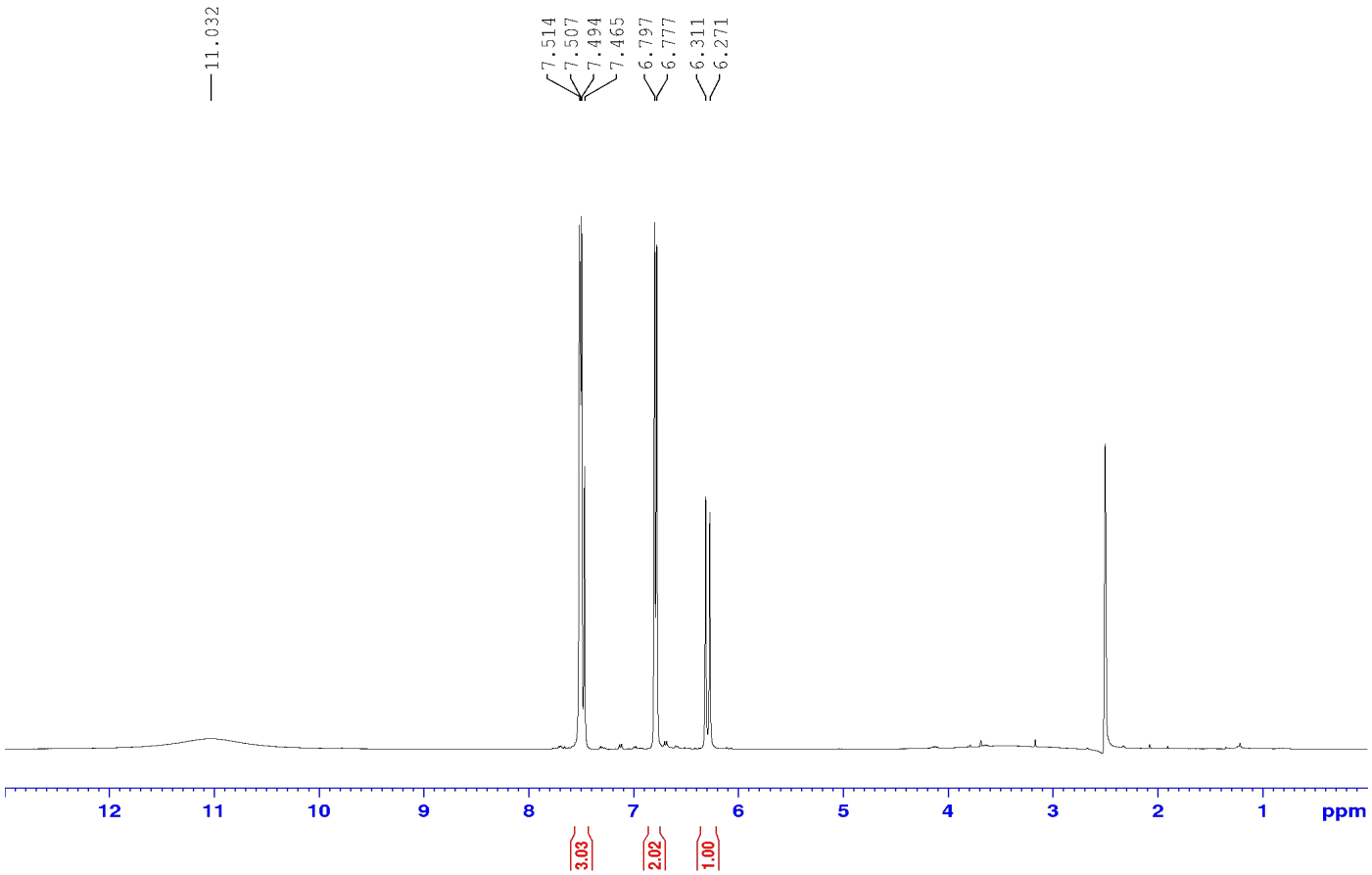
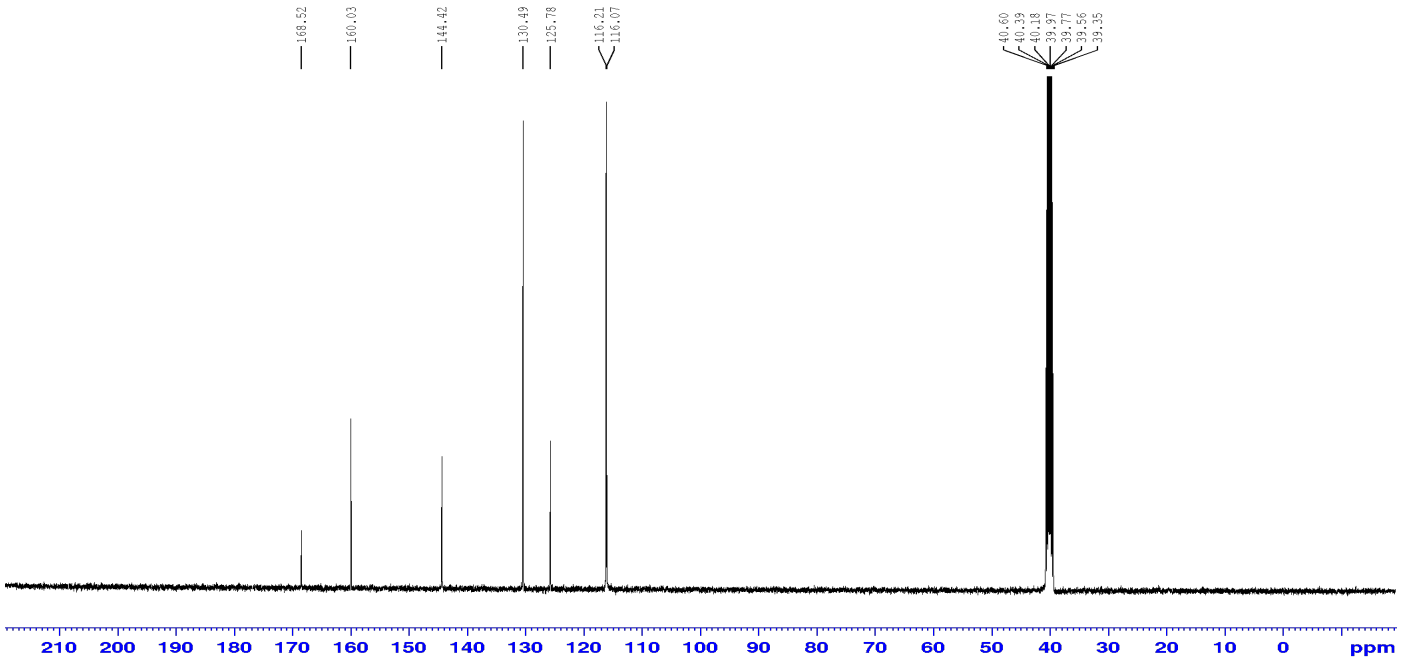


Figure A9: The reported Rf value of ferulic acid was 0.56 with 50/50 % ethyl acetate and petroleum ether (a) without UV-light (b) Under UV-light

© University of Venda





© University of Venda

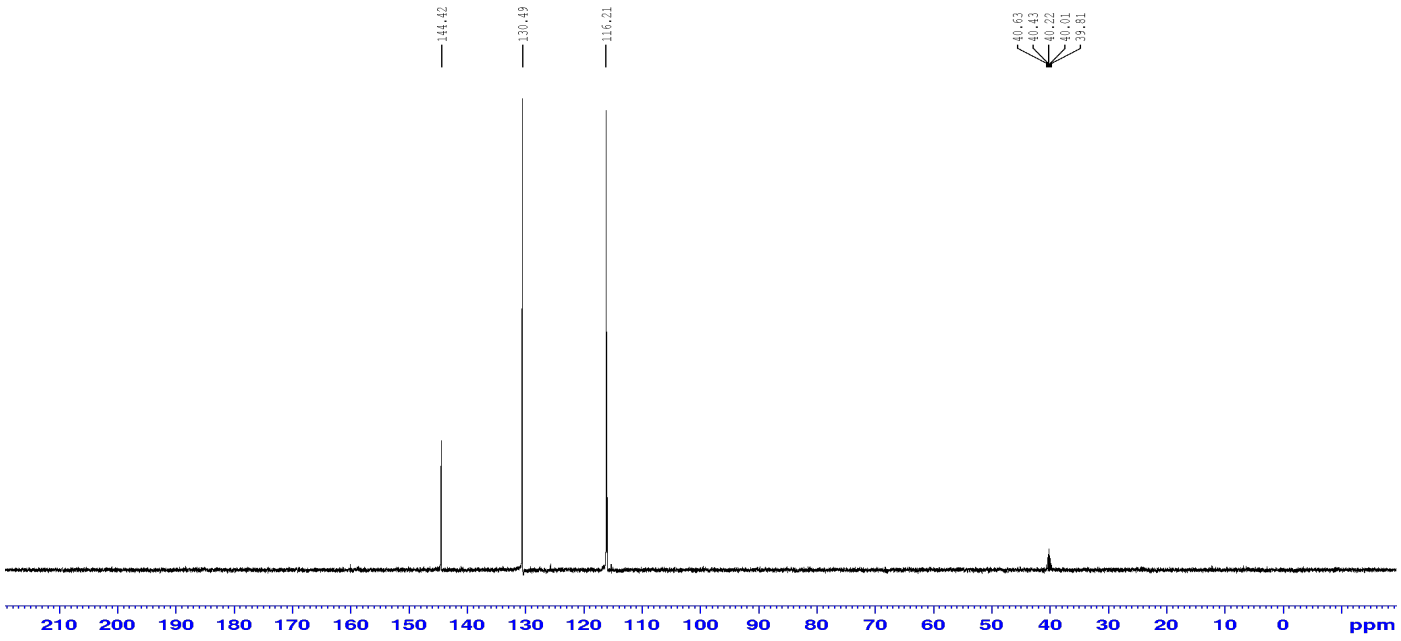


Figure A10: ^{1}H-NMR/^{13}C-NMR and DEPT 135 spectra of 4-Hydroxy cinnamic acid synthesized by procedure B

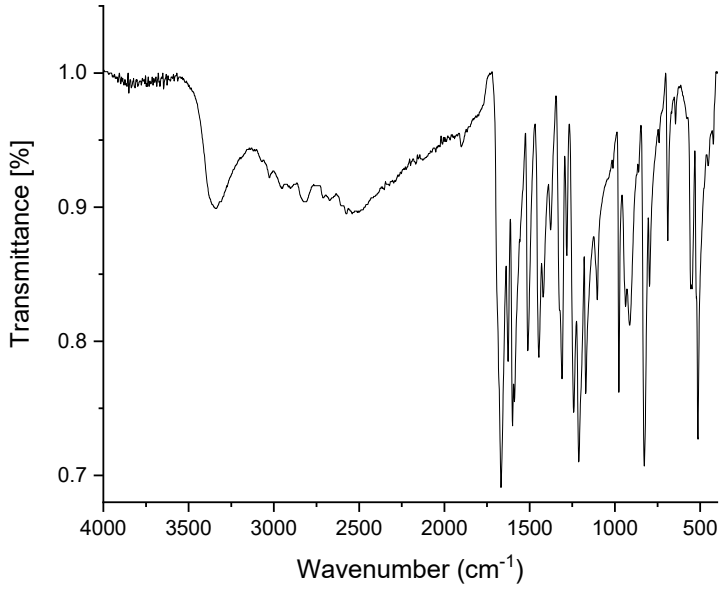
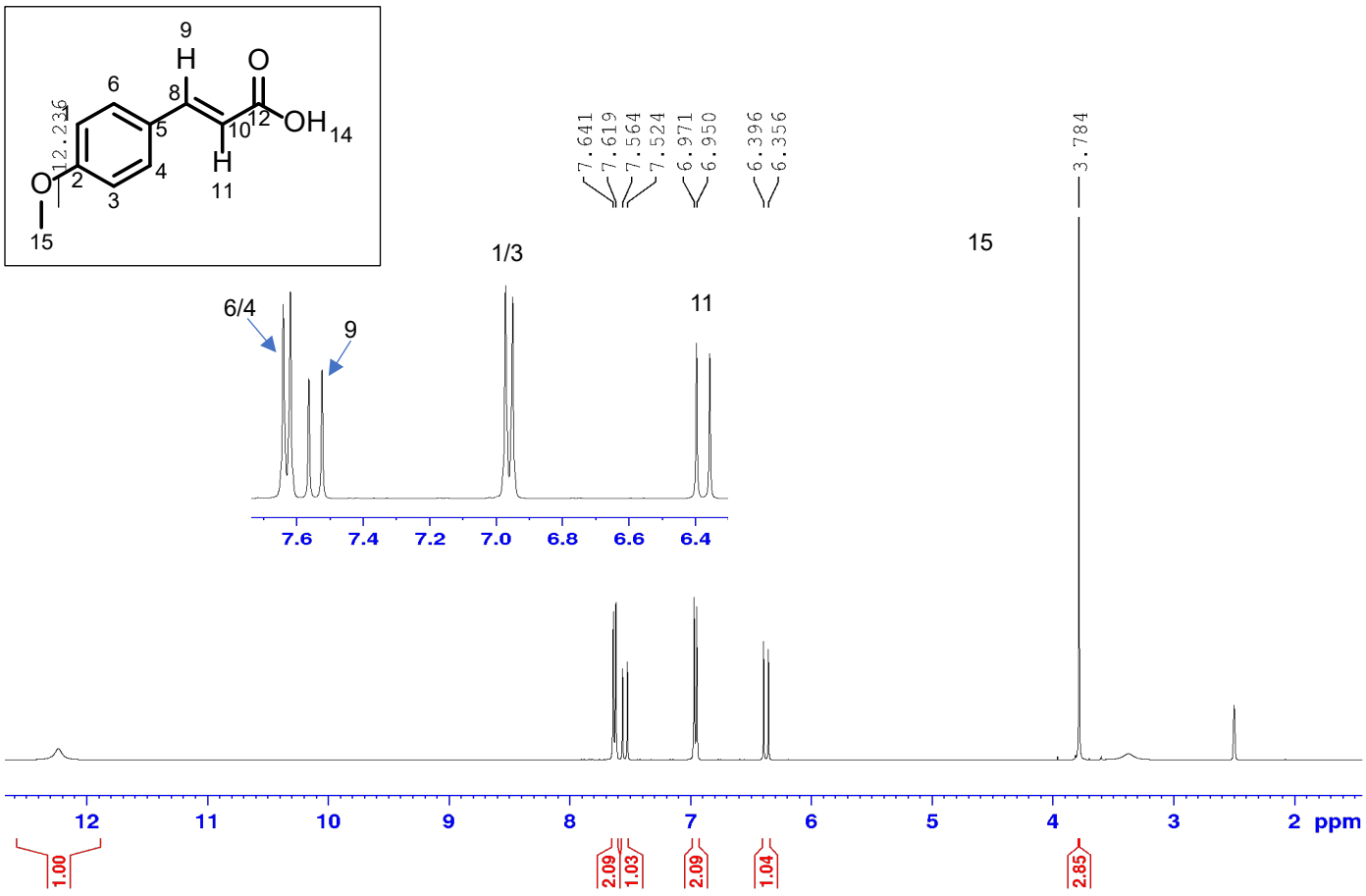


Figure A11: FTIR spectra and TLC visualization of hydroxycinnamic acid

© University of Venda



Figure A12: The reported Rf value of hydroxycinnamic acid was 0.69 with 50/50 % ethyl acetate and petroleum ether (a) without UV-light (b) Under UV-light



© University of Venda

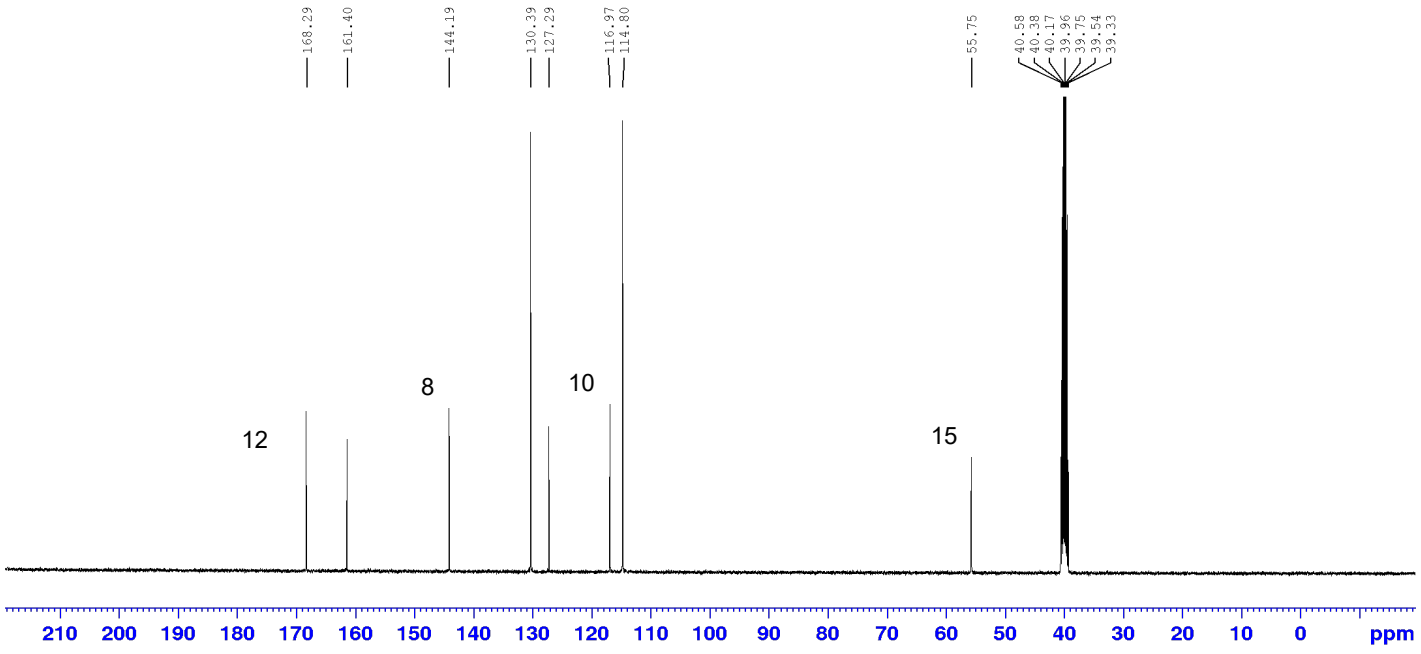


Figure A13: ^{1}H-NMR/13C-NMR spectra of trans-4-methoxy cinnamic acid synthesized by procedure C (Wittig)

© University of Venda

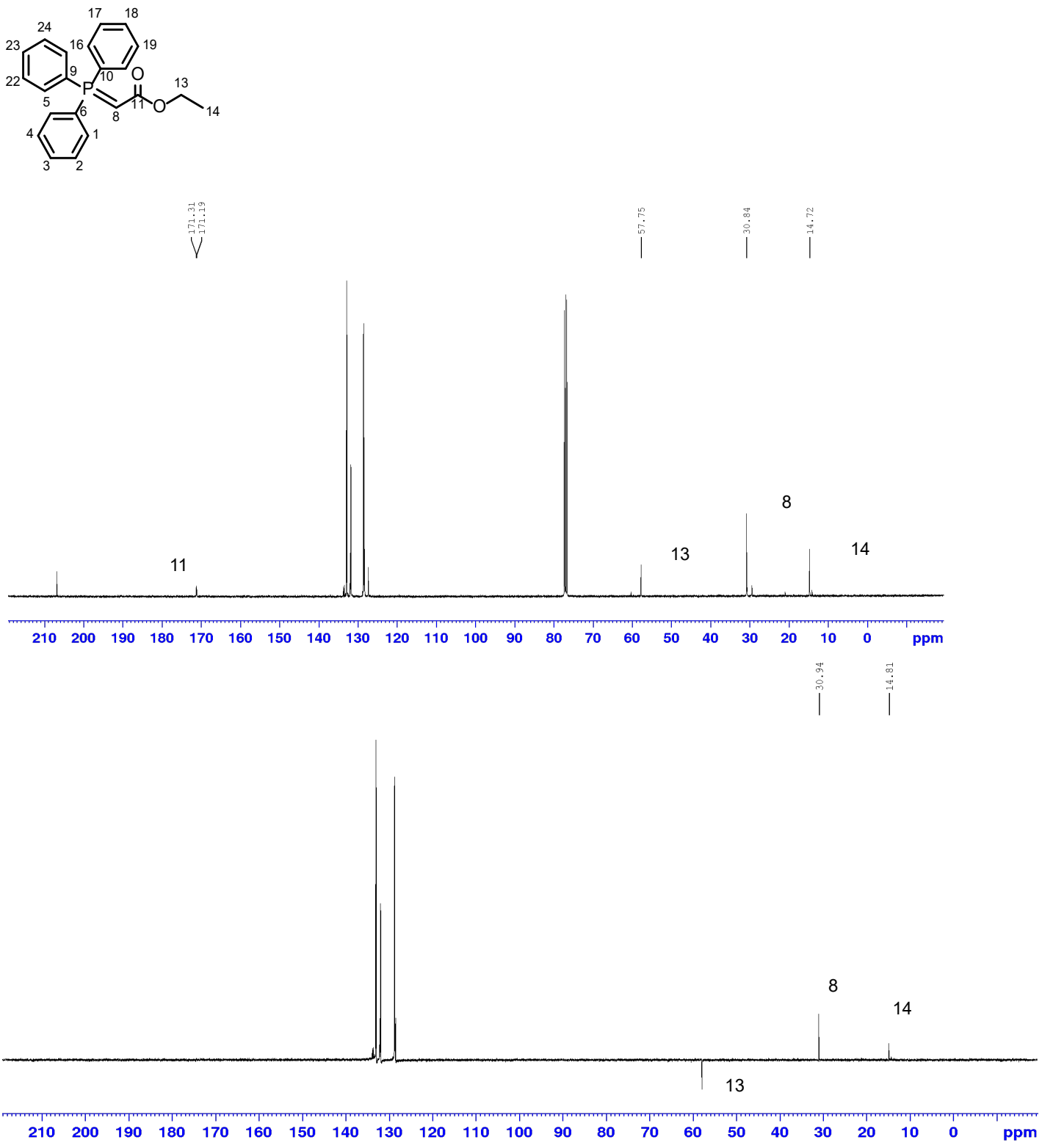


Figure A14: ^{13}C-NMR/dept-90 spectra of Ethyl 2-(triphenylphosphoranylidene) acetate

© University of Venda

Table A1: Computational study results for the optimization of synthesis solvent

Compound	Medium	Energy (a.u)	ΔE (a.u)	ΔE (kJ/mol)
(t-4MCA)	Acetonitrile	-612.80670	0.01208	31.70003
	Methanol	-612.80660	0.01204	31.60080
	Ethanol	-612.80650	0.01190	31.24223
	THF	-612.80520	0.01058	27.76883
	Chloroform	-612.80400	0.00952	24.99289
	Vacuum	-612.79460	0.00000	0.00000
Paracetamol (PCM)	Acetonitrile	-515.5392	0.0151	39.7058
	Methanol	-515.5392	0.0151	39.5758
	Ethanol	-515.5390	0.0149	39.1065
	THF	-515.5373	0.0132	34.5818
	Chloroform	-515.5360	0.0118	30.9978
	Vacuum	-515.5241	0.00000	0.00000
(MAA)	Acetonitrile	-306.51564	0.00720	18.90158
	Methanol	-306.51562	0.00718	18.84304
	Ethanol	-306.51554	0.00710	18.63120
	THF	-306.51476	0.00631	16.57530
	Chloroform	-306.51413	0.00569	14.92916
	Vacuum	-306.50844	0.00000	0.00000
4-vinyl pyridine	Acetonitrile	-325.71576	0.00636	16.70786
	Methanol	-325.71573	0.00633	16.62833
	Ethanol	-325.71576	0.00637	16.72345
	THF	-325.71463	0.00523	13.74109
	Chloroform	-325.71391	0.00452	11.86054
	Vacuum	-325.70939	0.00000	0.00000

© University of Venda

Table A5: Swelling % of MIPs in different solvents

Swelling % of NIP				
Weight in (mg)	Methanol	Ethanol	acetonitrile	Ethanol/Acetonitrile
Initial mass (dry MIP + vessel)	1123.6	1096.7	1098.7	1130.3
Final mass (swollen + vessel)	1162.5	1125	1124.9	1165.9
Final mass polymer (dry)	20.2	20.1	20.2	20.2
Final mass polymer (wet)	38.90	28.30	26.20	35.60
	92.57	389.05	29.70	76.24
Swelling % of t-4MCA				
Weight in (mg)	Methanol	Ethanol	Acetonitrile	Ethanol/Acetonitrile
Initial mass (dry MIP + vessel)	1130.1	1136.7	1097.3	1131.3
Final mass (swollen + vessel)	1185.4	1199	1160.4	1191.1
Initial mass polymer (dry)	20.1	20.2	20.1	20.1
Final mass polymer (wet)	55.30	62.30	63.10	59.80
	175.12	208.42	457.71	197.51
Swelling % of PCM				
Weight in (mg)	Methanol	ethanol	acetonitrile	Ethanol/acetonitrile
Initial mass (dry MIP + vessel)	1145.6	1198.7	1132.2	1142.6
Final mass (swollen + vessel)	1267.4	1290.9	1220.8	1237.5
Initial mass polymer (dry)	20.1	20.3	20.2	20.3
Final mass polymer	121.8	92.2	88.6	94.9
	505.97	231.03	338.61	367.49

© University of Venda